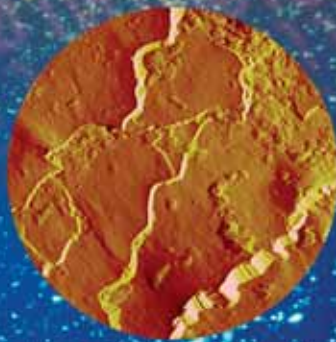
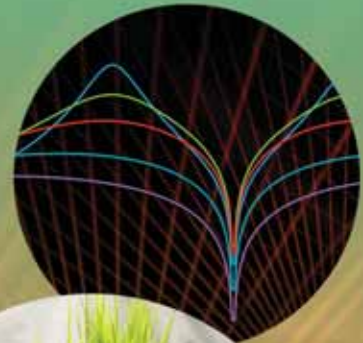


ISSUE THREE • 2007

Agilent Measurement Journal



Agilent Technologies

Applying Ingenuity to the Measurement of Emerging Technologies



Darlene J.S. Solomon
Chief Technology Officer, Agilent Technologies
Vice President, Agilent Laboratories

In many established fields, we sometimes take for granted the ease with which we can make direct measurements of fundamental properties. Digital multimeters measure voltage, current and resistance. Oscilloscopes measure and display analog and digital waveforms. Spectrophotometers measure the intensity of absorbed light as a function of excitation wavelength.

When working with emerging technologies, direct measurements are seldom easy. Stumbling points typically occur during the transitions between research, development and manufacturing — and indirect measurements can often provide the missing information.

In all cases, tremendous ingenuity goes into the indirect measurements and associated derivations that ultimately reveal the sought-after characteristics or behaviors. These measurements often require insightful combinations of general-purpose instruments, one-off black boxes and elaborate post-processing of measured data. Sometimes the evolution ends with this approach because the indirect measurement satisfies the need. In other cases, market demand pushes us to create new classes of direct-measurement tools.



Examples of direct and indirect measurements abound in electronics. In the early days of computer technology, designers relied on oscilloscopes to view the square-wave ones and zeroes coursing through their designs. With too few channels and inadequate triggering, oscilloscopes made it difficult to find timing problems and data-flow bottlenecks — until the oscilloscope evolved into the multi-channel logic analyzer, which provides a more direct way to understand digital circuitry.

In chemical analysis, octane number is an empirical measure of gasoline performance traditionally tested in a standard reference engine. Using techniques developed in the 1990s, chemists have identified mathematical correlations between octane number and gasoline's near-infrared spectrum. As a result, the near-infrared spectrometer replaced the reference engine and we can make gasoline-performance measurements indirectly through near-infrared spectroscopy without the arduous process of identifying individual gasoline components and their concentrations.

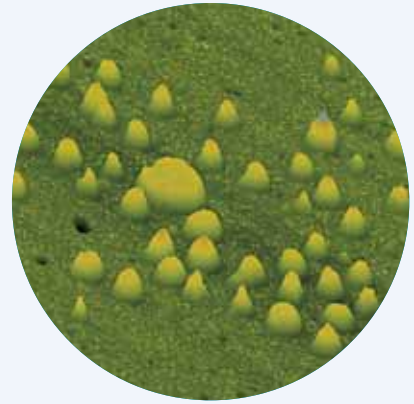
Life sciences bring another perspective, where reduction in sample complexity can be equivalent to increasing direct-detection performance. Up-front sample preparation is often overlooked as a core measurement component. For example, simplification of a complex biological mixture through



specific biochemical reactions — an indirect measurement — simplifies the direct measurement task for instruments such as bioanalyzers and mass spectrometers. The key specification then becomes the overall solution performance, which includes direct-measurement instrument performance as an important — but not necessarily defining — contributor.

At the nanoscale, atoms, molecules and structures play by the rules of atomic forces, molecular bonds and quantum mechanics. This is why observing, measuring and characterizing nanoscale materials will require clever combinations of existing instruments to make direct or indirect measurements until application-specific tools are available.

For example, in the R&D environment, an atomic force microscope (AFM), which physically touches the sample as it scans its surface, can be used in conjunction with a network analyzer or impedance/materials analyzer for direct measurement. In such cases, the AFM's scanning tip also serves as a probe that contacts the nanoscale device and enables electrical measurements of current, voltage, capacitance, magnetic force, impedance and even scattering or S-parameters. Ideally, within this decade we will begin to combine these separate modes of direct measurement into integrated and synchronous multimodal measurements.



When nanoscale products move into manufacturing, sample characterization through direct physical measurements can be too cumbersome, costly and time-consuming outside of the R&D environment. Instead, surrogate, ensemble and systems-level measurements enable statistical characterization of a material's functional properties, thereby confirming its physical integrity. Once we understand the correlation of structure/function measurements, it may be far easier to indirectly measure functional stability than to physically probe structural integrity.

These measurements are leading to new paradigms in data analysis and new methods for the correlation, visualization and integration of heterogeneous data sets. These "nano-informatics" tools are beginning to emerge and may leverage today's bioinformatics solutions. Progress in nano-informatics will drive nanotechnology insight and facilitate its transition into production.

In all of these disciplines, the transitions from research to development to manufacturing require ingenuity and innovation at two key times: when solving the indirect measurement problem and when creating a new instrument that can make the measurement directly. As you'll see in this issue of *Agilent Measurement Journal*, we're making progress in both areas.

Emerging Innovations Department

- 6
- High-speed digitizer
 - Fibre Channel
 - 3GPP LTE
 - Metabolite ID software
 - Upgraded mass spectrometer
 - EMI analysis
 - PXIT modules
 - BFD testing
 - Wireless test set

Insight Department

- 2 **Applying Ingenuity to the Measurement of Emerging Technologies**
Innovative thinking produces the indirect measurements and associated derivations that reveal the characteristics and behaviors of new technologies.
- 8 **Delivering Bigger Benefits by Optimizing Customer Workflows**
Guided by opinion-leader customers, Agilent's Life Sciences and Chemical Analysis group is extending its core products into increasingly comprehensive solutions.

10 **Measuring Material Properties at the Nanoscale**

Nanomaterials present diverse measurement challenges to cross-disciplinary research teams, and no single tool provides all the information they seek.

18 **Utilizing *In Situ* Atomic Force Microscopy in Life Science, Pharmaceutical and other Bio-Related Applications**

As new technologies simplify sample preparation and handling, use of powerful *in situ* techniques is becoming increasingly prevalent in biological research.

24 **WiMAX™: Plotting a New Path to Global Mobility**

Realizing the global potential of WiMAX will require innovation in its development and commercialization — and in the required measurement solutions.

28 **Addressing the Triple Complexity of Triple-Play Networks**

As service providers race to develop and deploy robust bundles of voice, data and video, powerful test instruments enable system-wide monitoring and troubleshooting.



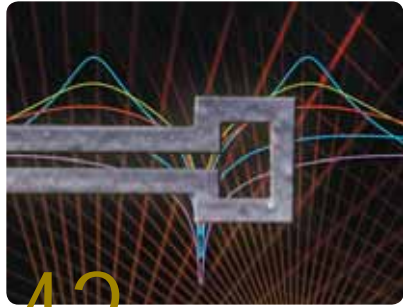
32 **What Next for Mobile Telephony?**

Peak data rates continue to rise but there are implications for data densities, system cost and the quality of each customer's experience.

38 **Exploring the Inner Workings of Tire-Pressure Monitoring Systems**

Because under-inflated tires can lead to dangerous situations, warning indicators became mandatory on most new passenger cars and light trucks in the United States after September 1, 2007.

www.agilent.com/go/journal



42 Developing, Assessing and Applying a High-Resolution Thin-Film Magnetic Probe

In EMI testing, the ability to pinpoint surface currents depends on ultra-fine spatial resolution, excellent electrical field rejection and stable relative phase at harmonic frequencies.

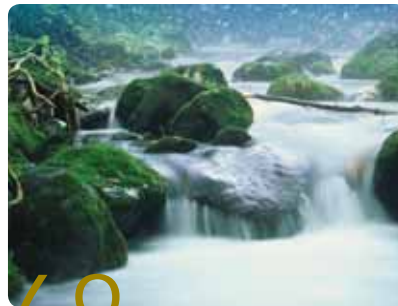
50 Making Accurate Settling-Time Measurements Using a Vector Network Analyzer

The faster a circuit settles, the faster communication can begin — and we present two practical measurement methods that are easy to set up and apply to switched or pulsed devices.

Campus Connection *Department*

56 Applying Metabolomics Methods to the Study of Bacterial Leaf Blight in Rice Plants

Collaborative work with the University of California, Davis exemplifies the rapid progress that has been made in hardware, software and biological applications for metabolomics.



68 Measuring Stream Dynamics with Fiber Optics

Researchers at Oregon State University are using distributed temperature sensing to measure and understand regional environments and ecologies.

Subscribe to *Agilent Measurement Journal*

Give yourself an edge in today's dynamic world of technology: Subscribe to the *Journal* and receive your own copy of the print edition in the mail.

To activate your free subscription, go to www.agilent.com/go/journal and look for the link "Manage your *Agilent Measurement Journal* subscription".

AGILENT MEASUREMENT JOURNAL

William P. Sullivan | President
and Chief Executive Officer

Darlene J.S. Solomon | Agilent
Chief Technology Officer and Vice President,
Agilent Laboratories

Chris van Ingen | President
Life Sciences and Chemical Analysis

Heidi Garcia | Editor-in-Chief

ADVISORY BOARD

David Badtorff | San Diego, California, USA

Lee Barford | Santa Clara, California, USA

Bert Esser | Amstelveen, Netherlands

Johnnie Hancock | Colorado Springs
Colorado, USA

Theresa Khoo | Singapore, Singapore

Jean-Claude Krynicki | Palaiseau,
Essonne, France

Yat Por Lau | Penang, Malaysia

Rick Laurell | Santa Rosa, California, USA

Craig Schmidt | Loveland, Colorado, USA

Roger Stancliff | Santa Rosa, California, USA

Kazuyuki Tamaru | Tokyo, Japan

Boon-Khim Tan | Penang, Malaysia

Daniel Thomasson | Santa Rosa,
California, USA

Kenn Wildnauer | Santa Rosa, California, USA

EDITORIAL

Please e-mail inquiries and requests to
journal@agilent.com

Agilent Measurement Journal

Emerging Innovations

● Greater measurement throughput with Acqiris digitizer

Agilent introduced the Acqiris DP1400 high-speed digitizer, the first release under the Acqiris brand, which Agilent acquired in November 2006. The compact DP1400's highly integrated components are designed for very low, 15-watt power consumption, while the standard short PCI card format features a simultaneous multibuffer acquisition and readout (SAR) mode that improves measurement throughput.

Usable in all standard PCI bus slots, the digitizer performs in a variety of application environments including semiconductor component, hard disk drive production and industrial nondestructive testing. The eight-bit, dual-channel DP1400 features an analog front-end mezzanine with signal conditioning and high-speed analog-to-digital components.

● Pioneering Fibre Channel test module

Agilent released an industry first in its dual-purpose SAN tester and protocol analyzer for 8 Gb/s Fibre Channel (FC). The 1736 Series Fibre Channel test module assists storage equipment manufacturers by providing realistic tests early in the development and qualification cycle, ensuring that the device under test (DUT) meets strict data-storage requirements. It also serves as a protocol analyzer, helping users identify protocol and performance issues. The new module supports a full line rate of 8 Gb/s as well as 4 Gb/s, 2 Gb/s and 1 Gb/s, allowing users to fully test all supported Fibre Channel line rates with a single module. Other capabilities include error-injection features and a flow-control stress test that validates ASIC designs early on and increases test coverage.

● Extended simulation coverage for 3GPP LTE Wireless Library

The 3GPP Long Term Evolution (LTE) Wireless Library has been updated with extended simulation coverage and improved uplink receiver capabilities, helping designers keep pace with the developing 3GPP LTE standard. With new uplink receiver models and improved uplink/downlink source models, this major update will help wireless system designers and verification engineers more quickly develop 3GPP LTE designs for next-generation mobile communications equipment.

The wireless library works within the Agilent Advanced Design System (ADS) EDA software using the Agilent Ptolemy simulator to provide preconfigured simulation setups with signal sources for downlink and uplink, as well as transmitter analyses including spectrum, complementary cumulative distribution function (CCDF) and waveform measurements.

● Metabolite ID software for biological analysis

Adding to the MassHunter Workstation software suite, the MassHunter Metabolite ID software system assists researchers studying modifications that pharmaceuticals and agrochemicals undergo in biological systems. Features of the metabolite identification system include an easy-to-use interface; integrated acquisition through reporting workflow; a combination of multiple algorithms to increase identification confidence; a sample/control comparison based on Agilent's molecular feature extraction (MFE) algorithm; a new molecular formula generation (MFG) algorithm using both MS and MS/MS accurate mass information; a customizable mass defect filter (MDF) to locate metabolites more selectively; and confirmation of metabolites via MS/MS spectral correlation using the Novatia Autoshift algorithm.

● Triple-quadrupole mass range extended in spectrometer

The Agilent 6410 triple quadrupole (QQQ) mass spectrometer is set for a significant upgrade that will extend its mass range to 2,000 m/z from 1,650 m/z. Combined with the new version of the Agilent MassHunter workstation software that provides automated tuning for microfluidic HPLC Chips for nanoflow liquid chromatography/mass spectrometry (LC/MS), the 6410 QQQ enables specific small-molecule assays and can quantify peptides in serum or plasma digests at the attomole level using optimized multiple-reaction monitoring scans. The equipment also provides femotogram-level sensitivity, and ion optics enhance ion transmission and spectral resolution.

● RF preselector helps locate EMI trouble

The Agilent N9039A RF preselector offers 20 kHz (typical) frequency accuracy in a 100-MHz span and up to 8,192 data points in a single, continuous sweep. Previous frequency acquisition methods required multiple sweeps to achieve similar accuracy levels. Measurements can be acquired independent of reference level due to the device's all-digital IF and high-frequency accuracy. When combined with an Agilent PSA Series spectrum analyzer and Agilent MXG sources, the N9039A becomes a fully CISPR-compliant EMI receiver.

● PXIT modules enhance test efficiency

Four next-generation PXIT modules for optical transceiver manufacturing promise to reduce test cost and increase production throughput. The modules, which now provide double the bit-rate coverage and improved performance over previous-generation equipment, have both a combined bit error ratio tester (BERT) and digital communication analyzer (DCA).

The four new modules are: the N2100B PXIT 8.5 Gb/s four-slot digital communications analyzer; the N2101B PXIT 10.7 Gb/s three-slot BERT with high-accuracy clock source; the N2102B PXIT 11.1 Gb/s two-slot pattern generator; and the N2099A PXIT two-slot synthesizer covering a 2-GHz tuning range.

● World's first BFD test solution

Network equipment manufacturers and service providers now have a single-platform solution for protocol emulation and conformance testing of bidirectional forwarding detection (BFD). Agilent's N2X BFD emulation software allows users to test an IP/MPLS device's BFD implementation against similar emulated devices numbering in the thousands, without the need to test individual devices.

The new BFD protocol provides rapid service detection and link faults in IP/MPLS networks. Particularly critical in Ethernet networks that do not have inherent fault-recovery mechanisms, the N2X is billed as the world's first test tool capable of measuring performance and ensuring interoperability of BFD-enabled devices in large, multivendor networks.

● Combined test solution for 3GPP protocol

Agilent's wireless communications test set (E5515C) running the special high data rate W-CDMA/HSDPA lab application (E6703T) has been upgraded with 7.2/2 Mbps HSPA data connection and HSUPA RF measurement capabilities. It is the first one-box benchtop test solution combining these capabilities with real-time 3GPP network emulation and HSPA/W-CDMA/GGE RF measurements, enabling cellular network designers to effectively evaluate a device's ability to process HSPA IP data flowing at rates of 7.2 Mb/s downstream and 2 Mb/s upstream. It also singularly provides all HSUPA functions, including RB test mode, PS data and power, ACLR, spectrum emissions mask and code-domain measurements with real-time connection status reporting and HSPA IP data.

Delivering Bigger Benefits by Optimizing Customer Workflows

Chris van Ingen

President, Life Sciences and Chemical Analysis, Agilent Technologies

INSIGHT

Thirty years ago, it would have seemed out of character for an equipment manufacturer to think too far beyond its instrument-centric product portfolio. In recent years, broad conceptualization has become the rule rather than the exception within Agilent's Life Sciences and Chemical Analysis (LSCA) group.

Our ongoing dialog with key opinion leaders and customers in the markets we serve helps us see the world through the eyes of practitioners in life science, chemical analysis and materials science. They are constantly looking for ways to gain a competitive edge in their businesses, and their needs range from reduced cost per analysis to greater compliance with regulatory requirements to increasingly efficient workflows.

Workflow is the broadest of these topics. Whatever the application — genomics, proteomics, drug discovery, forensics, food safety, environmental or petrochemical testing — the inherent processes and procedures can be made more efficient and productive. In addition to providing meaningful business benefits, effective workflows provide researchers more time for the creativity that leads to new insights and breakthroughs in their respective businesses.

Creating new synergies

Agilent has a strong technology foundation in several analytical- and life-sciences-based solutions — and we are continually refreshing our core platforms and extending them into more comprehensive workflow solutions. This means adding more value in areas such as sample preparation, chemistry, consumables, services and informatics to deliver application-specific solutions.

One recent large-scale example is Agilent's June 2007 acquisition of Stratagene, a leading developer, manufacturer and marketer of specialized life-science research and diagnostic products. Coupling our range of product platforms, software and data-management capabilities with Stratagene's bio-reagents portfolio provides full workflow solutions to academic and pharmaceutical researchers investigating genomics and proteomics.

Extending our instrumentation

At the other extreme, a single instrument provides another important example. In the analysis of DNA, RNA, proteins and cells, the Agilent 2100 bioanalyzer is the most successful of today's commercially available microfluidics-based platforms. Using lab-on-a-chip technology, it can answer research questions within 30 minutes, delivering automated, high-quality digital data.

Looking across the entire workflow of gene-expression studies, we identified numerous possible extensions to the 2100 bioanalyzer that would benefit researchers. One high-leverage addition was

the creation of application-specific LabChip® kits that address the four major steps of a typical workflow in life sciences research:

1. RNA isolation (RNA 6000 Nano LabChip kit)
2. Gene-expression analysis (DNA LabChip kit)
3. Protein expression (cell fluorescence LabChip kit and cell assay extension)
4. Protein purification (Protein 200 Plus LabChip kit)

Step by step, researchers can pursue a complete workflow by learning and using one instrument and its set of application-specific analysis kits.

Automating complex analyses

Analyzing environmental samples that contain a large number of target compounds is a complex application performed thousands of times every day. To improve efficiency and reduce costs, environmental laboratories can benefit from application-specific software that automates these complex workflows.

The Agilent deconvolution reporting software (DRS) provides fast and accurate interpretation of gas chromatography/mass spectrometry (GC/MS) data, especially in complex samples with high matrix contamination. DRS locates and isolates target spectra from co-eluting interferences and then compares the extracted spectrum with application-specific databases to detect the target compound, saving time and improving data quality by reducing the false negatives that often occur in manual comparisons. We have extended DRS with databases specific to environmental, food-safety and forensic applications.

Extracting insights from large data sets

Numerous experiments across multiple lines of inquiry can generate tremendous amounts of data. Breaking down barriers between the scientific disciplines depends on researchers' ability to efficiently sift through multiple data sets, find significant results and pinpoint meaningful connections. We offer a variety of life sciences informatics tools to enhance this part of the workflow.

One example is our GeneSpring analysis platform, which was developed to answer biological questions at the intersection of genomics, genetics, proteomics and biomarker screening. The

platform integrates data and results from multiple applications and provides comprehensive statistical analysis, data-mining and visualization tools to answer myriad research questions.

The results are impressive. In one case, the use of parallel gene expression profiling (GeneSpring GX) and genotyping analysis (GeneSpring GT) revealed new potential disease pathways in a pioneering study on schizophrenia and bipolar disorder. As another example, GeneSpring GT let researchers identify a specific gene that contributes to sudden infant death syndrome. In the past, this may have taken years, but it took less than a week with GeneSpring.

Working at the enterprise level

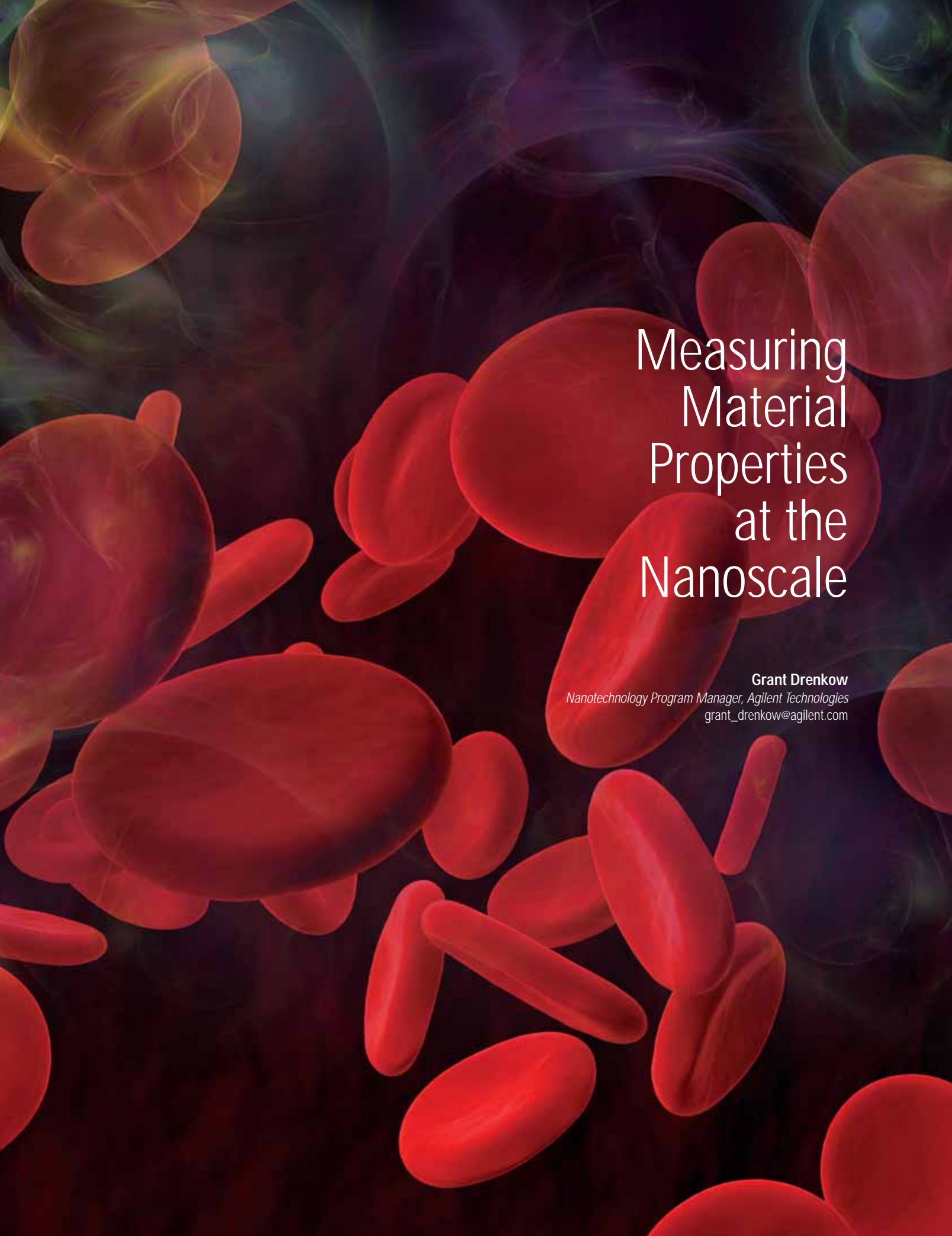
Experiments and measurements exist within the larger context of today's business environment, which includes challenges such as employee productivity, operational and performance metrics, and corporate and regulatory mandates. Factors such as resource constraints, competitive pressures and industry consolidation further complicate the situation.

The Agilent business process management (BPM) solution helps organizations address these challenges by streamlining, automating and optimizing mission-critical business processes while enabling collaboration between people, processes and information. With modules such as an enterprise workflow engine for managing business process execution, BPM helps identify and eliminate process bottlenecks, shortens process cycle times, reduces the risk of noncompliance, optimizes resource utilization and increases process automation.

Looking to the future

Our ongoing dialog with opinion-leader customers will continue to help us identify new ways to augment our solutions and further optimize their workflows. Every aspect of the workflow — from sample preparation to informatics analysis — contributes to improved business results and better collaboration within and across organizations. For our customers, the ultimate payoff is the ability to achieve new breakthroughs sooner while meeting their overall business goals, which will help them thrive in an increasingly competitive business environment.

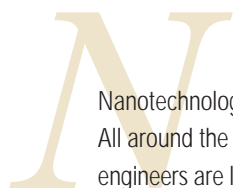
LabChip and the LabChip logo are registered trademarks of Caliper Technologies Corp. in the U.S. and other countries.



Measuring Material Properties at the Nanoscale

Grant Drenkow

Nanotechnology Program Manager, Agilent Technologies
grant_drenkow@agilent.com



Nanotechnology is one of today's best-funded areas of research. All around the world, multidisciplinary teams of scientists and engineers are looking for ways to create a variety of materials, devices and products by exploiting the unique properties of nanoscale structures.

These teams are exploring a truly small world: A nanometer is one billionth of a meter. To put this into perspective, assume that a meter is the distance from New York to Los Angeles. At this scale, the diameter of a human hair would be the equivalent of eight football fields, a human cell would be the size of a basketball court and nanotechnology would encompass any device or structure smaller than a basketball. One nanometer would be the size of a red ant.

In the nanoscale world, atoms, molecules, proteins and nanoscale devices play by the rules of atomic forces, molecular bonds and quantum mechanics. As a result, materials developed with nanotechnology exhibit significantly different properties in the macro world. Observing, measuring and characterizing these properties and behaviors at the nanoscale is a challenge for researchers — and for companies such as Agilent that provide measurement tools.

Creating remarkable properties

In general, products designed with nanoscale structures and devices will be stronger, lighter, faster and more energy efficient than their conventional counterparts. For example, carbon nanotubes — tubular arrays of carbon atoms — are the strongest structure known to man. These can be inserted into metals or polymers, increasing their strength by 10 to 50 percent. Used alone, they can serve as semiconductors or high-performance sensors.

Some products already on the market have been given remarkable characteristics by applying nanotechnology:

- Textiles woven with carbon nanotubes can be both waterproof and stain resistant.
- Nanotech-enhanced fabrics are strong enough to be bullet proof.
- Paints and coatings enhanced with nanoparticles are highly scratch resistant.
- Batteries made with nanoparticles enable industrial power tools to run all day on a single charge, and projects are under way to extend this technology into battery-powered vehicles.

Researchers are also investigating nanotubes and nanoparticles as materials that may someday revolutionize medicine. As an example, nanoparticles coated with antigens can pass through the body and attach themselves to diseased cells. When illuminated with light they will glow, making it possible to locate and destroy affected cells without damaging the surrounding tissues or causing harmful side effects in the patient.

Making meaningful measurements

To create new products based on nanotechnology, researchers must be able to image, manipulate and measure at the nanoscale. Unfortunately, nanoscale devices cannot be viewed with ordinary optical microscopes because they are smaller than the wavelength of light. Instead, observation requires advanced instruments that scan the surface. When nanoscale devices are used as sensors, special care is needed to characterize their electrical properties. These sensors can, for example, change their electrical characteristics when a molecule binds to their surface. Highly sensitive multimeters, semiconductor analyzers or impedance analyzers — along with good measurement techniques — are needed to detect changes measured in femtoamps (10^{-15} A) or nanovolts (10^{-9} V).

The chemistry of nanoscale fabrication faces similar challenges stemming from extremely dilute chemistries and very small amounts of analytes. Measuring and controlling these processes requires highly precise chromatographic and electrophoretic

separation equipment coupled to sensitive mass spectrometers (MS). Example instruments include chemical analyzers such as gas chromatographs (GC) or liquid chromatographs (LC), sometimes augmented with MS instrumentation. Measurements of biological materials at the nanoscale require a highly sensitive instrument called a bioanalyzer that uses electrophoresis techniques to identify key molecules such as proteins.

Looking across all disciplines, it's clear that meaningful results depend on highly sensitive measurements that are also reliable and repeatable. Fortunately, a variety of solutions are available — some that provide direct measurements and others that act as surrogate measurements to enable indirect derivation of nanoscale characteristics and behaviors.

Imaging with advanced microscopy

Although scanning probe microscopes (SPM) and the popular subset of atomic force microscopes (AFM) are called “microscopes,” they are quite different from conventional optical microscopes. For instance, an AFM works much like a phonograph needle with a tip that is moved across a surface in two dimensions while sensing vertical motion (Figure 1). The resulting set of data points is combined to create a three-dimensional topography of the scanned surface.

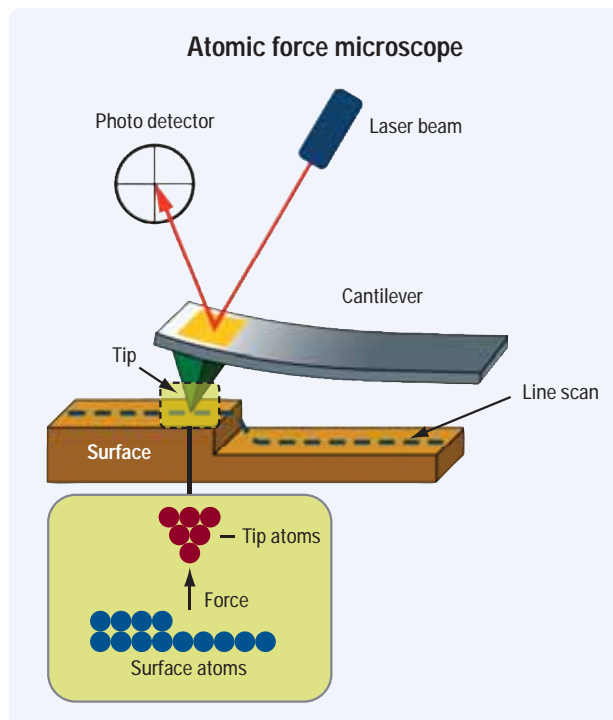


Figure 1. In an AFM, vertical motion of the tip is detected by bouncing laser light off the cantilever and measuring it with a photo detector.

By carefully measuring the tip/sample interaction, an AFM can detect the adhesion, friction and roughness of the surface as it scans. By measuring the force of cantilever motion, an AFM can also derive sample properties such as hardness, stiffness, elasticity, magnetic force or electrostatic force. AFMs can be configured to image materials immersed in liquids, a capability that is useful because many surfaces behave differently in such environments. In addition, AFMs are suitable for making mechanical measurements on living cells and locating molecules with high specificity.

The AFM is also an important tool in the identification and manipulation of nanoscale devices. By attaching a specific molecule to the tip of the AFM and dragging it across a surface, the molecule can be used to find a specific nanoscale object such as a protein. Once found, the AFM tip can be used to push the protein (if the molecule repels) or pull it (if the molecule attracts). Manipulating nanoscale devices is a common use for the AFM.

The AFM also can be used in conjunction with electronic instruments to make measurements on devices or surfaces. If the tip is connected to an electronic instrument (as a probe), it can measure properties such as current, voltage, capacitance or impedance as it moves across the surface. For example, connecting a network analyzer to an AFM makes it possible to extract S-parameters from nanoscale devices (Figure 2).

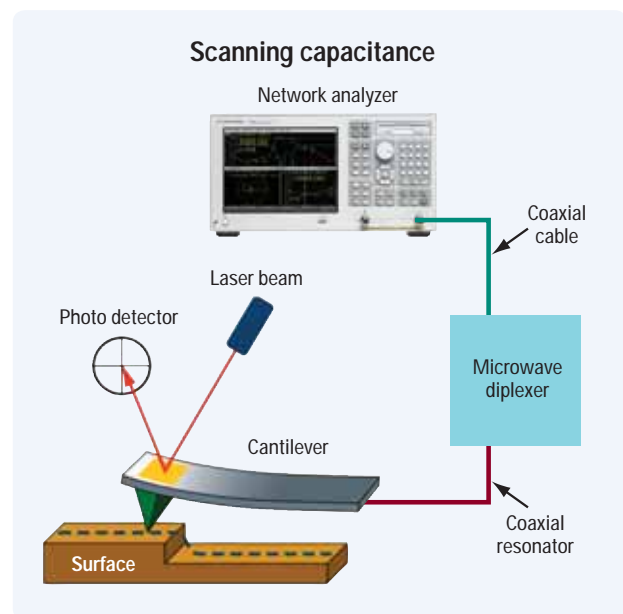


Figure 2. Coupling an AFM with a network analyzer creates a solution for scanning-capacitance microscopy.

Traditional optical and electron microscopy techniques are widely used in nanotechnology research. Electron microscopes, used in both scanning and transmission configurations, make it possible to see small details on large surfaces. The scanning electron microscope (SEM) uses a focused electron beam to see areas as small as 1 nm on the surface of a sample (Figure 3). As the beam is scanned (rastered) across the surface, many types of signals (e.g., secondary electrons, backscattered electrons or Auger electrons) are collected and used to generate an image.

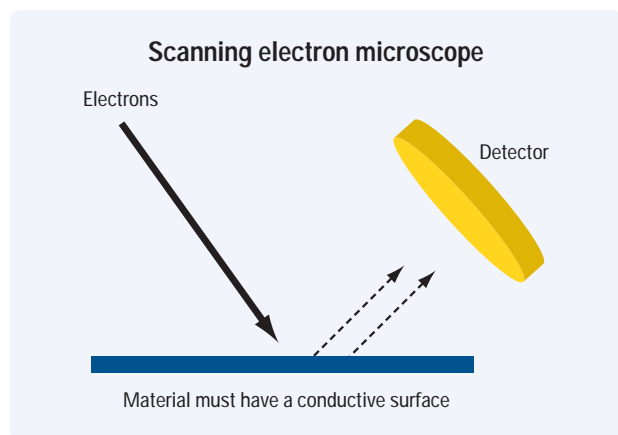


Figure 3. An SEM streams electrons at a conductive surface and creates an image based on the reflected information.

Another popular imaging tool is the transmission electron microscope (TEM). These expensive machines project high-energy electrons through the sample, making it possible to image at very high resolution because electron wavelengths are much smaller than 1 nm (Figure 4). For the TEM to work properly — and provide atomic resolution — the sample material must be reduced in thickness to a few hundred nanometers.

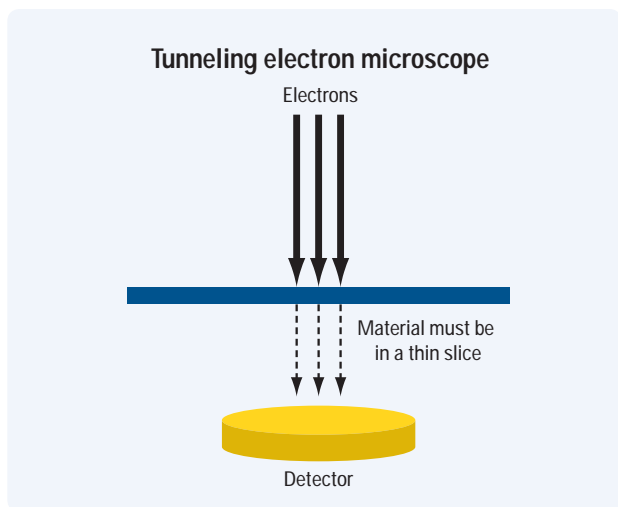


Figure 4. A TEM sends high-powered electrons through the sample to create a 3D view.

Analyzing chemical composition

Chemists were among the earliest nanotechnology researchers, building molecules at the nanoscale. Gas and liquid chromatography are the most popular tools for the separation of complex mixtures of molecules by their chemistry. In liquid chromatography, the chemical mixtures of interest are transported by a liquid solvent through a column packed with solid particles (stationary phase), causing the molecules to progress through the column at different rates based on their chemical affinity to the stationary phase. In gas chromatography, the chemical mixture is similarly transported in gas phase by a carrier gas through a column treated to have variable affinity for the constituents of the mixture (Figure 5).

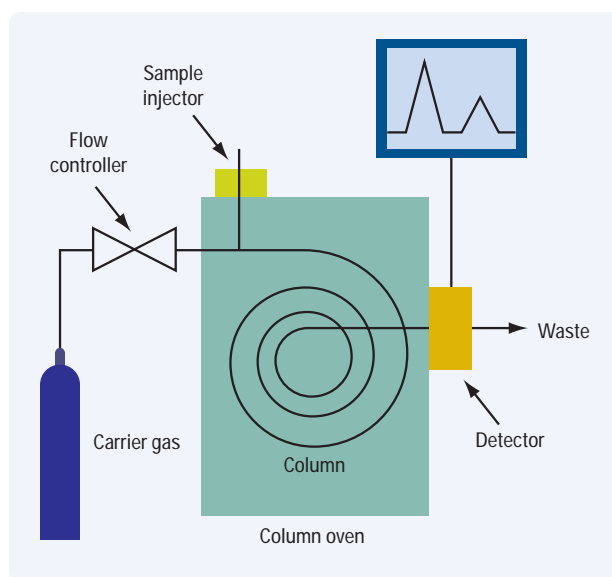


Figure 5. A gas chromatograph ionizes chemical compounds and detects individual molecules of the constituent materials.

An MS can measure the mass-to-charge ratio of individual molecules (Figure 6). It is quite often used in conjunction with a gas chromatograph (GC/MS) or liquid chromatograph (LC/MS), either of which can separate a complex mixture for subsequent quantitative identification by the MS. As an example, Yonsei University in Korea uses an LC/MS to examine byproducts from the creation of core-shell nanoparticles, which have a core of one element surrounded by a shell of another element.¹

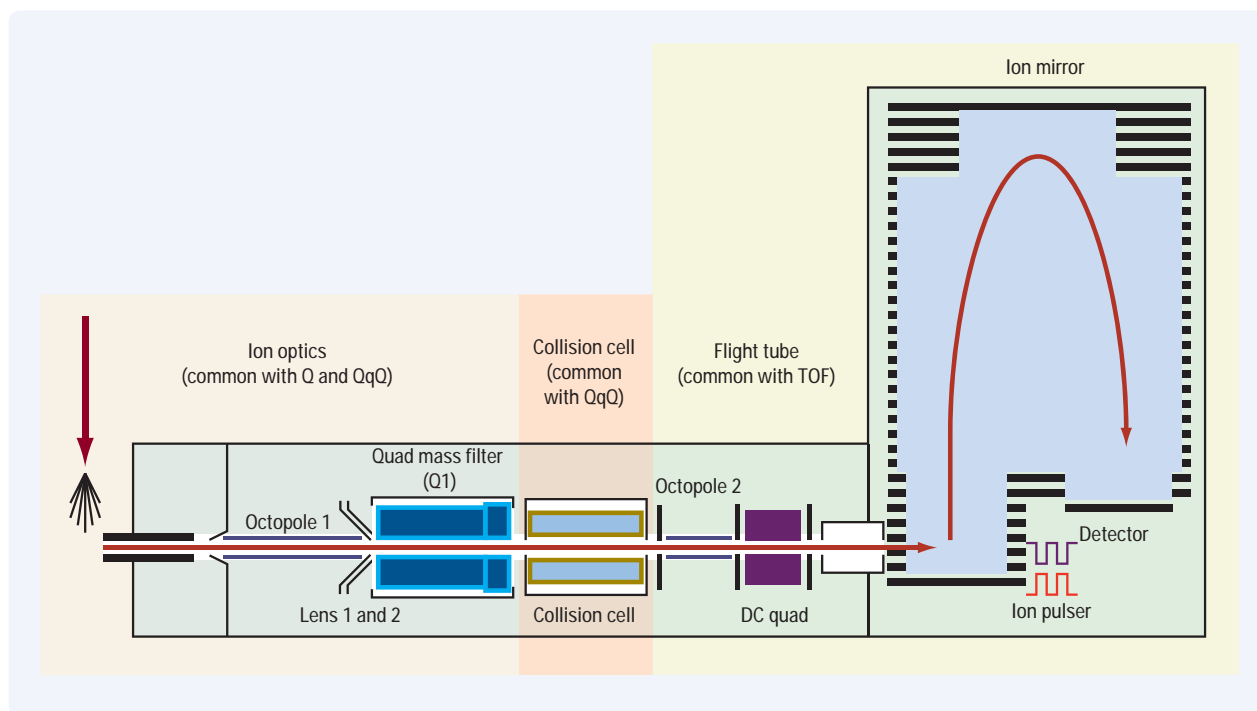


Figure 6. A mass spectrometer separates compounds based on their molecular weight.

Health and safety concerns

Nanotechnology promises products that will revolutionize our way of life. However, some organizations and individuals have expressed concern about possible health and safety risks posed by nanometer-sized particles. While nanoparticles are ideal for removing hydrocarbons in rivers or heavy metals from smokestacks and are small enough to potentially deliver therapeutic agents to individual human cells, there may be risks if the wrong nanoparticles enter the human body through the air or in drinking water. Consequently, governments in the United States and Europe are working on regulations — and appropriate measurement standards — to prevent possible health and safety problems. The National Nanotechnology Initiative in the United States estimates it will spend \$44M in 2007 directed at environment, health and safety.²

Examining biological properties

The analysis of DNA, RNA and proteins is sometimes carried out with a technique known as capillary electrophoresis. The sample is loaded into a lab chip filled with gel and an electric charge draws the molecules through the gel at different rates (Figure 7). This can be done using microfluidics to operate on small volumes in an instrument known as a bioanalyzer. As an example, the Robert Koch Institute in Germany uses the bioanalyzer to separate and analyze antibiotic resistance markers.³

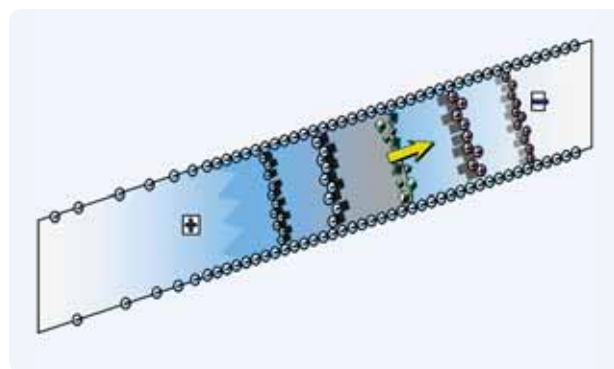


Figure 7. In gel electrophoresis, an electric charge causes the components of a biological sample to move across the gel slab at different rates, forming distinct bands.

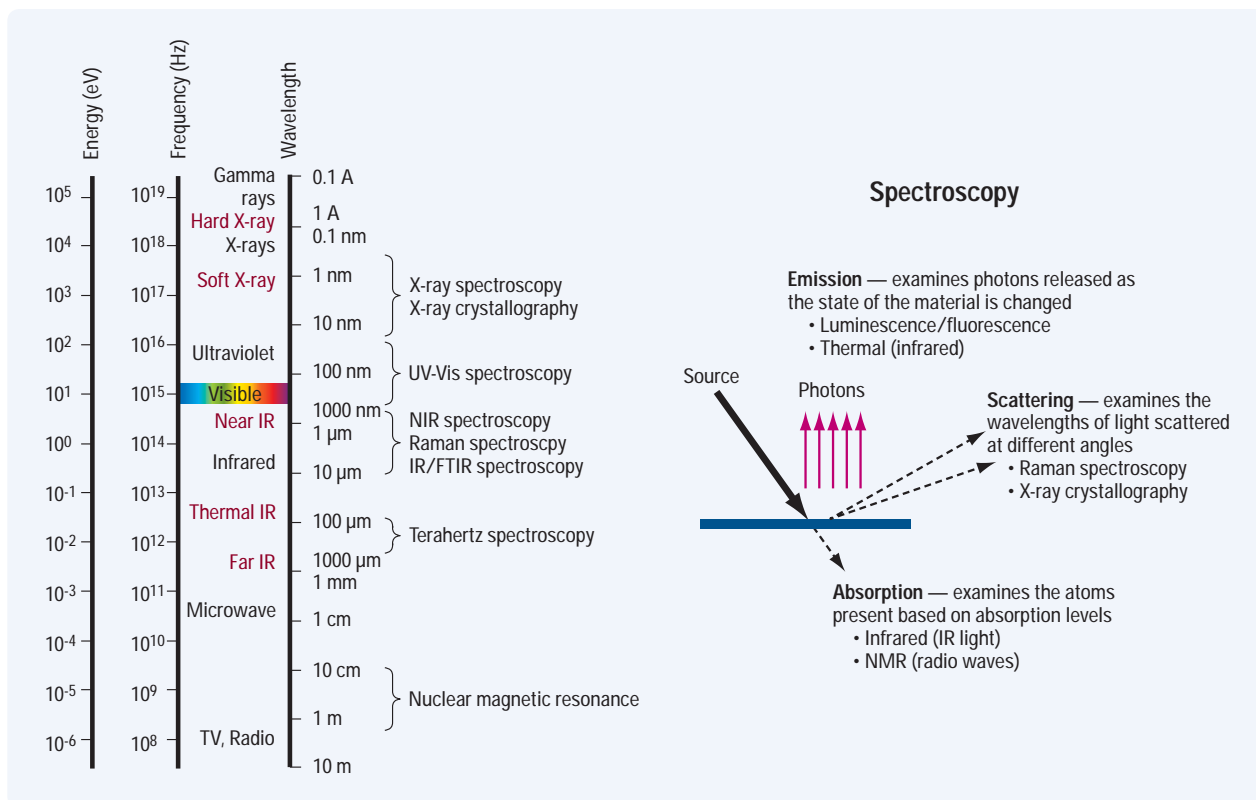


Figure 8. Spectroscopy uses light energy from across the spectrum to reveal surface details and material structures.

Mapping surfaces and structures

Spectroscopy instruments are important in nanotechnology because they provide a nondestructive way to look at the chemistry and physics of materials. These measurement tools illuminate the sample with visible, ultraviolet, infrared and X-ray waveforms and measure the resulting waves that reflect from or are absorbed by the sample. The chart in Figure 8 maps the various types of spectroscopy tools versus the light spectrum.

Characterizing electrical properties and behaviors

Electronic measurements serve an important role in nanotechnology. For nanoscale devices used in electronic applications, measurements can characterize the efficiency of nanoscale electronics. For non-electronic applications, electronic measurements serve as surrogate measurements for other characteristics. For example, the twist (chirality) of a carbon nanotube can be determined by its current/voltage (IV) curve. If the nanotube is not twisted, it acts as a superconductor with an IV curve that is essentially a straight line (right side of Figure 9). However, if the carbon nanotube is twisted, it acts as a semiconductor with an IV curve much like that of a transistor (left side of Figure 9). Note: The graphs are from measurements of a carbon nanotube field effect transistor (CNT FET) performed with an Agilent semiconductor analyzer.⁴

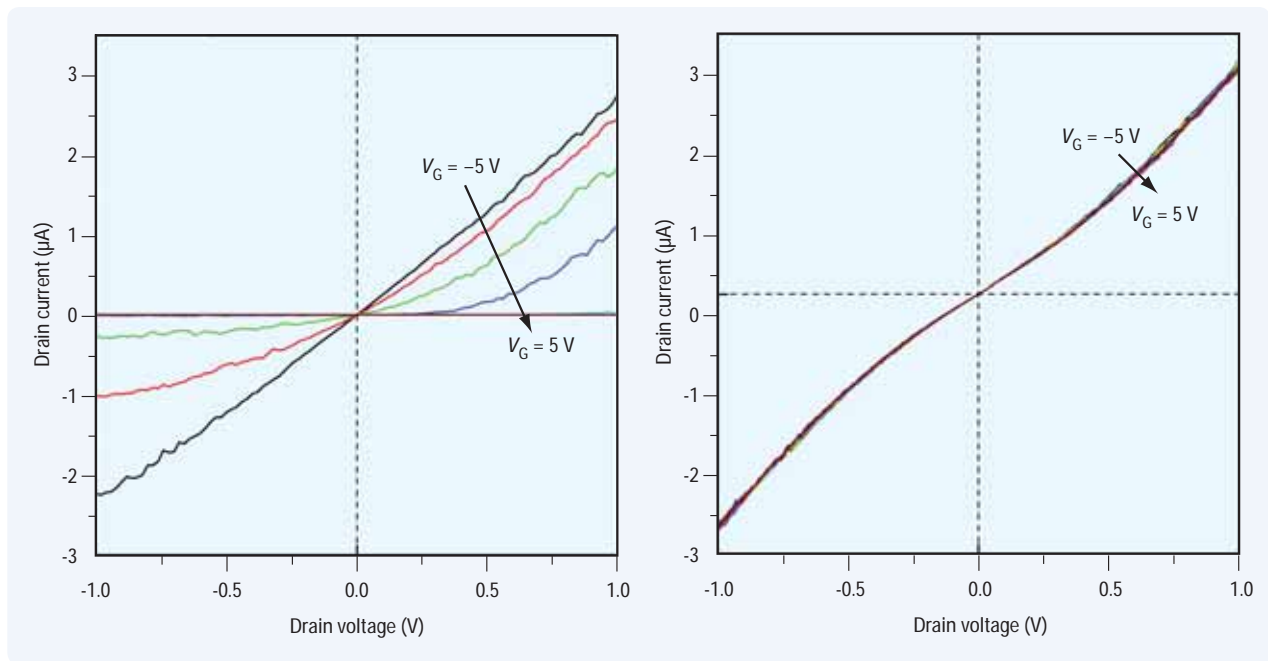


Figure 9. The IV characteristics of CNT FET vary with the amount of twist applied to a nanotube.

Dielectric measurements are important surrogate measurements on materials. Instruments such as an RF impedance/material analyzer can make permittivity and permeability measurements on nanotechnology materials. These measurements can be used to check bulk materials for changes caused by the addition of nanoscale structures. One example comes from Sandia National Labs, which uses an LCR meter to measure the dielectric values of doped ceramics at various temperatures.⁵

Network analyzers are designed to make S-parameter and reflection-coefficient measurements and can be applied to various types of materials engineered with nanoscale structures. Such measurements help determine the effectiveness of a material in electronic applications. In one example, China's Nanjing University is using a microwave network analyzer to measure the reflection coefficients of piezoelectric superlattice.⁶ Various other instruments such as multimeters, nanovoltmeters, oscilloscopes and microammeters are used to analyze DC and AC currents and voltages.

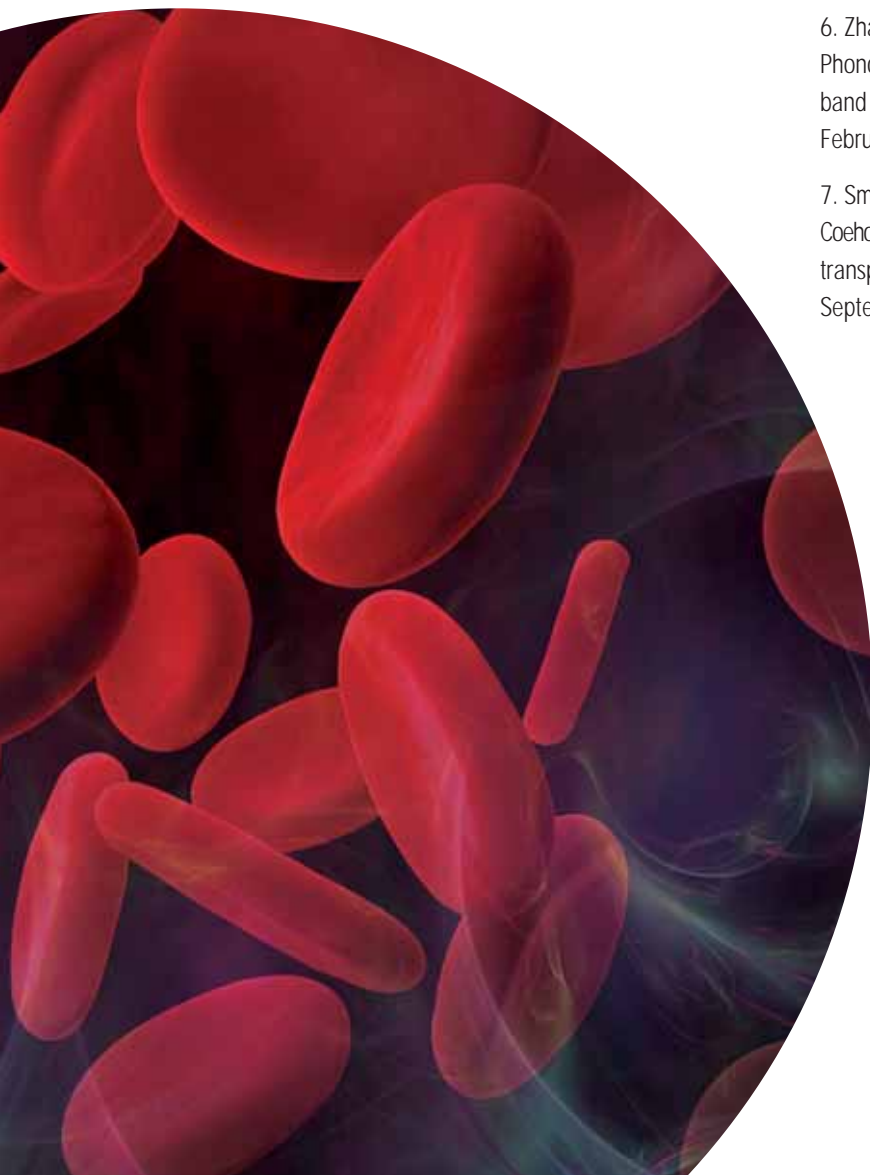
General-purpose instruments are also used as stimulus devices in nanotechnology measurements. One example is power supplies, which are commonly used because they supply very precise low-level voltages or currents to low-power nanoscale devices such as nanotubes and nanowires. Function generators are popular because they supply sine, square, pulse or arbitrary (custom) waveforms. High-precision pulses created with a pulse generator are another popular stimulus. For example, the University of Groningen in the Netherlands uses a pulse generator to drive a ferroelectric polymer transistor and a semiconductor analyzer to measure the resulting IV and CV curves.⁷


Conclusion

Because materials exhibit novel properties at the nanoscale, they present many measurement challenges to cross-disciplinary teams of researchers, and there is no single tool that provides all the information researchers seek. Instead, they must rely on a variety of measurement tools to image, manipulate and characterize nanoscale devices. They confront myriad problems that are as diverse as the measurements they need to make: imaging of surfaces; measurement of electrical, mechanical, thermal, physical, chemical or biological properties of surface and bulk; imaging the distribution of components; quantitatively understanding the composition of complex mixtures and composites; and developing highly specific identification and location of species down to the level of individual molecules. To make such measurements, researchers must draw upon a broad range of microscopy, spectroscopy, chemical analysis and physical measurement tools to further their research, development and commercialization activities.

References

1. Lee, W-R, Kim, M.G., Choi, J-R, Park, J-I, Ko, S.J and Cheon, J. 2005. Redox-Transmetalation Process as a Generalized Synthetic Strategy for Core-Shell Magnetic Nanoparticles. *Journal of the American Chemical Society*, 127, June 3, 2005.
2. The full report is available online at www.nano.gov/nni_societal_implications.pdf.
3. Strommenger, B., Kettlitz, C., Werner, G. and Witte, W. 2003. Multiplex PCR Assay for Simultaneous Detection of Nine Clinically Relevant Antibiotic Resistance Genes in *Staphylococcus aureus*. *Journal of Clinical Microbiology*, 41, June 2, 2003.
4. Agilent Application Note B1500-1, *Measuring CNT FETs and CNT SETs Using the Agilent B1500A*. 2005. Publication number 5989-2842EN, available online at www.agilent.com.
5. Grubbs, R. K., Venturini, E. L., Clem, P. G., Richardson, J. J., Tuttle, B. A. and Samara, G. A. 2005. Dielectric and magnetic properties of FE- and Nb-doped $\text{CaCu}_3\text{Ti}_4\text{O}_{12}$. *Physical Review*, B 72, September 23, 2005.
6. Zhang, X-J, Zhu, R-Q, Zhao, J., Chen, Y-F and Zhu, Y-Y. 2004. Phonon-polariton dispersion and the polariton-based photonic band gap in piezoelectric superlattices. *Physical Review*, B 69, February 27, 2004.
7. Smits, E., Anthopoulos, T., Setayesh, S., Veenendaal, E., Coehoorn, R., Blom, P., Boer, B. and Leeuw, D. 2006. Ambipolar charge transport in organic field-effect transistors. *Physical Review*, B 73, September 6, 2006.

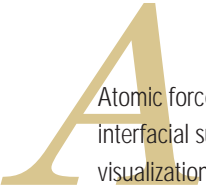




Utilizing *In Situ* Atomic Force Microscopy in Life Science, Pharmaceutical and Other Bio-Related Applications

Joan Horwitz

Marketing Communications Manager, Agilent Technologies
joan_horwitz@agilent.com



Atomic force microscopy (AFM) has revolutionized the field of interfacial surface science by enabling direct, high-resolution visualization of surface morphology in various solutions and gas environments. As new technologies simplify the preparation and handling of diverse sample types, the use of a powerful class of *in situ* AFM techniques is becoming increasingly prevalent in biological research.

AFM works by bringing a cantilever tip into contact with the surface to be imaged. An ionic repulsive force from the surface applied to the tip bends the cantilever upward. The amount of bending, measured by a laser spot reflected onto a split photodetector, can be used to calculate the force. By keeping the force constant while scanning the tip across the surface, the vertical movement of the tip will follow the surface profile and be recorded as surface topography.

Imaging in liquid

Manufacturers of AFM instrumentation have introduced several technologies designed specifically for *in situ* applications. Especially important are those techniques that enable AFM imaging of biological samples in water, physiologically relevant solutions, and buffers. One such development is the advent of an intermittent-contact AFM imaging mode that utilizes an AC magnetic field to drive the atomic force microscope's cantilever into oscillation. The precision control afforded by this magnetic AC (MAC) technique enables gentle, artifact-free measurement of samples in fluid or air.

The newest version of this technology — MAC Mode III from Agilent — employs lock-in amplifiers to determine the oscillation amplitude and phase response of the cantilever, resulting in superior force regulation and phase imaging. Furthermore, there is less system noise and the cantilever can be operated at much smaller amplitudes. Subsequently, sample damage is decreased, probe sharpness is preserved, and resolution is greatly improved.

In addition to facilitating high-resolution AFM imaging of delicate samples in fluid, this oscillating probe technology permits single-pass imaging concurrent with Kelvin force microscopy and electric force microscopy to acquire simultaneous, high-accuracy topography and surface potential measurements. Higher resonance frequencies of the AFM cantilever can be utilized to provide contrast beyond that seen with fundamental amplitude and phase signals, allowing researchers to collect additional information about mechanical properties of the sample surface.

Heating or cooling the sample

The addition of temperature control greatly enhances *in situ* AFM research. Physiological processes can be accelerated or decelerated, structures of many biological molecules can be altered, and biomolecular binding events can be controlled by heating or cooling.

Agilent temperature controllers thermally isolate the sample plate from the rest of the AFM system and insulate the surrounding apparatus from the effects of heating or cooling. Advanced temperature controllers also provide a rapid settling time, thereby allowing the sample plate to reach temperature quickly and hold constant temperature for long periods of time. Agilent sample plates offer built-in temperature control, excellent thermal stability ($\pm 0.1^\circ\text{C}$ or better), and the ability to heat, cool and precisely maintain extreme temperatures (from -30°C to $+250^\circ\text{C}$) during AFM imaging.

Controlling the sample environment

Another area of technological innovation critical to the growth of *in situ* AFM research is the progressive optimization of environmental isolation chambers. High-performance chambers typically mount directly to the atomic force microscope and provide a hermetically sealed sample compartment that is isolated from the rest of the system. To permit the flow of different gases into or out of the sample area, modern chamber designs include multiple inlet/outlet ports.

State-of-the-art environmental isolation chambers also enable humidity levels to be controlled, oxygen levels to be monitored and controlled, and reactive gases to be introduced into and purged from the sample chamber. To ensure utmost application versatility, the environmental isolation chamber should use low-mechanical-drift sample plates that are fully compatible with open liquid cells, flow-through cells, salt-bridge cells (for electrochemistry), Petri dishes (for live-cell imaging) and glass microscope slides.

The AFM scanner should always reside outside the environmental isolation chamber so as to be protected from contamination, harsh gases, solvents, caustic liquids and other damaging conditions. The scanner should also allow researchers to switch imaging modes quickly and easily. One highly practical option is simple-to-load scanner nose cones made from polyetheretherketone (PEEK) polymers that have low chemical reactivity and can be used in a wide range of solvents.

Analyzing structural and molecular biology

AFM studies on DNA, RNA, protein, lipid, live-cell and sub-cellular structures in different biological buffers can give detailed structural information in native environments. When combined with immunofluorescence and electrophysiology, AFM is a very powerful tool for studying the structure/function relations of cell membrane proteins and channels.

Figure 1 presents AFM images of DNA in H_2O containing $MgCl_2$ (top) and $ZnBr_2$ (bottom). The average width of the double helix measured is about 3.5 nm, the highest resolution reported. In $MgCl_2$, the DNA looks circular, whereas in $ZnBr_2$, the DNA is kinked. These images provide the first direct evidence of DNA kinking *in vivo* as a function of ionic conditions.

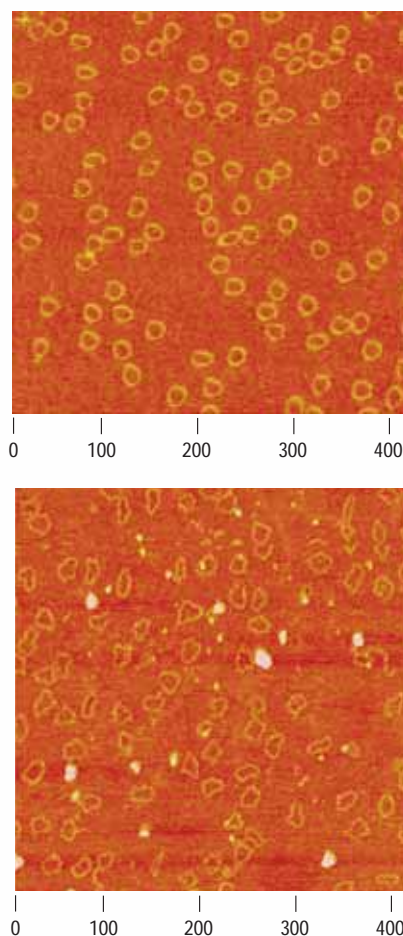


Figure 1. MAC Mode AFM images of 168-bp DNA minicircles in H_2O containing $MgCl_2$ (top) and $ZnBr_2$ (bottom). Scan size = 425 nm x 425 nm.

Figure 2 shows an AFM image of ferritin, an iron-storage protein, in H_2O . The average size of the protein is 10 nm, demonstrating a resolution of about 1 nm.

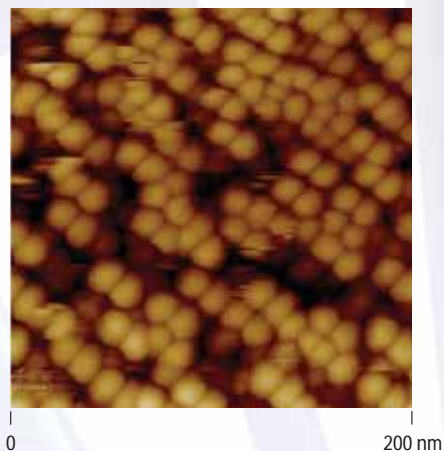


Figure 2. MAC Mode AFM image of ferritin in H_2O . Scan size = 200 nm x 200 nm.

Figure 3 shows AFM images of a chicken chromatin sample in buffer without (top) and with (bottom) the addition of Mg^{2+} . A flow-through liquid cell was used to change the buffer. Upon adding Mg^{2+} , the nucleosomes condensed, exhibiting a final height reduction of 25 percent.

Characterizing liposomes and other drug carriers

Liposomes are widely used protein and DNA drug carriers. Liposome structure is crucial to function and is often measured using light-scattering techniques, an approach that yields only size information and is limited by concentration. When deposited on a suitable substrate, the size and shape of liposomes in buffer can be directly visualized with AFM. The surface structure of other drug carriers, such as lactose crystals for spray powders, can also be studied with AFM under various conditions. AFM techniques, therefore, can greatly facilitate research in the pharmaceutical industry.

Figure 4 is an AFM image of dimyristic phosphatidyl-choline (DMPC) liposomes in phosphate buffer. The liposomes are round and have diameters ranging from 50 to 200 nm.

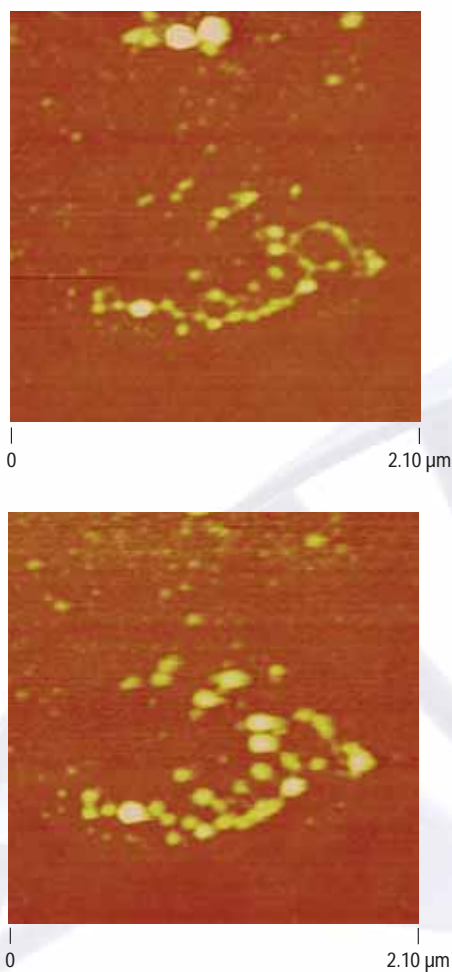


Figure 3. MAC Mode AFM images of chicken chromatin in buffer without (top) and with (bottom) the addition of Mg^{2+} . Scan size = $2.1 \mu\text{m} \times 2.1 \mu\text{m}$.

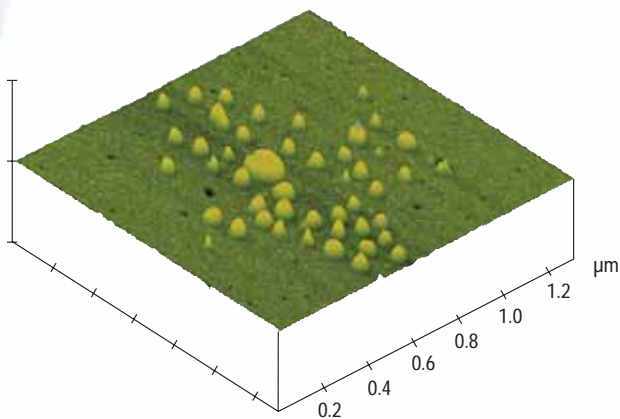


Figure 4. MAC Mode AFM image of DMPC liposomes in phosphate buffer. Scan size = $1.15 \mu\text{m} \times 1.15 \mu\text{m}$.

Figure 5 is a series of AFM images of a lactose crystal surface under increasing humidity, from 13 to 96 percent. The crystals are used as an inhaled drug carrier. Surface structures appear to “melt” at about 80 percent humidity.

In situ AFM monitoring of the swelling effects of biological materials and polymer membranes in H₂O can assist researchers in the recognition of hydrophilic surface locations. This type of observation can be performed at the single-macromolecule level. Figure 6 shows the swelling of a block copolymer based on n-butyl methacrylate (BMA) and poly (ethylene glycol) methyl ether methacrylate (PEGMA) using multifunctional macro initiator (Klok, H.-A., et al. 2006. *Macromolecules*, 39: 4507). Macromolecules of multi-arm star block copolymer extend their arms toward a mica substrate from the lipophilic molecular core. Upon humidity increase, the hydrophilic arms swell and the macromolecules adopt a spherical shape. Contrast of the phase images suggests the macromolecule core is harder than the core formed by the swelled hydrophilic arms. Such macromolecules are suggested as unimolecular drug containers. *In situ* AFM monitoring of uptake and release of drugs will be essential for proving this capability.

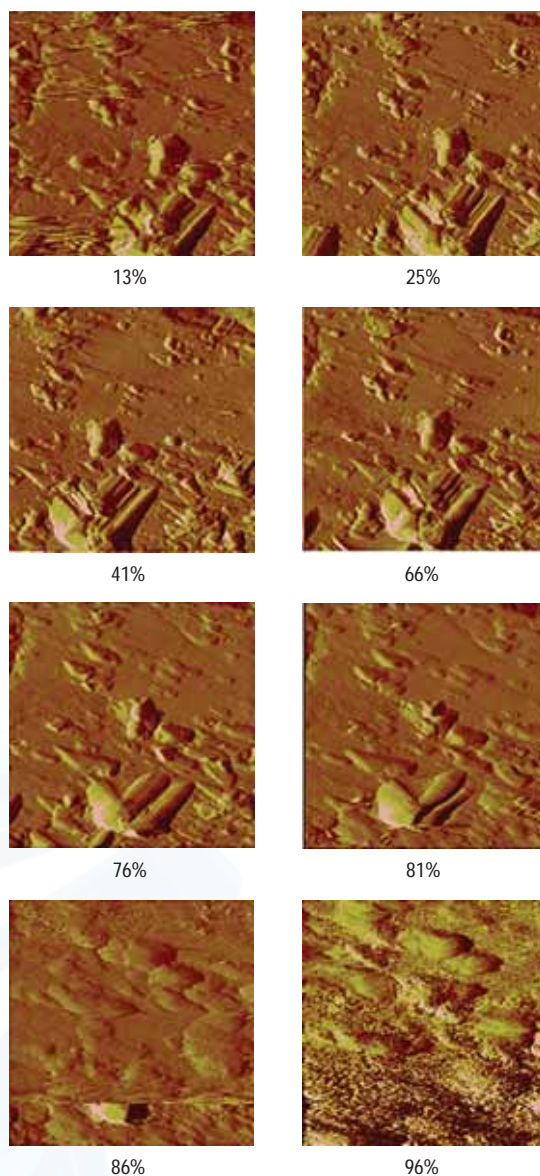


Figure 5. MAC Mode AFM images of a lactose crystal surface under increasing humidity. Scan size = 5 μm x 5 μm . Sample courtesy of Drs. Gary Ward and Mike Maniaci of Dura Pharmaceuticals.

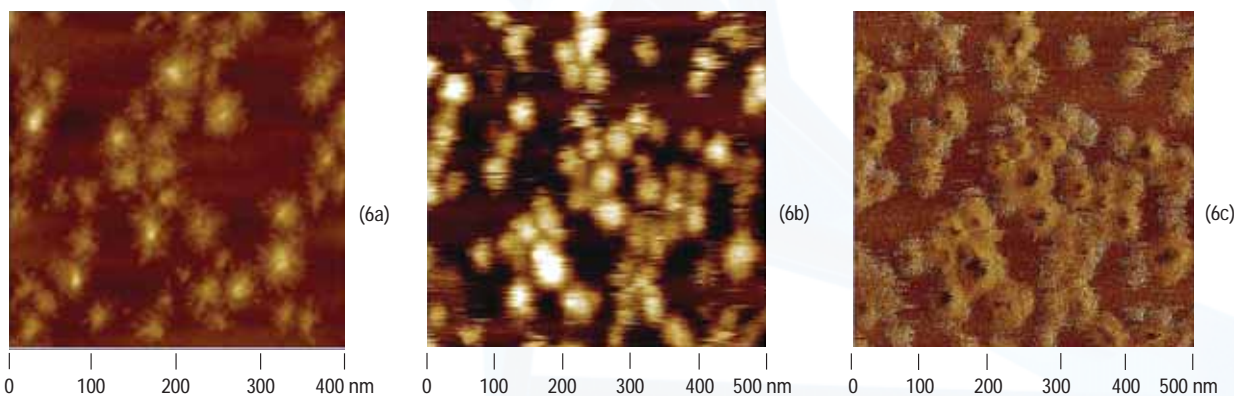


Figure 6. AFM images of BMA/PEGMA macromolecules of multi-arm star block copolymer. Scan size = 400 nm. (6a) Topography image of the single macromolecules on mica at 20 percent humidity; (6b and 6c) Topography and phase images of the macromolecules at 98 percent humidity.

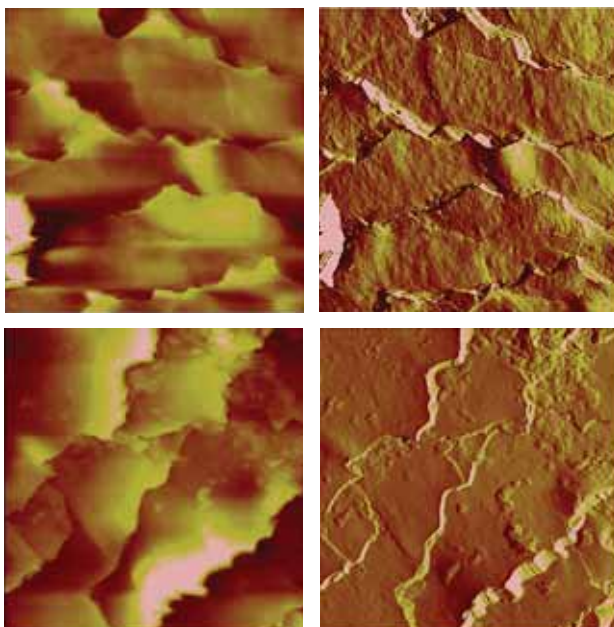


Figure 7. MAC Mode AFM images of an area of human hair before (left) and after (right) treatment with shampoo. Scan size = 22 μm x 22 μm .

Imaging in the cosmetics and hygiene industries

In the cosmetics and hygiene industries, the surface of materials such as fabric or human hair is routinely studied before and after applying a cleaning agent. AFM provides a quick way to obtain high-resolution images of material surfaces with little or no sample preparation. Figure 7 shows AFM images of an area of human hair before (left) and after (right) treatment with shampoo. Studies of this type aid in the development of safer, more effective products.

Looking to the future

In the future, manufacturers of AFM instrumentation will be asked to address numerous new challenges, such as the rapid analysis of large microarrays of biological molecules. Microarray technology has made its biggest impact in the areas of gene expression profiling and DNA sequence identification, but materials other than nucleic acids — including proteins, membranes, cells and small molecules — can also be arrayed and assayed for activity with microarrays.

Although various biological molecules can be attached to AFM cantilevers, using AFM with large arrays of biological molecules will require advances in hardware and software. Microarrays are typically composed of individual micron-sized spots of discrete chemical identity organized on glass microscope slides. Hundreds or thousands of these spots can be arranged on a typical microarray. The arrays can be reacted with various assay reagents and, with the aid of specialized instrumentation and software, thousands of specific interactions evaluated.

Current microarray technology calls attention to thousands of molecular interactions on the array; it typically does not quantify the forces of interaction between interacting species, nor does it evaluate these interactions at the single-molecule level. By combining AFM with microarray technology, the forces of molecular interaction between array elements and assay reagents can be determined.

This requires an AFM scanning mechanism in a top-down configuration as well as an AFM cantilever affixed to the scanning mechanism in order to permit a large enough space under the sample plate to accommodate a translatable stage for aligning individual microarray elements with the cantilever. Modular AFM systems, such as the Agilent 5500 atomic force microscope, provide ready platforms for future development of microarray capabilities.

Conclusion

Atomic force microscopy is well on its way to becoming an indispensable measurement method for many life science, pharmaceutical and other bio-related investigations. With continued advances in instrumentation and *in situ* technologies, AFM will find utility in an ever-widening range of emergent biological applications.

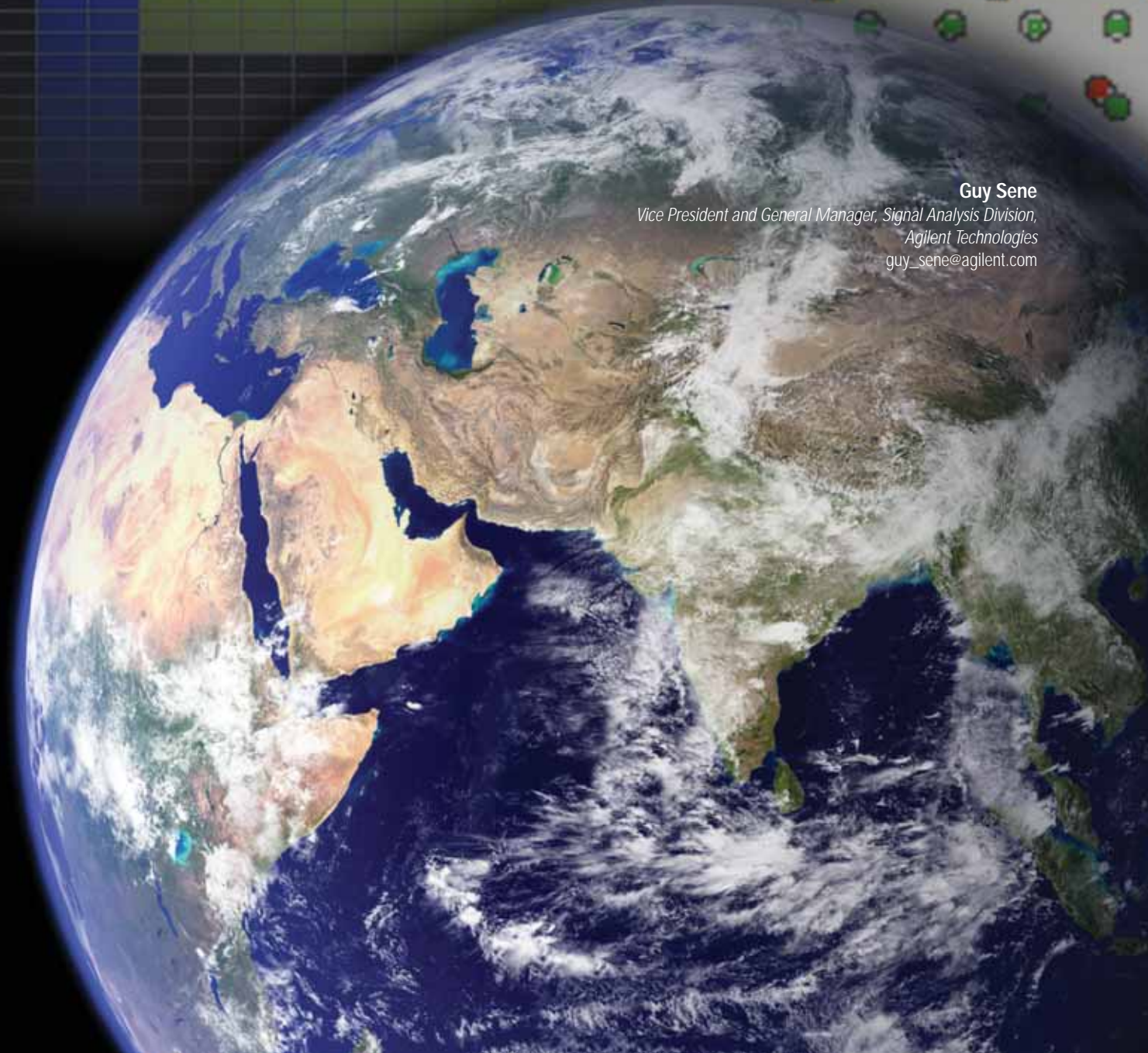
DL-MAPUL-MAPBurst#1

Burst#2

Burst#3

WiMAX™: Plotting a New Path to Global Broadband Mobility

Guy Sene
*Vice President and General Manager, Signal Analysis Division,
Agilent Technologies*
guy_sene@agilent.com



Increasingly, the world today is being defined by anytime, anywhere connectivity. Digital entertainment and communication is everywhere and available to billions of people personally, worldwide. Nearly two billion people use mobile phones on a daily basis — not just for their voice services but for a growing number of social and mobile, data-centric Internet applications. Average consumers now not only expect pervasive, ubiquitous mobility, they demand it. One technology hoping to further cement this trend toward mobility on a global basis is Worldwide Interoperability for Microwave Access, otherwise known as WiMAX.

Although a relative newcomer to the commercial arena, WiMAX and Mobile WiMAX™ have garnered increasing attention from both consumers and technologists alike. Its popularity has been driven by its promise to quickly and cost-effectively deliver super-fast broadband wireless access to underserved areas around the world, as well as recent worldwide developments in spectrum allocation and standardization. Also bolstering its popularity is the global support it has received in Europe, South Korea and the United States (see the sidebar, *WiMAX deployment around the world*).

Proceeding with cautious optimism

While such information creates a very compelling story for Mobile WiMAX, the technology is not without its detractors. Critics cautiously point to the fact that phones and laptop cards combining technologies such as Wi-Fi and cellular might well prove to be less expensive and more reliable in the short term; however, large-scale deployments will be necessary to prove the validity of that claim.

With a few exceptions, even traditional cell phone companies seem reticent to adopt WiMAX, having already invested a fortune in building their own wireless voice and data networks and still hurting from having to write off monumental 3G costs. Instead, they hope to recoup some of this investment through enhancements to UMTS in the form of the new 3G Long-Term Evolution (LTE) standard. This standard aims to evolve 3G toward

a high-data-rate, low-latency and packet-optimized radio-access technology, thereby ensuring that UMTS remains a highly competitive technology through 2010 and beyond. As no commercial deployments of Mobile WiMAX yet exist, though, its performance in a real network implementation remains to be seen.

In spite of these criticisms, there is no denying the growing global awareness — and momentum — of WiMAX and Mobile WiMAX. Of course, realizing its full potential on a worldwide basis will require device manufacturers, service providers and network operators alike to effectively address the myriad technical challenges they now face. As a derivative industry, measurement stands as an enabler of emerging industries such as WiMAX and Mobile WiMAX, supporting technology commercialization within that industry. New measurement solutions, therefore, will need to be created alongside the development and commercialization of WiMAX technology. More and more, such solutions will become critical to adequately addressing the challenges now facing device manufacturers, service providers and network operators.

Sketching the challenges

The widespread global interest in WiMAX and Mobile WiMAX has created a number of daunting new challenges. In the case of the device manufacturer, many of these challenges stem from the fact that the IEEE 802.16 standard specifies minimum performance requirements, but gives the implementer room to interpret how a device such as a WiMAX handset is built. With this amount of leeway, standards-compliant devices can vary widely from one company to another. As a result, the ability to take advantage of emerging market opportunities is closely tied to the manufacturer's ability to test its products for regulatory and standards compliance. It is also tied to the manufacturer's ability to keep pace with emerging WiMAX applications in light of shrinking design cycles and time-to-market schedules. Regular WiMAX Forum®-sponsored Plugfests also help ensure interoperability, but there is more work to be done. Another challenge is how to decrease costs in product design, manufacturing and test while increasing product performance, functionality and quality.

Service providers and network operators face their own challenges when it comes to deploying and maintaining WiMAX and Mobile WiMAX systems. They must ensure that the network and services offered are free from problems at the base station and on the network, for example. This is especially crucial to capturing market share in this fast-growing segment of the industry, and reducing subscriber churn requires that the network be properly tested to guarantee both optimal quality and performance.

Clearly, WiMAX is a challenge to build, deploy and maintain, especially given that there are numerous possible points of failure throughout its lifecycle. Each mobile device has to work properly, and must be able to seamlessly receive and transmit data from the base station and vice versa. The network must be able to handle this activity for multiple subscribers simultaneously without resulting in dropped calls or slow data throughput. Quality therefore cannot be an afterthought. Rather, it must be built into all areas of the lifecycle. Doing so is the only way to ensure that the devices, networks and services all work as expected. It is also the only way to consistently deliver a high-quality experience that instills confidence in subscribers.

Easing the burden

How well a company deals with these challenges will ultimately determine its level of success in the burgeoning Mobile WiMAX market. It will also influence the acceptance of WiMAX in the commercial marketplace. This is where measurement comes in. It can play a critical role in easing this burden by providing the assurance, quality and data sources companies require for technology development and commercialization.

When utilized appropriately, measurement solutions can offer a number of significant benefits. They help proliferate standards such as WiMAX and Mobile WiMAX by ensuring that devices, networks and services comply with any and all standards, certification, conformance and regulatory requirements. They also provide the tools R&D engineers and manufacturers, as well as wireless communication service providers, need to successfully test their products, speed time-to-market and maximize return-on-investment. Measurement solutions also ensure that consumers using WiMAX are protected against substandard quality either in the device, network or service. As a result, measurement is a key enabler for accelerating the delivery of next-generation wireless communication based on WiMAX.

Agilent is a prime example of a company that offers advanced measurement solutions in support of emerging WiMAX technology. Our fixed and Mobile WiMAX measurement solutions span the entire lifecycle — from R&D, design validation and pre-conformance to conformance test and manufacturing — to provide engineers the reliable, repeatable and consistent results they need to deploy WiMAX devices, networks and services. Use of such solutions, which have been specifically optimized for the development, validation and manufacture of applications based on WiMAX, ensure that manufacturers and service providers can take full advantage of emerging market opportunities in the commercial sector.¹

Deploying WiMAX in the real world

With today's engineers now working with WiMAX-specific measurement solutions to address the challenges they face, the next logical questions become, "What's next? How will the ultimate vision of WiMAX come to fruition?" The answers come from understanding the technologies' various stages of implementation: fixed, nomadic, portable, simple mobility and full mobility.

Fixed deployments are defined as stationary access to a single base station, such as for wireless broadband backhaul that connects multiple Wi-Fi networks in a mesh network. In contrast, nomadic deployments are characterized by stationary, but movable, access to a single base station. This deployment is similar to the cyber café concept in which the user can connect from anywhere within the range of a Wi-Fi access point.

Applications that are portable or mobile (e.g., the device is in motion while a signal is being received and transmitted) are based on the IEEE 802.16e-2005 standard. Such Mobile WiMAX systems have the ability to hand off a signal from one base station to the next, thereby creating "metro zones" that seamlessly provide continuous portable outdoor broadband wireless access to customers in large cities and metropolitan areas.

To date, products for both fixed and nomadic WiMAX applications have been commercially deployed. Products for portable applications have now begun making their way to market. While not yet available, Mobile WiMAX will eventually provide mobile broadband wireless access (MBWA) without the need for direct line-of-sight to a base station.

Realizing the true global potential of WiMAX and the business opportunities it foretells will require innovation in the development and commercialization of WiMAX. Just as critically, it will require innovation in the test and measurement solutions that will enable the technology to succeed in the real world. Doing so will not only propel manufacturers, network operators and service providers toward an enhanced customer experience, but more and more it

will help to create a new means of connectivity that will redefine the way in which we, as a global society, communicate.

References

1. More information is available at www.agilent.com/find/wimax. "WiMAX," "Mobile WiMAX" and "WiMAX Forum" are trademarks of the WiMAX Forum.

WiMAX deployment around the world

There is little doubt that WiMAX is increasingly being embraced by countries worldwide. Consider, for example, that trials and commercial deployments are currently ongoing around the world and that services are now being rolled out in Europe, India, Puerto Rico, Russia, South Korea and the United States. And that's just the beginning: According to analysts with the Dell'Oro Group, the Mobile WiMAX market will grow by a compounded annual growth rate exceeding 50 percent through 2011.

With announcements of new deployments coming almost daily, it is easy to see how such growth might actually be possible. Firms such as WiMAX Telecom in Europe, Yozan in Japan and Enforta in Russia already offer commercial services over fixed WiMAX networks. Many operators are either planning similar fixed systems or biding their time while Mobile WiMAX equipment makes its way through the certification process.

Also on the horizon are deployments in France, Germany, Greece and Italy, where plans are now underway to sell WiMAX spectrum licenses. Sweden's telecommunications regulator has even announced that in the fourth quarter of 2007 it will hold an auction of licenses for WiMAX wireless broadband access in the 3.6 to 3.8 GHz frequency band.

As of June 2006, a popular WiMAX market tracking database listed more than 200 operators as either planning WiMAX rollouts or already deploying trial or commercial systems (Figure 1). Additionally, it counted over 117 total

networks in the world, with 14 new networks planned for North America, not including Sprint's widely publicized multi-billion dollar WiMAX rollout. With such positive growth, it's no wonder that many analysts expect fixed WiMAX to become as widely used as DSL or cable modem, and Mobile WiMAX to enable the long-touted delivery of triple-play applications offering voice, data and video services.

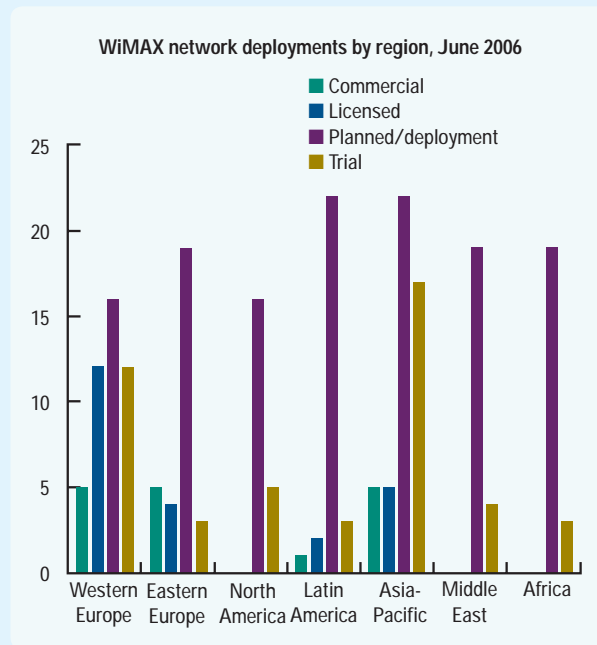
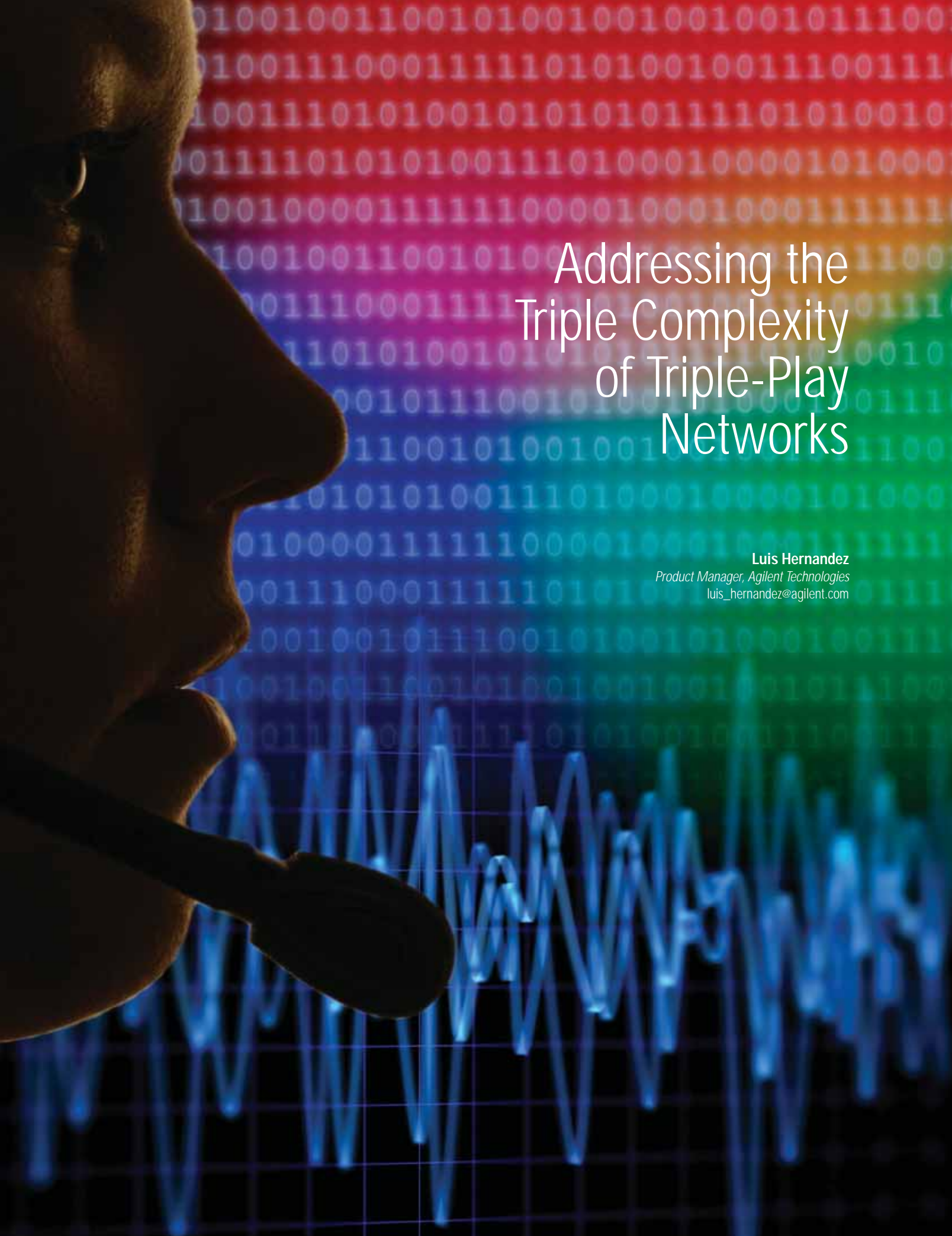


Figure 1. This chart, courtesy of TeleGeography, highlights recent deployments, with the most networks being planned and trialed in the Asia Pacific region.



Addressing the Triple Complexity of Triple-Play Networks

Luis Hernandez

Product Manager, Agilent Technologies

luis_hernandez@agilent.com



T

“Triple play” is a hot buzz phrase in the communications industry and is quickly becoming part of our common vocabulary. The triple play is a bundled offering of voice, data and video carried on a common infrastructure. Specifically, such systems carry voice over Internet Protocol (VoIP), broadband data and video over IP or IP television (IPTV). Because IPTV, in particular, brings extra complexity to the mix, it is shaking up the communications industry in terms of both technology and economics.

Triple-play services, including broadcast TV, video-on-demand (VoD), VoIP, gaming and data, represent serious challenges in the industry. As one example, IPTV is new to many people and the task of characterizing IPTV quality of service (QoS) is difficult and complex. It will become easier once a standard for measuring IPTV quality emerges from the numerous proposals currently under consideration.

Within the industry, service providers are racing to develop and deploy robust IPTV services before their competitors acquire significant market share. As a result, equipment manufacturers are quickly developing products and are seeking to standardize them among service providers.

Exploring the elements of complexity

With IPTV specifically and triple play in general, the inherent level of complexity becomes evident when services must be deployed quickly and with video quality comparable to cable or satellite. The scope of this complexity includes market and technology issues:

- The global market for integrated consumer devices that deliver triple-play services is growing explosively and there is always a new device that needs to be compatible with the others.
- The prime concern is maintaining combined high QoS for voice, data and video when transmitted over the same infrastructure. IPTV broadcast requires high bandwidth with near real-time service. VoIP is not bandwidth intensive but is very sensitive to delays and packet loss.
- Good quality of experience (QoE) has become imperative because revenue and profits depend on positive perceptions of each new service.
- IPTV and VoIP represent a highly distributed signaling architecture with a large number of signaling protocols (e.g., IGMP, RTSP and SIP).
- IPTV and triple play must support new and advanced services such as VoD and click-per-view advertising.

Sketching potential QoE problems

QoE is paramount. Consider the case of a subscriber trying to change the TV channel. First, they would press the “channel” button on the remote control. Behind the scenes, IGMP *leave* and *join* commands are sent from the set-top box to the residential gateway and on to the delivery network. Depending on traffic load and the location of the multicast video on the network, there is a variable delay between when the button is pressed and the appearance of the new channel. If the delay is too long, the subscriber might press the button again, thinking it did not work — and suddenly the channel will change twice. The main reason for this poor QoE is nonconstant channel “zapping.”

A similarly negative experience may result when a service provider changes the priority of services in a broadband connection after adding high-bandwidth IPTV services. A gaming user, who was accustomed to a fast, predictable network response, may experience a slow and irregular response because the service no longer has top priority (though this could potentially be corrected with a configuration change).



Figure 1. Agilent J6900A triple play analyzer

Monitoring and diagnosing problems

Tools such as the Agilent J6900A triple play analyzer aid in the successful monitoring, diagnosing and troubleshooting of such problems (Figure 1). For network equipment manufacturers and communication service providers, the triple play analyzer can be used as a dispatched tool or as part of a system-wide monitoring and troubleshooting solution.

To effectively monitor and diagnose the root problem within a network, the analyzer starts its measurements with a global view of the traffic, automatically separating and classifying data into TCP/IP traffic, MPEG2-TS streams (IPTV or VoD) and real-time transport protocol (RTP) streams (VoIP or IPTV). A breakdown of the different types of traffic is displayed, helping the user quickly identify which ones require further analysis.

To obtain further details on the performance of specific services in the network, the analyzer can drill down to specific voice, data or video streams, identifying the causes of media and signaling impairments in the network.

The RTP view provides a detailed analysis of the performance of voice and video streams in the network. MPEG2 transport streams can be encapsulated over UDP or UDP and RTP. The analyzer automatically identifies RTP streams and performs detailed analysis of parameters such as packet and byte count, packet loss and delay, throughput and percentage of bandwidth.

Media Delivery Index

Within the communications industry, MDI is gaining acceptance for media quality testing over an IP video delivery infrastructure. MDI is an industry standard defined in RFC 4445 and endorsed by the IP Video Quality Alliance. MDI is composed of two parts: the delay factor (DF) and the media loss rate (MLR). These are based on jitter and loss, two concepts that translate directly into networking terms. MDI correlates network impairments with video quality, which is vital for isolating problems and determining their root causes.

In the case of VoIP, R-factor scores and mean opinion score (MOS) are also available. MOS is a measurement of audio quality with scores ranging from 1 to 5 and values below 3.0 indicating poor voice quality. Because voice is a real-time service, it must be delivered with minimal delays and reproduced with a constant bit stream on the egress network or endpoint (150 ms end-to-end delay is a common recommendation).

A view of the MPEG2 transport stream allows network engineers to perform detailed real-time analysis of video streams present in the network (Figure 2). For example, IPTV multicast or VoD unicast streams contain critical information useful in troubleshooting video impairments. Also, ETSI TR 101-290 events can be analyzed with configurable thresholds for reporting. PCR jitter accuracy and errors are also reported to determine synchronization errors. Media delivery index (MDI) analysis allows engineers to determine buffer size issues and lost packets that directly affect the quality of video. Agilent's video MOS degradation function shows the impact of network impairments on video quality and provides an indication of video degradation. All of these events are calculated and presented per stream, including performance analysis per elementary stream. In addition, a viewer is available to visualize the video quality of a specific stream, allowing a direct visual assessment of subscriber QoE.

For video signaling analysis, the video control view keeps track of subscribers changing channels. Whenever this occurs, a series of IGMP *leave* and *join* commands are sent to the network. The J6900A records leaves, joins and zap/response times per subscriber, allowing detailed analysis of QoE.

Conclusion

The triple-play mix of voice, data and video brings with it new levels of complexity that can adversely affect subscriber QoE. The ability to ensure a positive experience can benefit from test solutions that enable end-to-end design, deployment, monitoring and maintenance of triple-play networks. One such solution is the Agilent J6900A triple play analyzer, which addresses network interoperability, IP network performance, voice and video service quality and QoE. Easily operable without advanced expertise or programming skills, it enables engineers to quickly identify QoE-related problems by providing test results for key parameters of IP telephony, IPTV and VoD network performance.

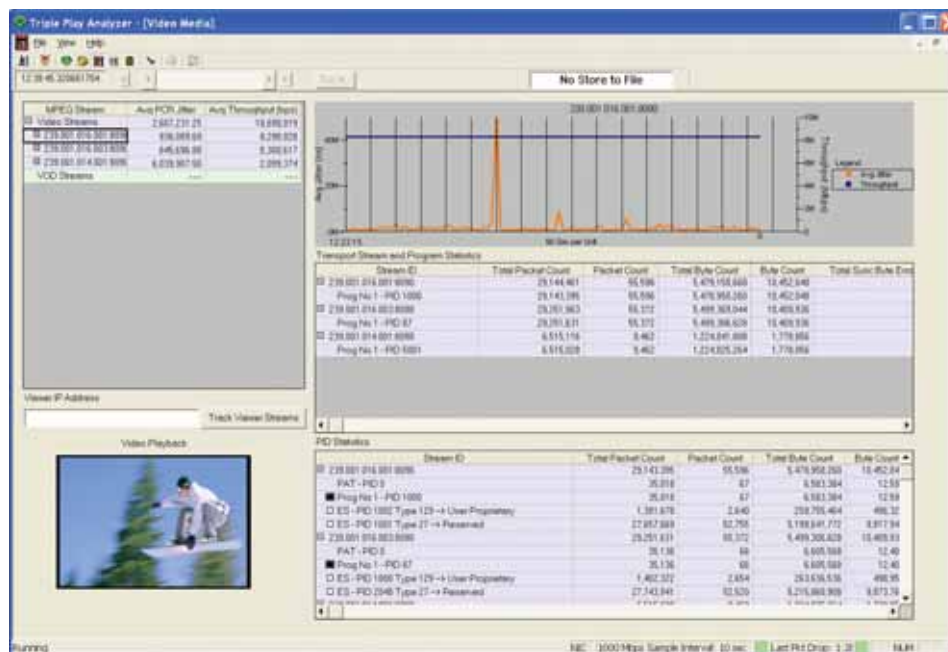


Figure 2. MPEG transport stream analysis

A tall yellow mobile phone tower with a worker on top, standing behind a row of old red telephone booths. The tower is a lattice structure with several antennas and a worker in a red helmet and safety gear on a platform near the top. The telephone booths are red with glass windows and some are damaged. The background is a blue sky with white clouds.

What Next for Mobile Telephony?

Examining the trend
towards high-data-rate
networks

Moray Rumney BSc, C. Eng, MIET
Lead Technologist, Agilent Technologies
moray_rumney@agilent.com

M

Many factors will define the evolution and adoption of commercial wireless technology. From the huge range of possible outcomes, it is useful to consider which factors are most relevant in predicting the future. Figure 1 shows the evolution of wireless since the start of the digital era in the early 1990s.

Much industry speculation and debate exists attempting to predict the next-generation market winners with the focus often being on the peak data rates possible. To take a more complete view, however, other important criteria should also be considered:

- Achievable data densities given the constraints of interference and deployment costs
- The consequences of format proliferation and spectrum fragmentation on system complexity and cost
- Customer-centric issues such as compelling end-user services and Quality of Experience (QoE)

This article will examine the continuing growth in peak data rates and consider implications on achievable data densities, system cost and customer QoE. The issue of interference and the growing gap between peak and average data rates will be considered.

Examining the trend towards higher data rates

Over the last 20 years, mobile wireless systems have evolved from expensive, low-tech niche markets into one of the world's biggest high-tech industries. Subscriber numbers this year will exceed 3 billion — or half the planet — with more to come. In addition to subscriber growth, Table 1 shows a parallel growth in cellular peak data rates of four orders of magnitude.

Table 1. Growth in cellular peak data rates and spectral efficiency

Radio system	Peak data rate	Channel BW	Freq reuse	Spectral efficiency
AMPS	9.6 kbps	30 kHz	7	0.015
GSM	9.6 to 14.4 kbps	200 kHz	4	0.032
GPRS	171 kbps	200 kHz	4	0.07
IS-95C (cdma2000)	307 kbps	1.25 MHz	1	0.25
EDGE	474 kbps	200 kHz	4	0.2
W-CDMA	2 Mbps	5 MHz	1	0.4
1xEV-DO(A)	3.1 Mbps	1.25 MHz	1	2.4
HSDPA	14 Mbps	5 MHz	1	2.8
HSDPA+ 2x2*	42 Mbps	5 MHz	1	8.4
802.16e WiMAX	74.8 Mbps	20 MHz	1	3.7
LTE	100 Mbps	20 MHz	1	5
802.16m 2x2*	160 Mbps	20 MHz	1	8.0
LTE 2x2*	172.8 Mbps	20 MHz	1	8.6
802.16m 4x4*	300 Mbps	20 MHz	1	15.0
LTE 4x4*	326.4 Mbps	20 MHz	1	16.3

* 2x2 and 4x4 = Downlink MIMO (multiple-input/multiple-output)

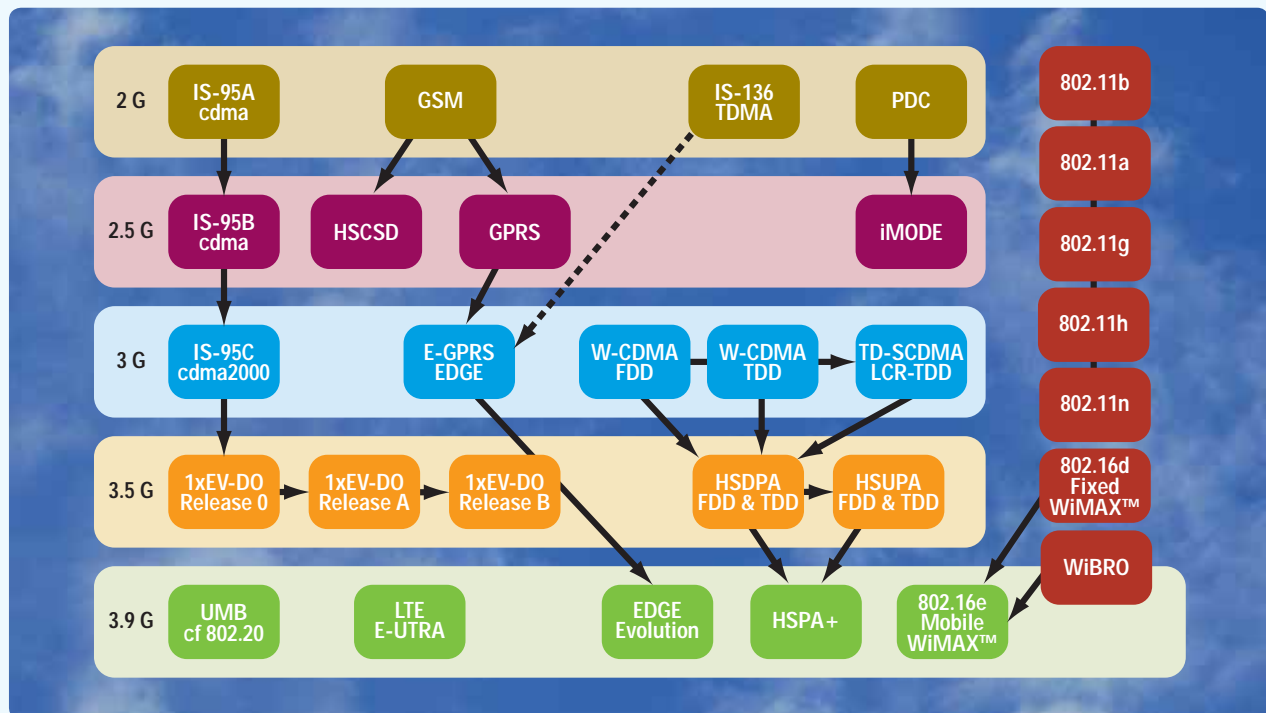


Figure 1. The evolution of wireless showing five competing new systems

At this point, it would not be unreasonable to conclude that Moore's law was predicting this growth in data rates, although with the doubling occurring every 18 months rather than two years. That said, Moore's law is an observation of the semiconductor industry. Although it is very tempting to hope, it is unlikely to be just a matter of time before we are able to download a 1 GByte operating system upgrade in 25 seconds at 326.4 Mbps from a cellular system to our laptop while riding an elevator on the way to a meeting.

To understand the significance of Table 1, we need to shift our attention from Moore's law to the Shannon-Hartley capacity theorem. Dating from the 1940s, the theorem is more fundamental than Moore's law and, like the law of gravity, is not merely an observation or recommendation. The theorem predicts the error-free capacity C of a radio channel as:

$$C = B \times \log_2(1 + \text{SNR}) \text{ where}$$

C = Channel capacity in bits per second
 B = Occupied bandwidth in hertz
SNR = linear signal-to-noise ratio

The capacity of the channel scales linearly with the bandwidth and as a log function of the SNR, indicating an efficiency upper limit with diminishing returns at very high SNR. When cellular systems operate at capacity, the SNR is always dominated by co-channel interference (other users) rather than sensitivity.

Probing the Shannon-Hartley theorem

Techniques such as interference cancellation (IC) and spatial diversity with multi-stream transmission appear to get around the theorem but looking a bit closer this is not strictly true. The potential of IC in cellular systems is due to most noise not being truly Gaussian as assumed by the theorem. If information can be extracted from this "noise" then it is "others' signal" and can be removed, thereby improving capacity. The challenge is in the processing power and advanced algorithms required to track, decode and then remove the dynamic interference from multiple users. This puts a practical and modest upper limit on what can be achieved. For spatial diversity, the theorem still indicates the capacity of each channel and it is the correlation between the channels that would determine the overall improvement possible using multiple-input/multiple-output (MIMO) techniques.

It is essential to point out from Table 1 that the newer radio systems do not themselves deliver ever-higher spectral efficiency; rather, they are designed to take advantage of good radio conditions when they occur. An automotive analogy can help here: Cars can be designed for a wide range of top speeds, but it is only when driving conditions (e.g., road quality and traffic) are good enough that high speeds are possible. When the system gets loaded and traffic slows to a crawl, a V-12 roadster is no better than a three-cylinder compact. In such conditions, the residual advantage of the V-12 is perhaps just looking good while you wait!

Another key point to make is that the throughput figures in Table 1 represent the capacity of an entire cell or cell sector and that the peak rates given must be shared among the active users in the cell. This has a substantial impact on QoE when the system becomes loaded.

Pinpointing the origins of higher data rates

If we take a closer look at the evolution of data rates and spectral efficiency for each system, we discover six technical factors that explain the growth:

- Allocating more time (TDMA duty cycle)
- Allocating more bandwidth
- Improving frequency reuse
- Reducing channel coding protection
- Using higher order modulation
- Taking advantage of spatial diversity (MIMO)

The first two factors increase peak data rates by allocating a wider or longer channel so will neither impact system spectral efficiency nor affect system capacity. For example, a Long-Term Evolution (LTE) 20 MHz channel consumes 800 times the spectral resources of a 200 kHz single-slot GSM channel. This largely accounts for much of the increase in data rates and predicts much higher delivery costs for high-speed services. There is no escape from the reality that high-rate services consume large amounts of spectrum, and usable cellular spectrum is very limited.

The other four factors all represent increases in spectral efficiency that can increase system capacity. However, these methods don't come for free since for them to work there are significant implications for the required SNR and radio-channel propagation conditions, which are not a function of the radio system.

Accounting for interference

Unlike wired communication channels such as copper or fiber which largely isolate signals from each other, electromagnetic propagation in free space knows no boundaries. On first inspection, the Shannon-Hartley theorem predicts that for LTE to deliver 100 Mbps in a single channel would require an SNR of better than 30 dB. This is a crucial point: In a typical environment, how often does the SNR reach such levels?

In the limit case of an isolated cell (e.g., a hotspot), demonstrating peak performance is straightforward and only limited at the cell boundaries when the self-noise of the system becomes dominant. However, when the cells become closer to the point where coverage is continuous, the interference situation is very different. A common measure for system interference is the geometry factor or “G factor” defined as:

$$G = \hat{I}_{or} / (\hat{I}_{or} + I_{oc}) \text{ where}$$

\hat{I}_{or} = received power of desired signal
 I_{oc} = all other co-channel received power

Figure 2 shows the familiar hexagonal cellular pattern and it can be shown that at the boundary of two cells the G factor will on average be no better than -3 dB, and at the boundary of three cells no better than -4.8 dB.

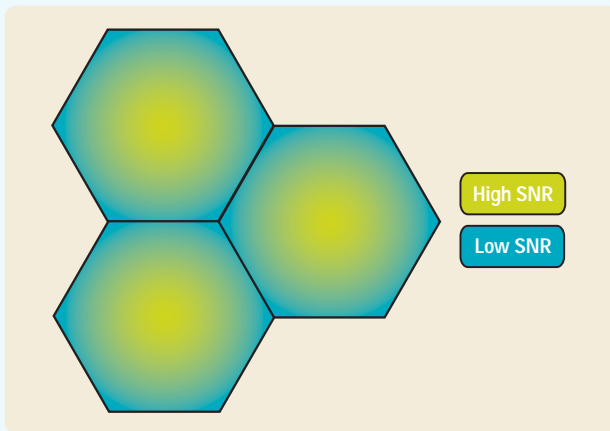


Figure 2. Variation of SNR in a single-frequency cellular system

It is not straightforward to directly relate the SNR in the theorem with the geometry factor and then conclude the capacity of the channel since there are other factors that need to be taken into account — not least the proportion of the transmitted cell power I_{or} allocated to the user and the dynamic effects of channel fading due to mobility.

The principle remains, however, that the potential capacity of the radio channel varies from excellent at the center and degrades significantly at the edges. Older systems such as GSM were designed to work to full specification at the cell edge and the better radio conditions further into the cell were used to reduce uplink and downlink transmission power rather than deliver higher-rate services. Newer systems take advantage of the variation in radio conditions across the cell to opportunistically deliver higher rate services. For example, GSM requires 9 dB SNR at the cell boundary but full-rate EDGE requires 24 dB SNR and so only performs at its peak rate towards the middle of a cell dimensioned for basic GSM. This phenomenon creates islands of high performance cellular in a sea of average performance, with the positions of the islands being defined by proximity to the cell sites.

Examining the distribution of geometry factor

Figure 3 shows the distribution of G factor that would be typical for randomly distributed outdoor users in a major metropolitan area. Of note, 20 percent of users experience a G factor below 0 dB, the 50 percentile point is at 5 dB, and only 10 percent of users experience better than 15 dB. For indoor — particularly at frequencies well above 1 GHz where building penetration loss is significant — conditions degrade and the distribution would move significantly to the left. This is a big concern for QoE given the high proportion of cellular calls that are made indoors. Dedicated indoor networks are the only realistic way round this.

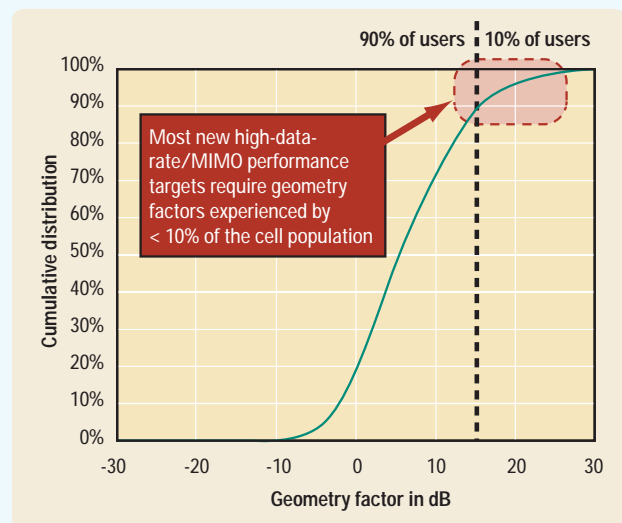


Figure 3. Outdoor geometry factor distribution in a metropolitan area

Comparing average vs. peak spectral efficiency

Figure 4 plots an approximation of the average spectral efficiency for different systems along with the peak efficiency required for operation at their maximum rates. There are several interesting points in this figure. First, it can be seen that the early (low efficiency) systems — AMPS and GSM — were deployed operating at their maximum rates. This was because these systems were designed to operate at their maximum rates at the cell edge. Subsequent systems starting with GPRS employed reduced channel coding then higher-order modulation, which increased the peak user data rate but required a better SNR than was available at the cell edge. Taking advantage of the variation in G factor across the cell is one of the reasons these newer systems show an increase in average efficiency.

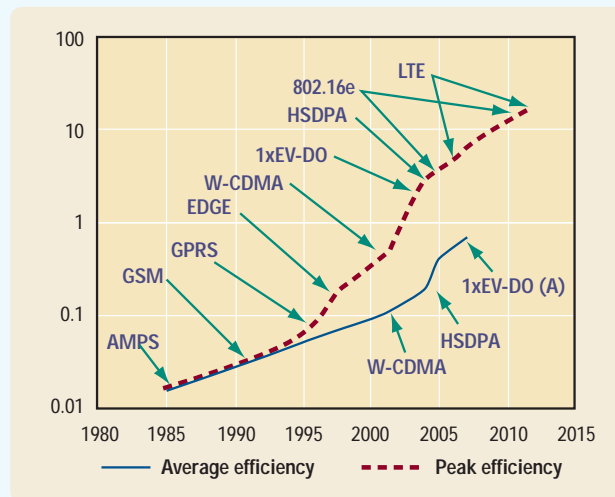


Figure 4. Average versus peak spectral efficiency over time

The other obvious trend is the widening gap between average efficiency and the efficiency required at a system's maximum rate. This is due to new systems specifying performance at very high G factors further into the cell. This has a direct consequence on QoE: G factor distribution is independent of the radio system so as rates rise, a smaller percentage of users can experience the system at its maximum rate. The performance for current HSDPA systems is on the order of 1 to 2 Mbps/sector. Given the recent history of mobile wireless this is a remarkable feat — but with this representing an average normalized spectral efficiency of 0.4 b/s/Hz, the gap to the 5 b/s/Hz peak is large (Table 1). Users close to the cell center should see better performance (provided the backhaul exists); however, the average efficiency — which drives system capacity, QoE and revenue potential — is rising much more slowly over time than the efficiency required to operate at the headline rates.

An HSDPA example from 3GPP TS 25.101¹ will illustrate the relationship between throughput, probability of coverage (G factor) and users/sector. These throughput figures require the advanced features of diversity receiver and equalizer and are for a pedestrian (3 km/h) environment.

Table 2. HSDPA throughput versus probability of coverage (G factor) and users/sector

Power per user	Users/sector	G factor	Approx. coverage (QoE)	Throughput Mbps
-2 dB	1	18 dB	5%	7.638
-2 dB	1	15 dB	7%	6.412
-3 dB	2	10 dB	25%	2.464
-6 dB	4	10 dB	25%	1.619
-3 dB	2	5 dB	50%	1.688
-6 dB	4	5 dB	50%	0.779

Adding closed-loop transmit diversity and MIMO may extract slightly more performance but existing receiver diversity has already gained most of the advantage, especially when line-of-sight exists to the base station (a factor that eliminates any MIMO advantage). Switching to a technology such as 3GPP2's 1xEV-DO or IEEE's WiMAX will change the details of Table 2 but not the substance. Interference is the great leveler that removes most of the performance differences between competing cellular systems. Contrasting the users/sector from Table 2 with the people/sector in dense areas illustrates the difficulty cellular systems face in providing dense high-data-rate networks.

Dimensioning for the average vs. peak

Average performance drives system capacity, revenue potential and QoE. HSDPA today achieves 1 to 2 Mbps per sector and new standards such as Mobile WiMAX, HSPA+, UMB and LTE can improve on this by as much as 4x using techniques such as interference cancellation, OFDM, equalizers and smart antennas including MIMO.

Peak performance mainly drives headlines and also carries the risk of driving down QoE due to the setting of unrealistic expectations. Perhaps of more significance, dimensioning future cellular systems for their peak rates has implications for the cost of terminals and the network. The peak LTE downlink throughput with 2x2 MIMO is 172.8 Mbps.² LTE terminal classes will be introduced which set lower limits, but the impact of the highest targets may influence phone infrastructure, leading to tougher design challenges and increased cost. Dimensioning the network to handle very high rates with reasonable QoE would be extremely

expensive. The two major infrastructure costs are the initial site acquisition and equipment costs plus the ongoing rental and backhaul costs. Capital expenditures and some operating expenditures scale linearly with system capacity, which, for satisfactory QoE, must grow substantially — and demands perhaps a 10 times increase in cell density. In addition, the backhaul costs must scale with the system's peak rate (not the average) which for the next generation represents nearly 100 times what is deployed today.

Matching technology to the problem

Technology should be appropriate to the problem. We could have our mail delivered by helicopter or commute to work using a drag racer, but we don't because transportation has had millennia to evolve and we understand what works best. By comparison the broadband wireless industry is in its infancy and remains in search of its *raison d'être*. Continuing to evolve the current centrally-managed cellular model to deliver peak rates presents many challenges. The physics, politics (site availability) and economics all look problematic. This suggests a bifurcation of the market will occur. Traditional cellular can focus on and optimize the all-important ubiquitous average macro-cell experience, and alternative low-cost approaches will have to be developed to deliver localized high-data-rate solutions much closer to the point of demand.

Designing cellular networks at just above the expected average performance would considerably simplify the cost and challenge of introducing technology that brings new service capabilities and valuable improvements such as reduced latency.

Comparing Wi-Fi and femtocells for high data rates

Today we have significant deployment of private and public wireless access based on IEEE 802.11 (Wi-Fi). These have improved in performance and coverage at a remarkable rate. Unfortunately, though, their simpler technologies and unlicensed operating band are very prone to interference and have become a victim of their own success in some areas. The lack of transmit power control considered essential for cellular is a major issue. Fortunately, with over 600 MHz of spectrum at 2.4 and 5 GHz, Wi-Fi has more room to expand and thus fewer efficiency worries than cellular. An alternative to Wi-Fi is the emerging cellular "home base station" or femtocell. These have been proposed and even standardized but have never taken off.³ Now, there is evidence that the situation may be changing. The two big challenges for femtocells are cost versus Wi-Fi and interference mitigation to protect the licensed cellular network.

Looking at costs, there are aggressive goals to introduce products in the \$300 range based on mobile rather than the more-expensive base station components. Ultimately, sales volumes will define the costs and this should not prevent the concept from taking off. As for interference mitigation, this cuts both ways. On the negative side, femtocells operating in licensed spectrum have much tougher expectations of not interfering with the cellular network than the *ad hoc* Wi-Fi systems operating in unlicensed spectrum. On the positive side, however, femtocells are based on cellular technology that is designed to be spectrally aware and has the potential to control its power and frequency in a more sophisticated way than is possible with current Wi-Fi.

That said, the 802.11 standard continues to develop and be deployed far faster than cellular with the introduction of 802.11n. The headlines for this evolution are almost always about its MIMO capability, which has perhaps not lived up to early expectations. Of more significance, though, especially in demanding enterprise or public environments, is the inclusion of cellular-style access control that prevents the system being brought down by excessive demand. Also, 802.11h has added power control and dynamic frequency selection to allow its use in the 5 GHz band currently occupied by radar.

Looking to the future

The physical and commercial constraints on implementing high-data-rate cellular services must be considered. As with transportation systems where there is a wide mix of vehicle types to match the range of channels, so it will be with wireless. The cellular industry needs to continue to optimize performance for the average user as defined by the statistics of the radio channel and not risk getting distracted by peak performance. Cellular's focus should move from technology towards the development of compelling services with high QoE. The battle for the high-data-rate home and enterprise wireless markets will continue, and whether the winner is based on Wi-Fi or the more advanced femtocells, Agilent is ready to provide the tools the industry needs to design and optimize the right wireless technology for the future.

References

1. 3GPP TS 25.101 v7.8.0 Tables 9.8D3, 9.8D4 and 9.8F3
2. 3GPP TR 25.912 v7.2.0 section 13
3. 3GPP TS 42.056 v4.0.0 GSM Cordless Telephony System

³WiMAX™ and Mobile WiMAX™ are trademarks of the WiMAX Forum.



Exploring the Inner Workings of Tire-Pressure Monitoring Systems

Hock Yew Yeap
Product Marketing Engineer, Agilent Technologies
hock-yew_yeap@agilent.com

Passenger safety is a major focus of all automotive designs, supported by ongoing efforts to continually enhance safety-related features. One such feature is the tire-pressure monitoring system (TPMS), which provides either real-time pressure readings or under-pressure warning indicators to the driver within the comfort of the vehicle cabin.

Studies have shown it is common to find vehicles traveling with under-inflated tires. This condition has unwanted side effects: additional stress on the steering system, accelerated tire wear and decreased fuel economy. Unfortunately, it also has some very sobering consequences: Statistics show that more than 400 fatal and up to 10,000 non-fatal accidents per year are caused by flat tires or blowouts. Twenty percent of flat tires and blowouts are the result of under-inflated tires.

Statistics such as these are one reason the United States enacted legislation requiring all new passenger cars and small trucks with gross vehicle weight (GVW) of less than 10,000 pounds be equipped with TPMS. The main purpose is to ensure better handling and greater safety by giving drivers real-time warnings about lost tire pressure. The gradual phase-in of the new requirements began in October 2005 (20 percent of new vehicles) and culminated on September 1, 2007, when all light vehicles sold in the United States must be equipped with some type of TPMS.

Comparing two approaches

The owner's manual of any recent vehicle includes the recommended tire pressure for the factory-installed tires. The United States legislation sets a threshold of no less than 25 percent deflation from the recommended pressure. Any reading lower than the threshold triggers the TPMS, which will then warn the driver.

Two types of monitoring systems are currently in use: indirect and direct. Indirect systems leverage signals measured by typical antilock braking systems (ABS) that use wheel-speed sensors to regulate ABS operations. Data from those same wheel-speed sensors can be used to compare the rotational speed of each tire; an underinflated tire has a smaller circumference and therefore rolls faster than the other tires. Unfortunately, this method requires a bit of time and distance before the problem becomes apparent. Also, it might not be detected if all four tires have deflated by the same amount and are rotating at the same speed.

In comparison, direct monitoring has proven to be a more accurate and reliable measure of tire pressure. This method uses one base receiver unit that monitors four transmitting pressure sensors — one affixed to each tire. The receiver unit is commonly placed inside the vehicle and drives an indicator on either the dashboard or a separate display. One sensor is mounted inside each tire where it measures pressure and transmits the reading over radio frequency (RF) to the base module. Each transmitter is normally encoded with a unique serial number or code, allowing the base receiver to identify each tire separately.

Looking inside a direct monitoring system

Tire-pressure sensors are made from piezo-resistive materials that pick up pressure variances electrically through a diaphragm that flexes with the pressure level. Sensor data is then electronically processed and encoded before being transmitted over the RF link.

Most transmitters use radio frequencies within the industrial, scientific and medical (ISM) band, typically at 315 MHz, 434 MHz, 868 MHz or 915 MHz. In many cases, the transmitted signal is modulated using either asynchronous-shift keying (ASK) or frequency-shift keying (FSK).

To illustrate the transmitted data, a unique serial number or ID for the pressure sensor is typically 32 bits in length, with the pressure data occupying eight bits or one byte. Depending on the design, the data stream may also include the battery condition and a status stream. In some designs, temperature is measured along with tire pressure and up to one byte of temperature data is included in the data stream.

Many of today's systems send data at 9600 bps using Manchester Code in which digital ones and zeros transition between high and low halfway through each bit period. A 9600-bps baud rate shortens the transmission time, which indirectly reduces interference.

Leveraging existing RF platforms

To reduce part count and vehicle cost, many auto manufacturers try to integrate the TPMS with another RF platform. One example is the remote keyless entry (RKE) system, which is a logical choice for two reasons. First, it is typically used when the vehicle is shut off and parked; the TPMS is in use when the vehicle is running and in motion. Second, the RKE and TPMS systems use the same frequency ranges within the ISM band.

Managing battery life

Batteries are presently the most common way to power direct-measurement sensor units mounted inside tires. Lithium cells are a common choice because they provide long life and reduce the likelihood that the battery will require replacement during the life of the vehicle. The aforementioned short transmission times also contribute to longer battery life.

Two more techniques help extend battery life: keeping transmitter power low and avoiding full-time transmission. Given the short communication distances, low-power transmission is a viable approach. It also is practical and efficient to let the transmitter remain in standby mode, sending data at fixed intervals programmed by the base receiver unit (which also can transmit to the sensor units). Current drain is typically 100 nA in standby mode and 1 to 5 mA when transmitting.

Testing TPMS and other systems

In the United States, more than 7 million passenger cars and 8 million light trucks are sold each year. With typically four tires each, that represents more than 60 million pressure sensors and 15 million base receiver units to be manufactured and tested every year. Faced with such massive volumes, manufacturing organizations are looking for ways to accelerate their time-to-market performance.



Testing such systems requires a broad range of technologies including battery simulators, RF signal analyzers, switching systems and more. Systems such as the Agilent TS-5020 provide a flexible platform that can test a variety of automotive subsystems — TPMS, RKE, supplemental restraints and others (Figure 1). The TS-5020 can be configured with not just instruments but also interfaces, test fixtures and the Agilent TestExec SL software. The result is a solution that adds flexibility, saves time and reduces the cost of testing automotive systems.

Conclusion

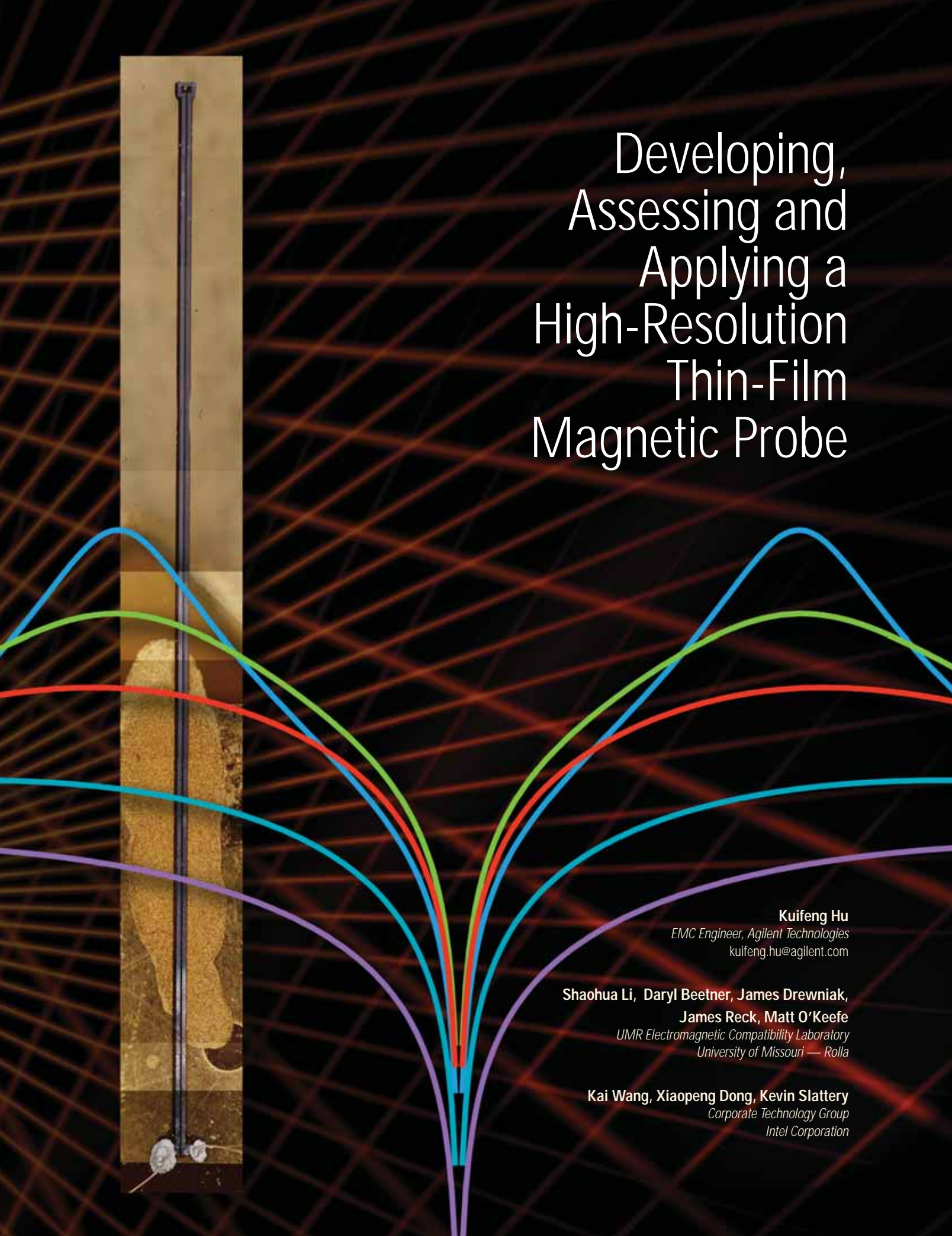
TPMS is one of many systems that make automobiles safer for drivers and passengers — and it became mandatory for all new vehicles of less than 10,000 lbs GVW sold in the United States after September 1, 2007. With a volume of more than 60 million pressure sensors and 15 million base receiver units, manufacturers face technical and time-to-market challenges in the production and testing of such systems. Whether TPMSs rely on battery-powered wireless systems or an emerging class of battery-free designs, flexible test systems capable of characterizing multiple types of automotive systems will help manufacturers meet their cost and delivery goals.

Additional reading

- Agilent application note, *Agilent TS-5020 Tire Pressure Monitoring System*, publication 5989-5736EN, available online from www.agilent.com
- Agilent application note, *Agilent TS-5020 Automotive Functional Test System*, publication 5989-5460EN, available online from www.agilent.com
- Agilent application note, *Testing Remote Keyless Entry using the Agilent TS-5020*, publication 5968-6080E, available online from www.agilent.com
- Agilent application note, *Testing Supplemental Restraint Systems using the Agilent TS-5020*, publication 5968-6356E, available online from www.agilent.com



Figure 1. An Agilent TS-5020 configured for TPMS testing



Developing, Assessing and Applying a High-Resolution Thin-Film Magnetic Probe

Kuifeng Hu

*EMC Engineer, Agilent Technologies
kuifeng.hu@agilent.com*

Shaohua Li, Daryl Beetner, James Drewniak,

James Reck, Matt O'Keefe

*UMR Electromagnetic Compatibility Laboratory
University of Missouri — Rolla*

Kai Wang, Xiaopeng Dong, Kevin Slattery

*Corporate Technology Group
Intel Corporation*

E

EMI compliance is becoming more and more challenging as clocks and data transmission rates shift to ever-higher speeds. The increasing switching currents presented on integrated circuit (IC) power grids and input/output (I/O) ports are very often the ultimate cause of both signal integrity issues and EMI compliance failures. Measurement of those high-frequency currents is therefore important. Accurately measured currents could be used in many important ways:

- Compare electromagnetic characteristics of ICs¹
- Distinguish inductive or capacitive coupling mechanisms²
- Estimate power-plane ground bounce³
- Predict far-field radiation⁴
- Optimize package pin assignment⁵
- Validate simulation results

Unfortunately, it can be especially difficult to make meaningful measurements of these high-frequency noise currents on an IC. Pinpointing the surface currents depends on ultra-fine spatial resolution, excellent electrical field rejection and the ability to extract stable relative phase at the harmonic frequencies.

This article presents the development, characterization and application of a high-resolution thin-film magnetic-field probe. Probe diameter ranged from 5 μm to 100 μm . The 100- μm probe exhibits a 250- μm improvement in spatial resolution compared to a conventional loop probe, measured at a height of 250 μm over differential traces with a 118- μm spacing. Electric field rejection was improved using shielding and a 180-degree hybrid junction to separate common-mode (electric field) and differential-mode (primarily magnetic field) coupling. A network analyzer with narrowband filtering was used to detect the relatively weak signal from the probe and to allow detection of phase information. An application of the probe shows how it can be used to identify the magnitude and phase of magnetic fields produced by currents in very closely spaced IC package pins.

Designing the probe

The electromagnetic receiving characteristics of the probe may be realistically derived by assuming quasi-static field conditions, since the probe is electrically small even to several gigahertz. Ideally, then, the probe's received power is a linear function of only one field component and the received power is an indication of that field's strength. For example,

$$P_{probe} = C_y(f)H_y$$

where P_{probe} is the received power, $C_y(f)$ is the frequency-dependent coupling coefficient between the y-directed magnetic field and the probe and H_y is the magnetic field in the y-direction. The coupling coefficient can be obtained by either measurement or numerical calculations from a known probe structure. Numerical models can be used, but care is required since not all conditions seen in the test environment may be captured in the simulations. Measurement of C_y requires that H_y is well controlled and known while assuming the coupling from other field components is minimal. In that case, $C_y(f)$ can be calculated from the measured received power as

$$C_y(f) = \frac{P_{probe}}{H_y}$$

In reality, however, negligible coupling from other field components cannot be guaranteed. If the probe is not designed to minimize other field components, the received power will be a function of multiple variables, for example,

$$P_{probe} = C_z(f)E_z + C_y(f)H_y$$

where E_z and $C_z(f)$ are the z-directed electrical field and the associated coupling coefficient. The measured power can not be used to interpret any single field component unless additional measurements are made. A good design should minimize coupling from all fields except the one of interest.

The unwanted field component coupling can be minimized using a balanced, shielded structure as shown in Figure 1. The inner conductors of two coaxial cables are connected at the tip to form a loop. The received power is measured at the two output ports, which consist of two orthogonal modes. The differential mode output is associated with the magnetic field and the common mode output is associated with the electric field. A shield underneath the inner loop helps to minimize electric field coupling. The shield is gapped to prevent interference with the magnetic field measurement.

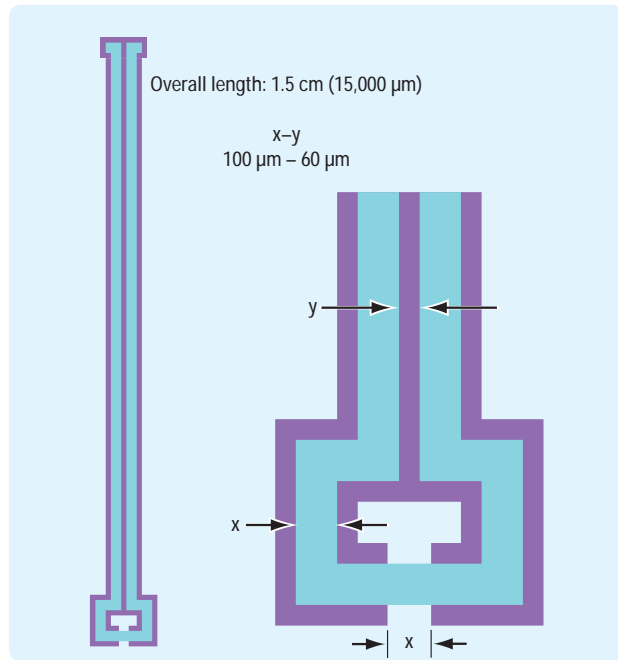


Figure 1. Layout of the thin-film probe

Fabricating the probe

The probe was constructed using a series of thin-film photolithography processes.^{6,7} A thin layer of silver was deposited on a silicon base and then was etched to form the traces and loop that constitute the main part of the probe. The traces were covered with an insulating material, SU-8, which is commonly used as part of many specialty photolithography processes. An additional layer of silver was patterned on top of the SU-8 to form a shield.

The wafer was diced to separate individual probes. A single die including a probe was then washed in a chemical bath to separate the silver and SU-8 from the silicon base, thus forming a probe from the shield, SU-8, and traces, with the SU-8 acting as an insulator between the two metal layers. Removing the probe from the silicon creates a probe that is flexible enough to

temporarily deform after unintentional contact with the device under test (DUT) while still maintaining structural integrity. Under these conditions, silicon would be too brittle and has the added drawback that it is difficult to cut the silicon in such a way to allow the probe to be placed very close (closer than the diameter of the probe) to the DUT.

After construction, the thin-film probes were bonded to a pre-fabricated printed circuit board (PCB) that connects the probe to the test equipment. Pictures of the probe connections and of the PCB are shown in Figure 2. After cleaning, the probe shield was attached to the ground plane of the PCB using an electrically conductive epoxy. Following a complete cure of the ground plane-epoxy connection, bonding pads on the probe traces were attached to matching bonding pads on the PCB using gold wire. The gold wire was attached by hand using an electrically conductive epoxy and a microscope. Optical micrographs of the final probe assembly are shown in Figure 3.

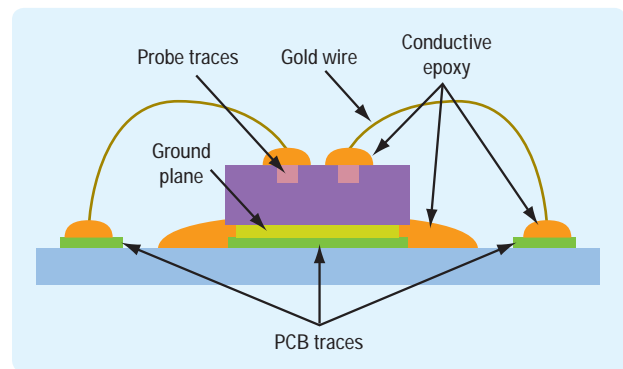


Figure 2. Cross section of the bonded probe

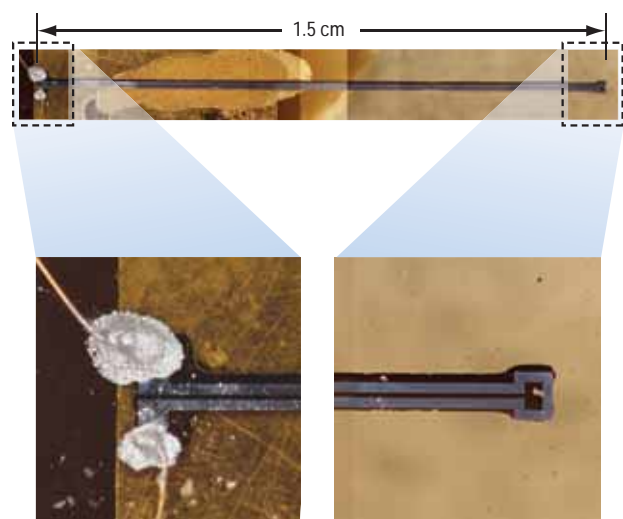


Figure 3. Optical micrographs of the 100- μ m probe: full length (top); a magnified view of the wire bonds (lower left); and a closeup of the probe tip (lower right)

Characterizing the probe

Five different probes were fabricated with trace widths ranging from 100 μm to 5 μm and line spacing ranging from 60 μm to 5 μm , respectively. The discussion included below describes testing of a probe with 100- μm trace width and a 60- μm line spacing.

The measurement setup

The electrical characteristics of the probe were measured using the setup shown in Figure 4. An AMP 96341 40 dB hybrid was used to help separate electric- and magnetic-field coupling. A differential-mode current is created on the two probe traces when a magnetic field couples to the probe through the loop-tip. Electric-field coupling primarily produces a common-mode current. The hybrid was connected to better measure the differential current produced by the magnetic field. The hybrid was designed to work from 2 MHz to 2 GHz. To improve sensitivity, low-noise amplifiers were inserted between the hybrid and the probe.

The frequency response of the probe was measured in three steps. The first step was to measure the response of the hybrid and low-noise amplifiers for de-embedding purposes, as shown in block one of Figure 4. An HP 8720ES four-port network analyzer was used to measure the single-ended three-port S-parameters from ports C1, C2 and D as indicated in the figure. These measurements were then transformed into mixed-mode S-parameters.⁸ A 20 dB attenuator was used at the output of the amplifier to prevent overloading of the network analyzer inputs.

In the second step, a two-port short-open-load-through calibration was made at ports T and D, as shown in Figure 4.

The response of the probe was measured in the third step. The 50 Ω trace was connected to the network analyzer through a 10 dB attenuator to reduce mismatch. The input power of the network analyzer was set to 10 dBm and the resolution bandwidth was reduced to 100 Hz to achieve a low noise floor and allow better measurements at low frequencies. The trace was terminated with a 50 Ω load at port T. The thin-film probe was placed 250 μm above the trace. The frequency response of the probe was calculated by combining the results from steps 1 through 3. Figure 5 shows the frequency response of the 100 μm thin-film probe. The data shows a linear frequency response up to 600 MHz with a slope of 20 dB/decade and a usable frequency range up to 2 GHz (the limit of the hybrid used in this experiment). A comparison of the frequency response from the 180-degree reversed position indicates the coupled energy is mainly from the magnetic field.

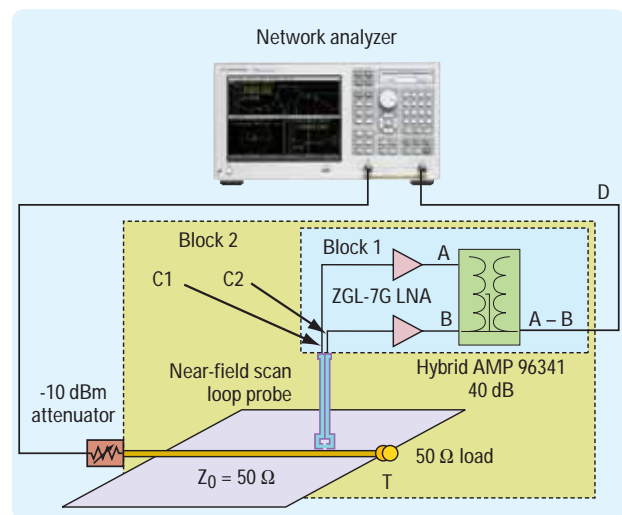
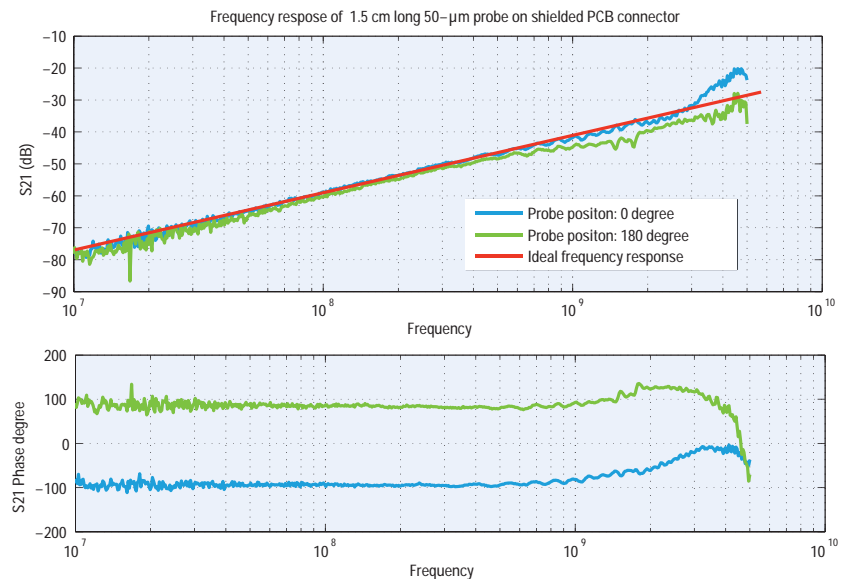


Figure 4. The measurement setup

Figure 5. Measured frequency response magnitude (top) and phase (bottom)



Assessing spatial resolution

The spatial resolution of the probe, relative to a typical loop probe, was determined by scanning the probe across a pair of differential traces. The reference probe, shown in Figure 6, has a loop area of approximately 1 mm². Ideally, the measurement will show a strong, narrow peak in the magnetic field over each trace that reduces quickly to zero between the traces. The width of the peak over the traces and the null between them is an indication of spatial resolution.

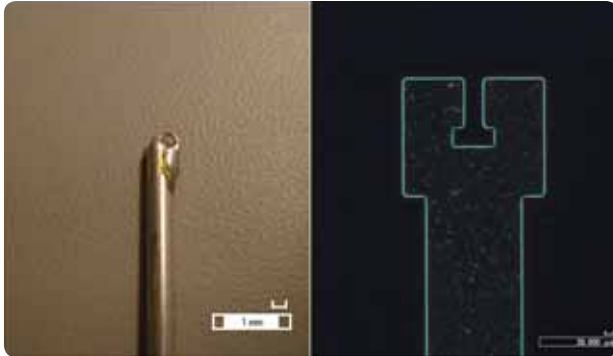


Figure 6. The thin-film probe and a simple loop probe

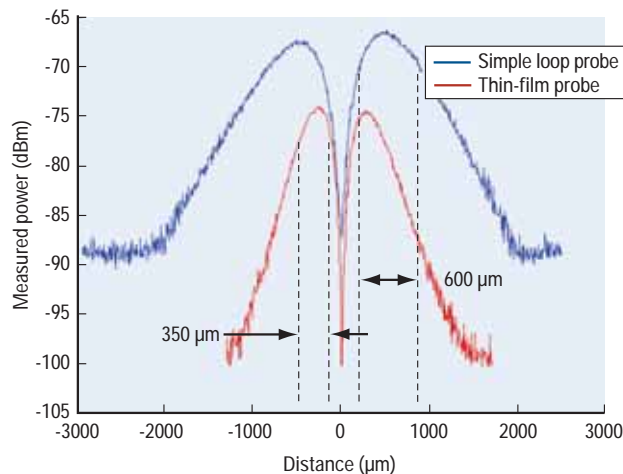


Figure 7. Comparison of the spatial resolution of the thin-film probe and of a simple loop probe

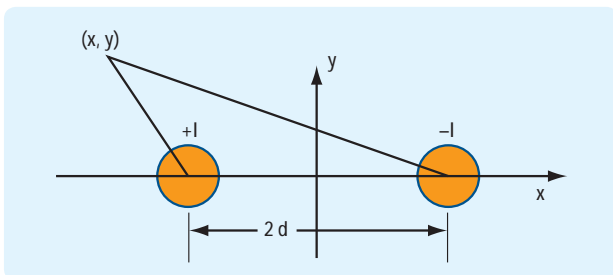


Figure 8. Model for the magnetic field produced by a differential pair

The thin-film probe and the conventional loop probe were scanned across the differential trace at a height of 250 μm. The measured signal power is shown in Figure 7. The thin-film probe has a 3 dB decrease over 350 μm, which is 250 μm less than the conventional loop probe.

The spatial resolution found in Figure 7 is a function of both the probe size as well as the height above the traces. Consider the differential traces shown in Figure 8. The position of the loop is indicated at coordinates (x, y). When the plane of the loop is perpendicular to the ground plane and parallel to the longitudinal axis of the trace (as indicated in Figure 9), only the x component of the magnetic field contributes to the magnetic flux through the loop. The magnetic flux is given by:

$$B_x = \frac{\mu_0 I}{2\pi d} \left(\frac{y/d}{((x/d - 1)^2 + (y/d)^2)} - \frac{y/d}{((x/d + 1)^2 + (y/d)^2)} \right)$$

The magnitude of the field is determined both by a ratio of the height of the probe to trace separation and the ratio of the horizontal position (x-direction) to trace separation. The effect is illustrated in Figure 10.

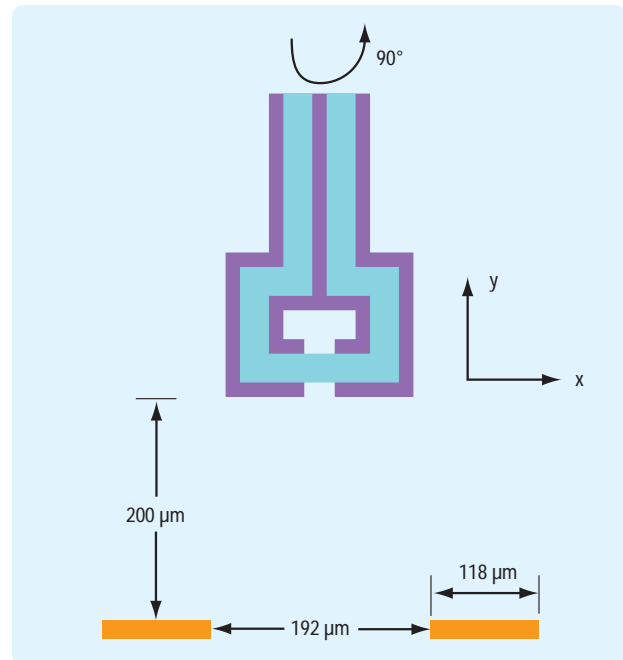


Figure 9. Measurement of differential traces

Examining field separation

The ability of the probe and associated measurement setup to separate the magnetic from the electric field was examined by scanning a 7 cm long microstrip trace that was shorted at one end to create a 900 MHz standing wave. Figure 11 shows the magnitude and phase of the magnetic field over the trace as given by simulation and as measured by the probe. For a pure standing wave, the voltage should reach a maximum at position $x = 40$ mm and should reach a minimum at $x = 10$ mm and $x = 70$ mm.

The current is a maximum at $x = 70$ mm and $x = 10$ mm and should be zero at $x = 40$ mm. While the measurement at $x = 40$ mm (when E is maximum and H is minimum) is not zero, it is about 25 dB lower than at $x = 10$ mm, illustrating that the probe predominately measures the magnetic field and not the electric field. The phase measurement further confirms this contention, since its value shifts by 180 degrees at the location of a current maximum.

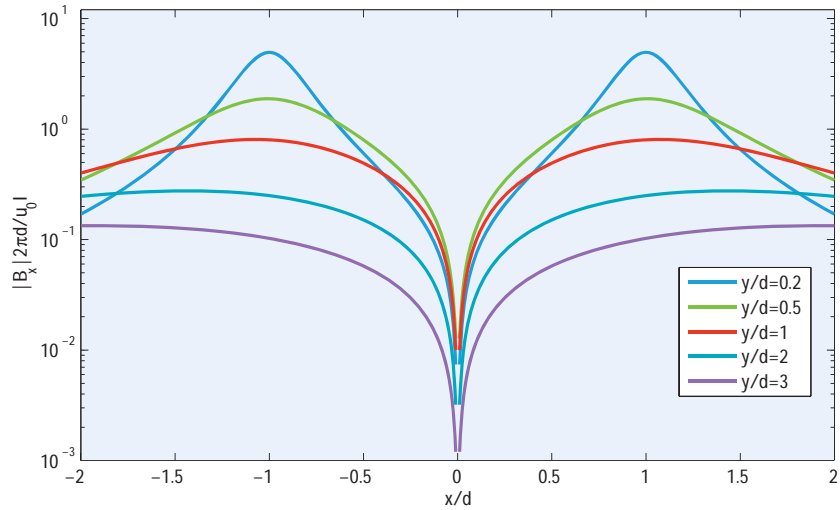


Figure 10. Normalized x component of magnetic field distribution over a pair of differential traces

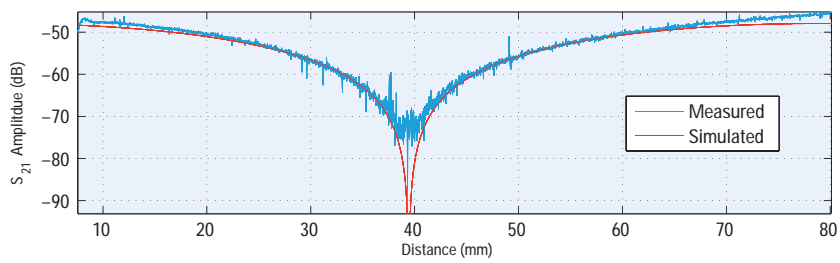
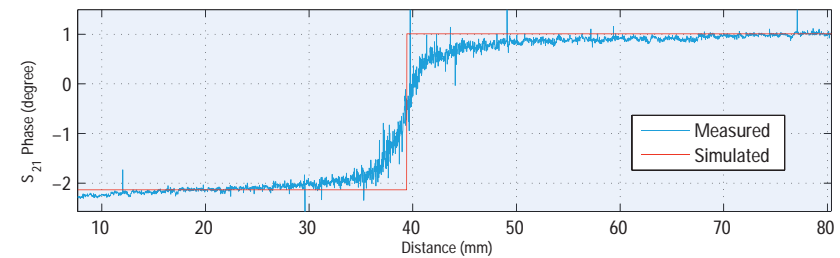


Figure 11. Measured and simulated power and phase from the thin-film probe over a shorted microstrip trace at 900 MHz. The simulation (red line) shows the performance of an ideal magnetic-field probe.



Measuring high-frequency current phase

The thin-film probe was used to measure the magnetic field distribution over the pins of an automotive microcontroller. The microcontroller was in a QFP 100-pin package with closely-spaced pins. Measurements were made at 96 MHz, the second harmonic of the 48 MHz clock. Traditionally, phase is measured using an oscilloscope, where signals are measured in the time domain relative to a known signal (such as the microcontroller clock) and then converted to the frequency domain. A side effect of making the probe small is a decrease in sensitivity. For this reason, the traditional broadband phase extraction method is not effective for the thin-film probe. To overcome this problem, a narrowband measurement setup utilizing a synchronized clock and a network analyzer was developed.

The measurement setup is shown in Figure 12. The microcontroller's clock originates from a high-precision clock generator. The network analyzer is set to the tuned-receiver mode, in which the internal reference clock is replaced by the external synchronized signal generator. The signal generator and the center frequency of the network analyzer are set to the same harmonic frequency, 96 MHz. S_{11} was measured for both magnitude and phase. In this case, phase is given relative to the microcontroller clock. The magnitude and phase of the magnetic fields over the 100 pins is shown in Figure 13. The result shows that the current on the V_{dd} and V_{ss} pins are 180 degrees out of

phase as expected, with the highest current on V_{dd} pins 12, 41, 67 and 92. The return current is on V_{ss} pins 9, 13, 21, 42, 51, 66, 84 and 93. The currents on adjacent V_{dd} pins and the V_{ss} pins do have different amplitudes, possibly causing an unbalanced current across the package. Such unbalanced currents have been associated with higher TEM cell emissions.²

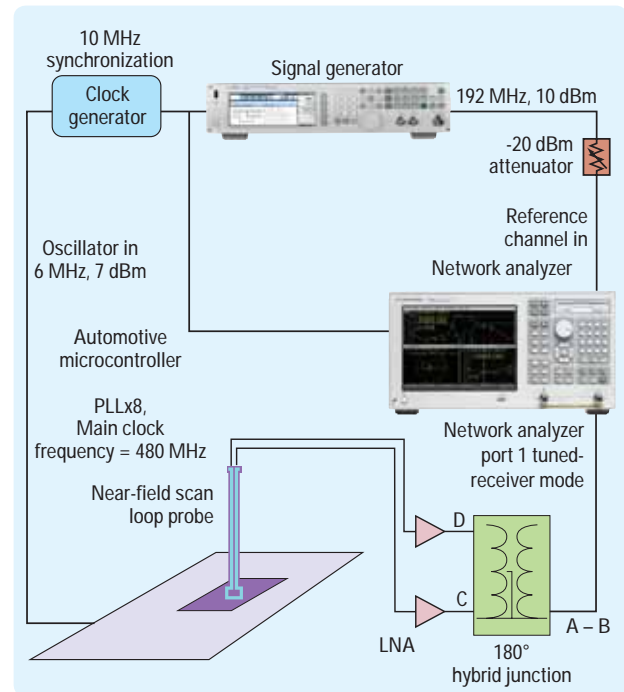


Figure 12. Setup for measuring magnitude and phase of package-pin currents

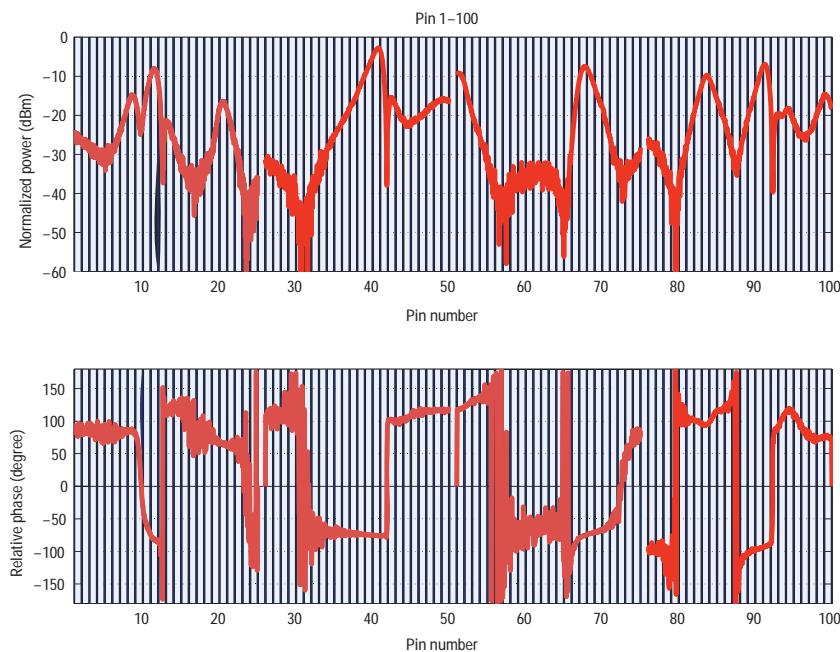


Figure 13. Magnitude and phase distribution of magnetic fields over package pins, measured at the second harmonic of the clock

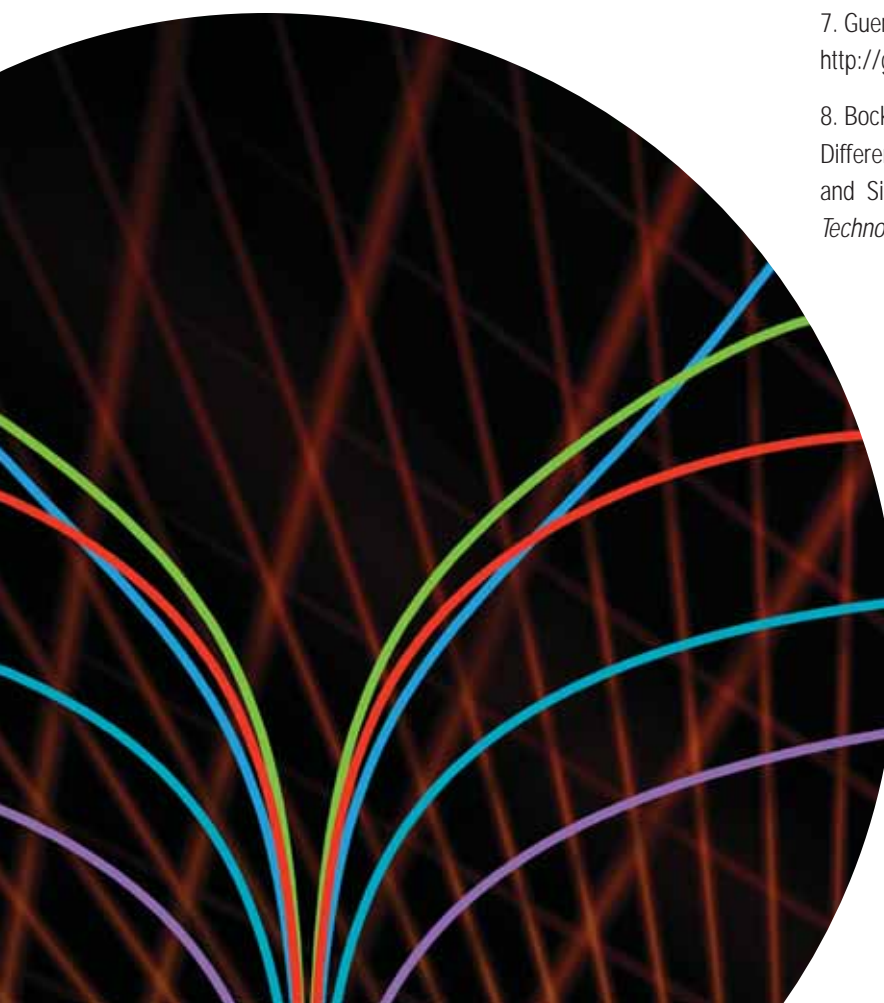
Conclusion

EMI compliance becomes more challenging as clocks and data transmission rates keep moving to ever-higher speeds. The increasing switching currents presented on IC power grids and I/O ports are very often the ultimate cause of both signal integrity issues and EMI compliance failures. It can be difficult to make meaningful measurements of high-frequency noise currents on an IC. Pinpointing the surface currents depends on ultra-fine spatial resolution, excellent electrical field rejection and the ability to extract stable relative phase at the harmonic frequencies.

Creating a probe with a balanced, shielded structure minimized the effects of unwanted field component coupling. In testing, the thin-film probe provided much higher resolution than conventional probes and measurements showed good separation between electric- and magnetic-field coupling. Measurement of the magnetic field was improved using a 40 dB hybrid. The probe demonstrated good response up to a 2 GHz, the limit of the working range of the hybrid. Greater range is expected in the future with modifications to the probe and its bonding structure as well as the measurement technique. The probe can measure phase as well as the magnitude of magnetic fields using a synchronized, high-resolution clock and a network analyzer.

References

1. Electromagnetic Compatibility Measurement Procedures for Integrated Circuits: Integrated Circuit Radiated Emissions Diagnostic Procedure, 150 kHz to 1000 MHz, Magnetic Field Loop Probe. *AE-J* 1752/2, March 1995.
2. Hu, K., Weng, H., Beetner, D., Pommerenke, D., Drewniak, J., Lavery, K. and Whiles, J. 2006. Application of Chip-Level EMC in Automotive Product Design. *Proceedings of the IEEE Symposium on Electromagnetic Compatibility*, Volume 3, August 2006: 842-848.
3. Dhia, B. S., Ramdani M., Sicard E., 2005. *Electromagnetic Compatibility of Integrated Circuits: Techniques for low emission and susceptibility*, Springer, 2005, ISBN-13: 978-0387266008.
4. Weng, H., Beetner, D.G., DuBroff, R.E. and Shi, J. 2005. Estimation of Current from Near-field Measurement. *Proceedings of the IEEE Symposium on Electromagnetic Compatibility*, Volume 1, August 2005: 222-227.
5. Hu, K. 2007. *Integrated Circuits Switching Current Modeling, Measurement and Power Distribution Network Optimization*. Ph.D. dissertation, University of Missouri-Rolla, April 2007.
6. Reck, J., Hu, K., Li, S., O'Keefe, M., Drewniak, J., Beetner, D., et.al. Unpublished. *Fabrication of Two-Layer Thin Film Magnetic Field Micro-Probes on Freestanding SU-8 Photoepoxy*.
7. Guerin, L.J. *The SU-8 Homepage*. <http://geocities.com/guerinlj/>
8. Bockelman, D. E. and Eisenstadt, W. R. 1995. Combined Differential and Common-Mode Scattering Parameters: Theory and Simulation. *IEEE Transactions on Microwave Theory and Technology*, Volume 43, July 1995: 1530-1539.





Making Accurate Settling-Time Measurements Using a Vector Network Analyzer

Daniel Gunyan

R&D Engineer, Agilent Technologies
daniel.gunyan@agilent.com

W

When amplifiers and switches are turned on, the output signal rises then settles. Measurements usually focus on rise time, which most device manufacturers will specify. In many cases, however, settling time is at least equally important and is often even more so since settling time is usually much slower than rise time. The faster an electronic circuit will settle, the faster communication can begin through the circuit. For example, faster switching increases measurement throughput, which reduces the cost of testing. It also boosts communication throughput, potentially increasing profit for a service provider.

Accurate measurements of settling time provide greater assurance that a device can meet customer requirements for fast switching. As an example, it may be required that the insertion loss of a switch settle to within 0.01 dB of its final value within 350 μ s. Dependable measurements will help the switch manufacturer ensure that its product can meet such a requirement. Better measurements also can enable streamlined device qualification as well as improved system margins and yields for the end user.

Practitioners use a variety of instruments and techniques to measure settling time. One common method requires an oscilloscope and a pulse generator. Two less common — but more accurate — approaches utilize a vector network analyzer (VNA). This article describes these three approaches and gives measurement examples using the VNA-based methods.

Measuring settling time with an oscilloscope

Using an oscilloscope and pulse generator, a DC voltage is applied to the input of the switch and a control pulse is used to close the switch (Figure 1). The scope input is applied to the output of the switch and is triggered by the control pulse. The settling time can be ascertained to within a specified range, usually in millivolts. This method has one key advantage: Rise time can be accurately measured if the scope has sufficient bandwidth.

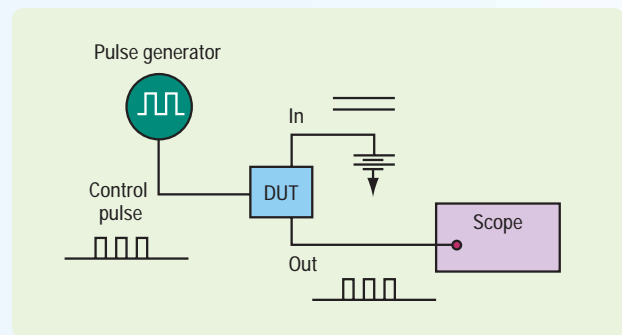


Figure 1. Example measurement setup for oscilloscope method

Unfortunately, this simple setup has three important shortcomings. First, it will not work with devices that have DC blocking on the input or output. Second, it cannot easily measure the frequency response of the device or account for mismatches and losses in the measurement path. Finally, measurement accuracy may be too low for many applications.

The DC-blocking issue can be alleviated by using a radio frequency (RF) input instead of a DC input. Even so, this method is hampered by issues such as scope frequency response, sampling rate, memory depth and envelope processing (settling-time information is contained in the envelope of the RF signal). Each of these issues can be addressed by performing settling-time measurements using a VNA.

Using a VNA with CW time sweep — the wideband method

As shown in Figure 2, the second method uses a VNA and a pulse generator, with the VNA set to a continuous wave (CW) time sweep. With this configuration, measurement resolution and accuracy are usually much greater than is possible with an oscilloscope, and the device is measured under RF stimulus. Calibrating the analyzer to the device ports removes the effects of loss and mismatch in the measurement system for a more accurate measurement.

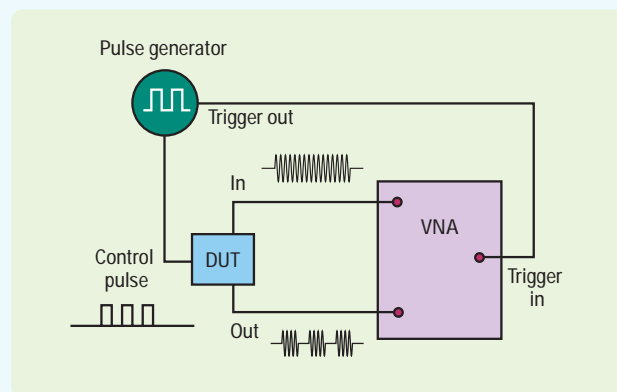


Figure 2. Example measurement setup for CW time-sweep (wideband) method

Averaging can be used to reduce measurement noise, though this is limited by measurement drift of the VNA. If averaging is used, it is necessary to trigger the VNA sweep on the control pulse. This can be done using the hardware trigger input usually found on the back panel of advanced VNAs.¹ If triggering is not available, the sweep time can be adjusted to double the period of the control pulse. This will assure that at least one full pulse is measured somewhere within the sweep. In this case, averaging will not work because multiple sweeps will not be aligned.

This setup has three key steps:

1. Determine the necessary sweep time and time-axis resolution
2. Select IF bandwidth, number of points, pulse width and pulse repetition frequency settings that meet the requirements of Step 1
3. Average to achieve the desired amplitude resolution

While the CW time-sweep approach can be very accurate, it has an important drawback: Minimum time resolution is limited by the maximum IF bandwidth. If either the sweep time or time-axis resolution at the maximum IF bandwidth is not sufficient to capture the settling time, then another approach must be used.

Applying pulsed-profile S-parameter measurements — the narrowband method

The third approach is shown in Figure 3. The hardware setup is nearly the same as the CW time sweep; however, the measurement method is completely different, using an approach similar to the pulsed-profile S-parameter measurements often applied when testing radar components.

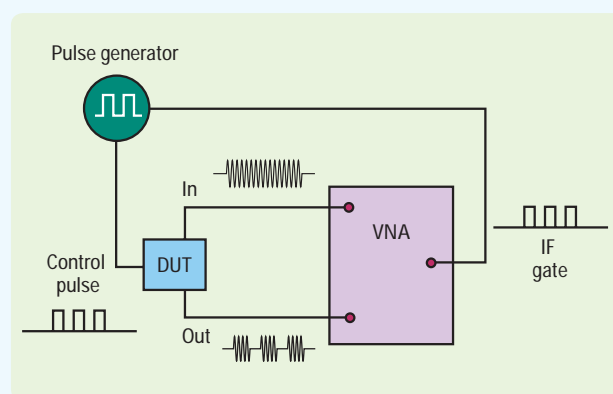


Figure 3. Example measurement setup for pulsed profile S-parameter (narrowband) method

As before, the input is a CW signal and the switching action generates a pulsed RF output. A pulsed-profile measurement filters and gates the IF outputs of the VNA receivers such that only a portion of the pulsed signal is measured. The gating window is then shifted sequentially in time to generate a pulsed profile. (Please see Reference 2 for a more detailed discussion of the theory behind the narrowband method.²)

This approach has three essential steps:

1. Determine the necessary sweep time and time-axis resolution
2. Select pulse width, pulse repetition frequency, IF gate width and number of points to satisfy the requirements of Step 1
3. Set the IF bandwidth and averaging to achieve the desired amplitude resolution

It is important to note that a tradeoff exists between the time-axis resolution and the accuracy of the measurement. Better time-axis resolution can be achieved by narrowing the IF gates; however, a narrow gate admits less energy into the VNA IF data acquisition circuitry, resulting in more measurement noise. A typical compromise for the IF gate-width setting is a 5 to 15 percent duty cycle, though at this setting the time-axis resolution is usually too coarse for rise-time measurements. Averaging can be performed on measured datasets to reduce measurement noise. The minimum possible time-axis resolution is determined by the minimum width of the IF gate switching circuitry (typically tens of nanoseconds).

Determining measurement accuracy

With so many variables in the measurement, it is often difficult to calculate accuracy. Fortunately, when measuring settling time, only the relative amplitude accuracy between the final value and a specified difference from the final value is important. Errors in the time scale are typically very small and need not be considered. Because only the relative amplitude accuracy is important, the measurement is dominated by trace noise, which is simple to measure. In contrast, absolute measurement accuracy depends on calibration quality (not discussed here).³

A simple way to test the trace noise on, for example, an Agilent PNA Series microwave network analyzer is to set up the system for the measurement and close the switch (or turn on the device). Then, set up a CW time sweep for the desired parameter and turn on the trace statistics function. This capability will provide the peak noise and standard deviation, which can be used to determine if the measurement can achieve the desired relative accuracy. If the trace noise is not acceptable, parameters such as IF bandwidth, averaging or IF gate width can be adjusted until the trace noise is within acceptable limits for the measurement. Using this simple method, amplitude noise can be less than 0.001 dB, allowing settling time measurements at this resolution.

A note on settling-time calculations

Settling time can be determined from the measurement using manual and automated methods. The manual approach relies on a visual confirmation that the signal has settled. This typically requires 10 to 15 measurement points to determine whether the device has settled. Next, a marker is placed in the settled area and a second marker is moved back in time until the value reaches the specified settling difference. The readout of the second marker provides the settling time of the switch.

This technique can be automated by transferring the trace data to a program that performs the same procedure. However, determining whether or not the switch has settled is often easier to do visually than programmatically. One useful approach is a smoothed derivative (e.g., derivative of the moving average) of the settling measurement: If the derivative reaches zero, it usually means the switch has settled. Some devices, however, may have a settling plateau, giving a false indication that the switch has settled. In such cases, prior knowledge of this behavior must be taken into account when determining if the measurement has actually settled.

In order to successfully determine the settling time, the peak-to-peak trace noise should be less than the settling time criteria. For example, if 0.01 dB settling time is to be measured, the peak-to-peak trace noise also should be kept below 0.01 dB — ideally two to 10 times less.

Settling time of return-loss measurements can be different since very low signal levels are typically being measured. Therefore, rather than measuring a very small deviation from a very small final value, it is usually more appropriate to measure the time it takes for the return loss to settle below a desired value.

Comparing measurement examples

Two packaged RF GaAs FET switches and one pulsed GSM amplifier were measured to show examples of settling time measurements. In these examples, an Agilent N5242A PNA-X microwave network analyzer was used to measure the settling time and an Agilent 81110A pulse pattern generator was used for the control pulse and PNA hardware trigger (the PNA-X also has internal pulse generators available). Calibrations were performed using a coaxial cal kit.

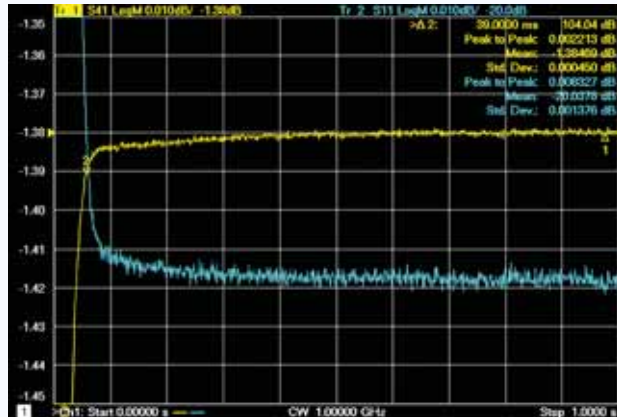


Figure 4. Settling time of switch using CW time-sweep method, showing insertion loss (yellow) and input return loss (blue)

The CW time-sweep method was used because the first switch has a 0.01 dB settling time on the order of tens of milliseconds. Figure 4 shows the settling-time measurement of insertion loss and input return loss. Figure 5a shows the resulting measurements of insertion loss settling time at four different RF frequencies. To measure the different frequencies, the initial setup was copied to three subsequent channels and the CW frequencies modified in each new channel. Note that the switch still seems to be settling even near the end of the sweep. A longer time sweep was used to investigate this, and 0.001 dB settling times greater than one second were measured as shown in Figure 5b. Surprisingly, a significant difference is seen at the selected RF frequencies. This behavior would not have been discovered using the scope method and a DC input.

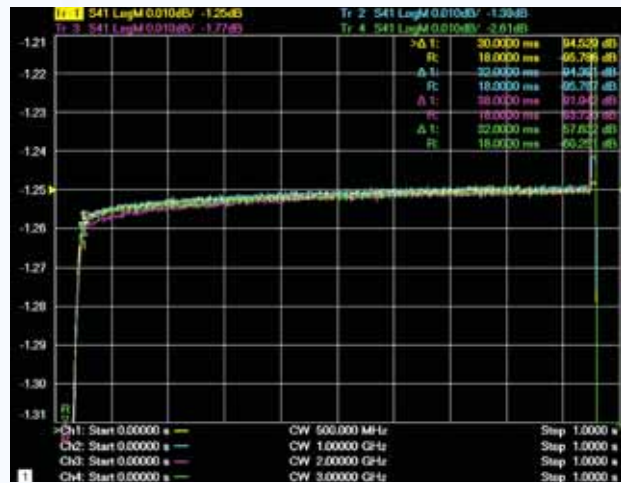


Figure 5a. 0.01 dB settling time of switch using CW time-sweep method at four different RF frequencies

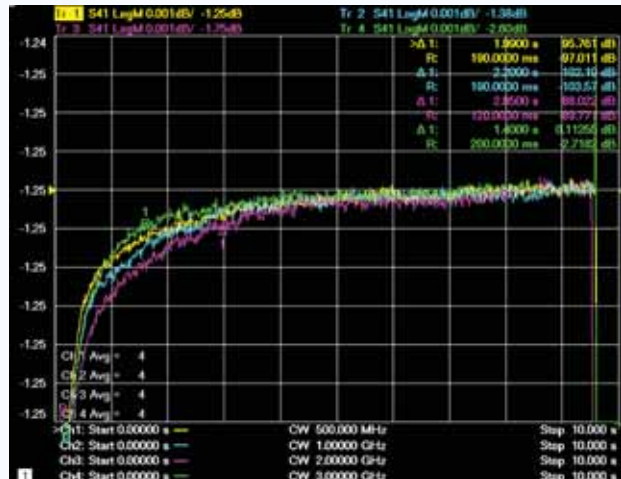


Figure 5b. 0.001 dB settling time of switch using CW time-sweep method at four different RF frequencies

The second switch has a 0.01 dB settling time on the order of hundreds of microseconds. Although the PNA-X is capable of performing this measurement in the CW time-sweep mode, the pulsed profile S-parameter method was used for illustration (Figure 6).

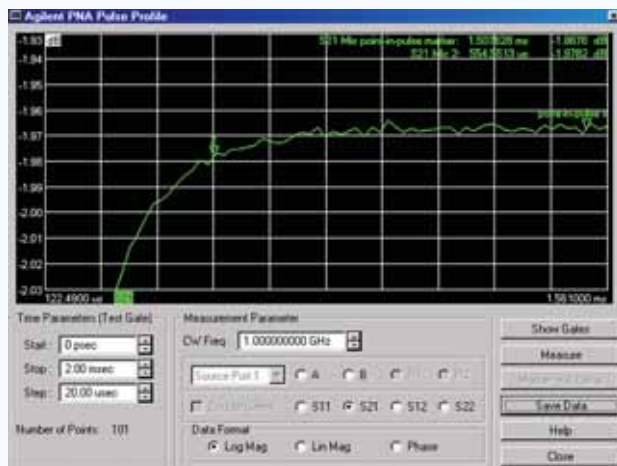


Figure 6. 0.01 dB settling time of switch using pulsed-profile S-parameter measurement

The GSM amplifier never settles to a final value within the measured time slot. Thus, instead of using the deviation from the final value as a measurement criteria, the deviation between two specified times is used. Using this criteria, the gain difference between 400 μ s and 2.5 ms is measured to be 0.022 dB as shown in Figure 7.

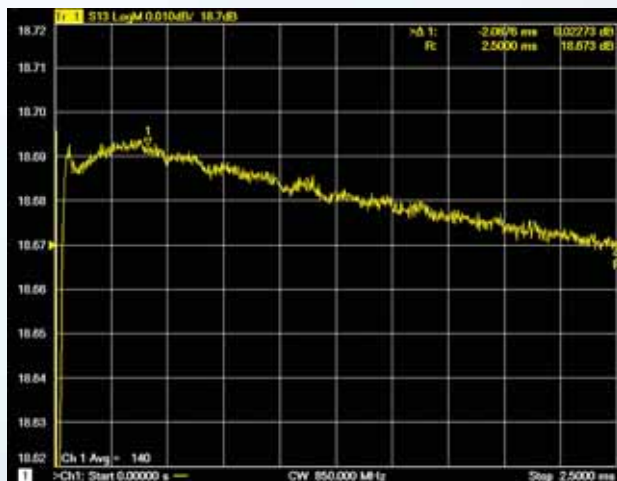


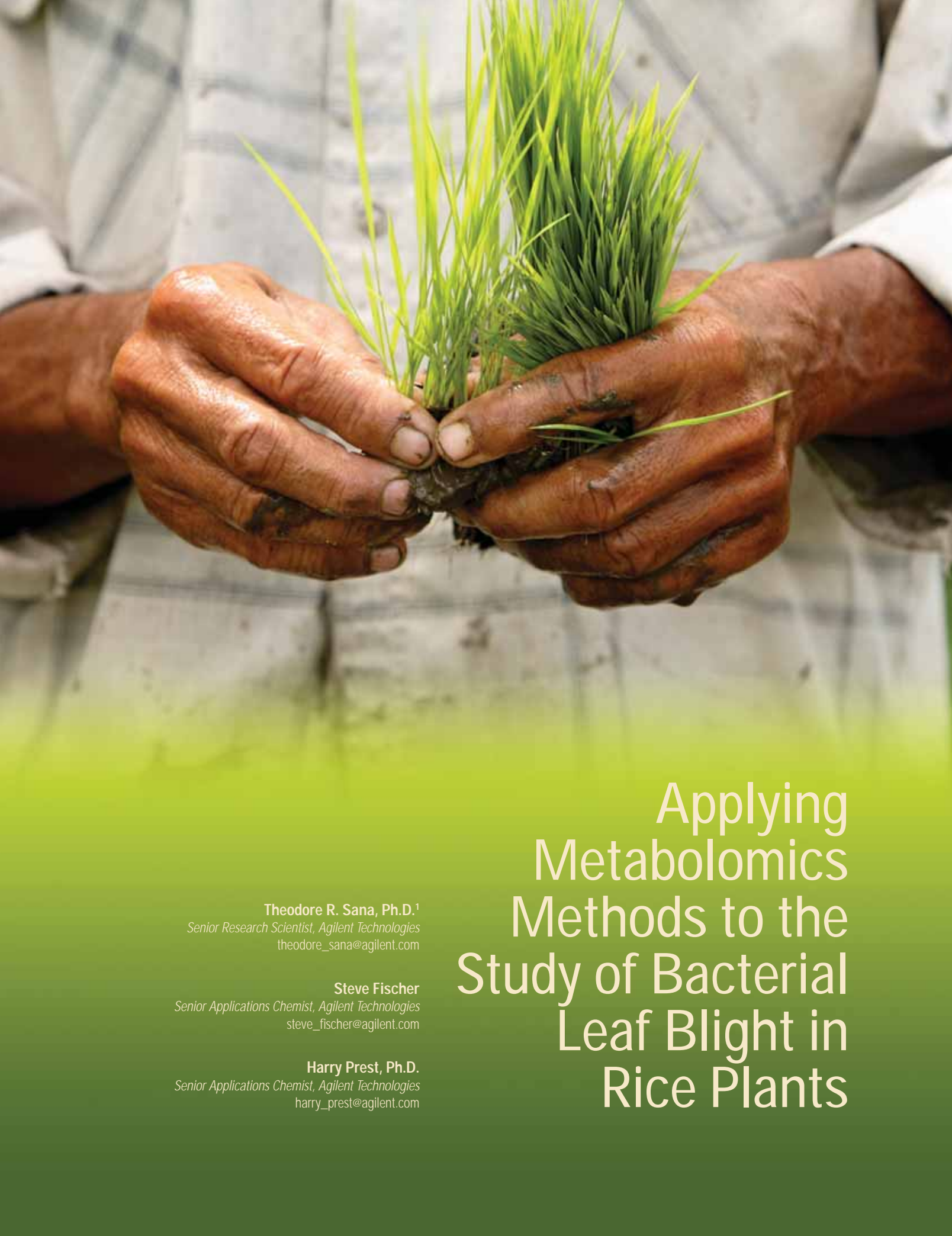
Figure 7. Settling of pulsed GSM amplifier using CW time-sweep measurement

Conclusion

Accurate switch settling times can be measured using vector network analyzers using either CW time-sweep or pulsed-profile S-parameter approaches. Accurate measurements will allow switch manufacturers and designers to ensure they meet customer requirements. VNAs are easily calibrated to the device ports, removing most of the fixture and measurement-system effects that can contribute significant errors to uncalibrated measurements. These practical measurement methods are easy to set up and apply to switched or pulsed devices.

References

1. Examples include the Agilent ENA Series RF network analyzers and PNA Series microwave network analyzers.
2. Agilent Application Note 1408-12, *Pulsed-RF S-Parameter Measurements Using Wideband and Narrowband Detection*, publication number 5989-4839EN, available from www.agilent.com.
3. The Agilent network analyzer uncertainty calculator can be downloaded from www.agilent.com/find/na_calculator.



Applying Metabolomics Methods to the Study of Bacterial Leaf Blight in Rice Plants

Theodore R. Sana, Ph.D.¹

Senior Research Scientist, Agilent Technologies
theodore_sana@agilent.com

Steve Fischer

Senior Applications Chemist, Agilent Technologies
steve_fischer@agilent.com

Harry Prest, Ph.D.

Senior Applications Chemist, Agilent Technologies
harry_prest@agilent.com

Rice is a primary food source for more than 3 billion people worldwide. Approximately 600 million people derive more than half of their calories from rice, and it is the third largest commercial crop behind wheat and corn. In 2005, an estimated 50 percent of the potential yield of the world rice crop was lost to diseases caused by bacteria, fungi and viruses.

In Africa and Asia, the most serious bacterial infection in rice is bacterial leaf blight (BLB), caused by *Xanthomonas oryzae pv. oryzae* (*Xoo*). Breeding and deployment of resistant rice cultivars carrying major resistance genes has been the most effective approach to combating BLB; one such gene, Xa21, has been successfully cloned into the rice variety Taipei 309 (TP309). PX099 is a bacterial strain of *Xoo* that spreads rapidly from rice plant to rice plant. Infected leaves develop lesions, become yellow, and wilt in a matter of days (Figure 1).



Figure 1. These rice leaves show both diseased and healthy states.

In collaboration with Dr. Oliver Fiehn and Dr. Pamela Ronald, our scientific partners at the University of California, Davis (UCD), we applied metabolomics methods to differentiate two rice genotypes: one susceptible (TP309) and the other resistant (TP309_Xa21) to infection by BLB. This work was facilitated by Agilent's University Grants Program, and the following is the first example of a joint metabolomics research project.

Defining metabolomics and the metabolome

Metabolomics is the comparative analysis of metabolites — the intermediate or final products of cellular metabolism — found in sets of similar biological samples. By measuring the “abundance profiles” of these metabolites, metabolomics can identify potential biomarkers and identify the effects drugs or diseases have on known or unexpected biological pathways.

Metabolomics is a *small molecule analysis problem* (molecular weight <1500), often of highly complex samples in which the analyte's chemical identity is usually unknown. The biological matrices containing the analytes typically include serum, plasma, erythrocytes, urine and cells. Due to the diverse physico-chemical properties of the analytes and orders-of-magnitude concentration ranges, metabolite detection requires a variety of extraction and analytical techniques.

The domain of this work is the *metabolome*, which is considered to be the small-molecule chemical equivalent of the genome. It represents the collection of all metabolites in a biological organism. Because the metabolome is closely associated with the genotype of an organism, metabolomics can play an important role in unraveling genotype/phenotype relationships.

Summarizing sample extraction and analysis workflows

Several key steps in metabolomics require careful consideration when planning an experiment. When performing either generic or targeted sample extractions, the method must effectively yield either a comprehensive or specific set of cellular or biofluid metabolites while excluding components that are not intended for analysis such as proteins and other compounds with high molecular weight. The extracted sample or analyte must also be in a state that is compatible with the downstream analytical techniques.

The protocol must be reproducible and take into account the distribution of metabolites that are greatly affected by the extraction method. Therefore, variability between samples due to processing methodology must be minimized where possible. This includes numerous factors: methods for quenching metabolic turnover to prevent degradation or interconversion of metabolites; selection of appropriate extraction solvents and cosolvents, and adjustment of pH for optimal extraction; minimizing metabolite oxidation; sample storage temperature; protein precipitation methods; and processing-time considerations.

Analytical reproducibility is very important for expression profiling. The combination of inherent biological sample variability and technical analytical variability determines the number of sample replicates required to verify the existence of statistically significant differences between sample sets. The smaller the analytical variance, the fewer replicates are required. Technical variability can be significantly minimized by including appropriate internal standards along different parts of the extraction and analytical workflows.

Outlining analytical approaches for metabolomics

Many methods can be used for metabolite profiling, and each one has advantages and disadvantages. Consequently, a combination of analytical techniques is often used to provide a more comprehensive view of the metabolome. The combinations used most often

are gas chromatography/mass spectrometry (GC/MS), liquid chromatography/mass spectrometry (LC/MS), nuclear magnetic resonance (NMR) and capillary electrophoresis/mass spectrometry (CE/MS). Figure 2 shows some of the chromatographic and detection techniques that are included in the Agilent metabolomics laboratory for profiling, identification and validation: GC/MS, LC, time-of-flight (TOF), quadrupole TOF (Q-TOF) and triple quadrupole (QQQ).

GC/MS offers the highest routine separation power (great analyte peak capacity) and potential sample identification with the use of electron impact (EI) ionization libraries. EI ionization has one big advantage relative to LC/MS ionization techniques: there is no ionization suppression effect. However, GC/MS analysis has four significant disadvantages:

- Most metabolites are nonvolatile and need to be chemically derivatized to become volatile prior to GC/MS analysis.
- Some metabolites are not volatile even after derivatization and hence cannot be analyzed.
- Thermally unstable metabolites lead to variable quantitation.
- They generally lack a molecular ion, which is extremely helpful in compound identification.

In contrast, LC/MS has the ability to analyze almost anything without the need for prior derivatization. This is because it operates in many ionization modes such as electrospray ionization (ESI) and



Figure 2. Agilent offers a complete set of instrumentation for metabolomics analysis.³

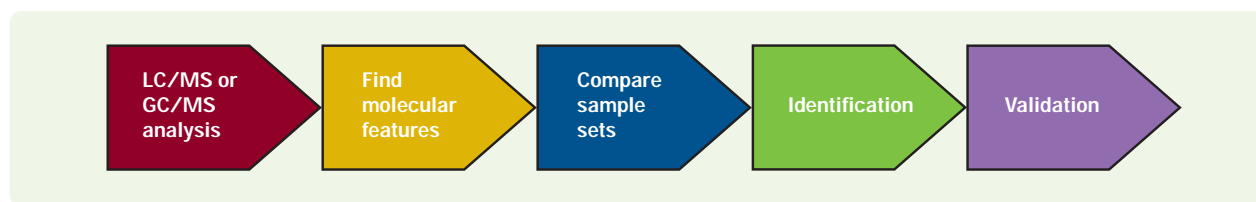


Figure 3. This diagram describes the Agilent mass profiling analysis workflow for metabolomics. Features (compounds) that are differential between sample sets are identified. The validation step requires a large number of samples.

atmospheric pressure chemical ionization (APCI) that have broad analyte applicability as well as the ability to produce both positive and negative ions to get full sample coverage. The separation power of HPLC is less than that of GC, however, resulting in longer analysis times. Also, comprehensive, publicly accessible spectral libraries are still in development and only currently becoming available.

The Agilent metabolomics analytical workflow (Figure 3) usually begins with a profiling approach using GC/MS, LC/MS, or both, to find statistically interesting “features” between different sample sets. A feature is an artificially constructed variable for each unidentified analyte and includes its retention time, mass and ion intensity.

Tools such as Agilent MassHunter software are used to find all the features in the raw total ion chromatograms (TICs) from LC/MS runs. A file is produced that contains a list of all the features found. Feature files from different samples are then compared using an application such as the GeneSpring-MS software. Features that are found to be statistically different are identified by searching the accurate masses against a metabolite database such as METLIN.² If the metabolite is not present in the database, it is possible to perform MS/MS analysis on a Q-TOF instrument for spectral interpretation of the data to a structure by generating

molecular formulae from the fragment ions. Finally, a relatively small number of identified metabolites can be purified, synthesized or purchased in a purified form for accurate quantitation on a QQQ mass spectrometer.

Metabolomics analysis of rice leaf infection

These methods were developed and tested during our collaboration with the team at UCD. The experiment design is outlined in Table 1 and includes appropriate controls. Two variants of PXO99 bacteria were used in this study: One was the wild-type, PXO99, and the other was a raxST gene knockout PXO99-raxST⁻.

The wild-type bacterium PXO99 produces a peptide (AvrXa21+) that is recognized by a cell-surface receptor encoded by the Xa21 gene in TP309_Xa21 transgenic rice but not present in TP309 (Figure 4). The raxST gene is critical for the correct processing of AvrXa21 peptide. The ability of transgenic rice to defend against the PXO99 bacterial pathogen is due to binding of the bacterial peptide to the plant Xa21 receptor, triggering the mitogen-activated protein 3-kinase (MAP3K) pathway that mediates signal transduction from the cell surface to the nucleus. This activates an

Table 1. Our experimental study design included two rice genotypes: wild-type TP309 (susceptible to infection) and transgenic TP309_Xa21 (resistant to infection). Rice were challenged with wild-type bacterium, PXO99, or PXO99 containing a raxST gene knock-out (raxST⁻), media-only mock infection or no treatment (NT). Six rice leaf biological replicates for each condition were analyzed. The average rice leaf weights (mg) for each condition and their standard deviations (SD) are shown.

Rice genotype	Challenge	Average_leaf weight (mg)	SD_leaf weight (mg)
TP309	PXO99	17.0	3.6
	Mock	16.6	1.6
	NT	19.0	3.2
TP309_Xa21	PXO99	17.3	1.5
	Mock	18.3	2.4
	NT	19.3	2.1
	PXO99-raxST ⁻	18.4	1.3

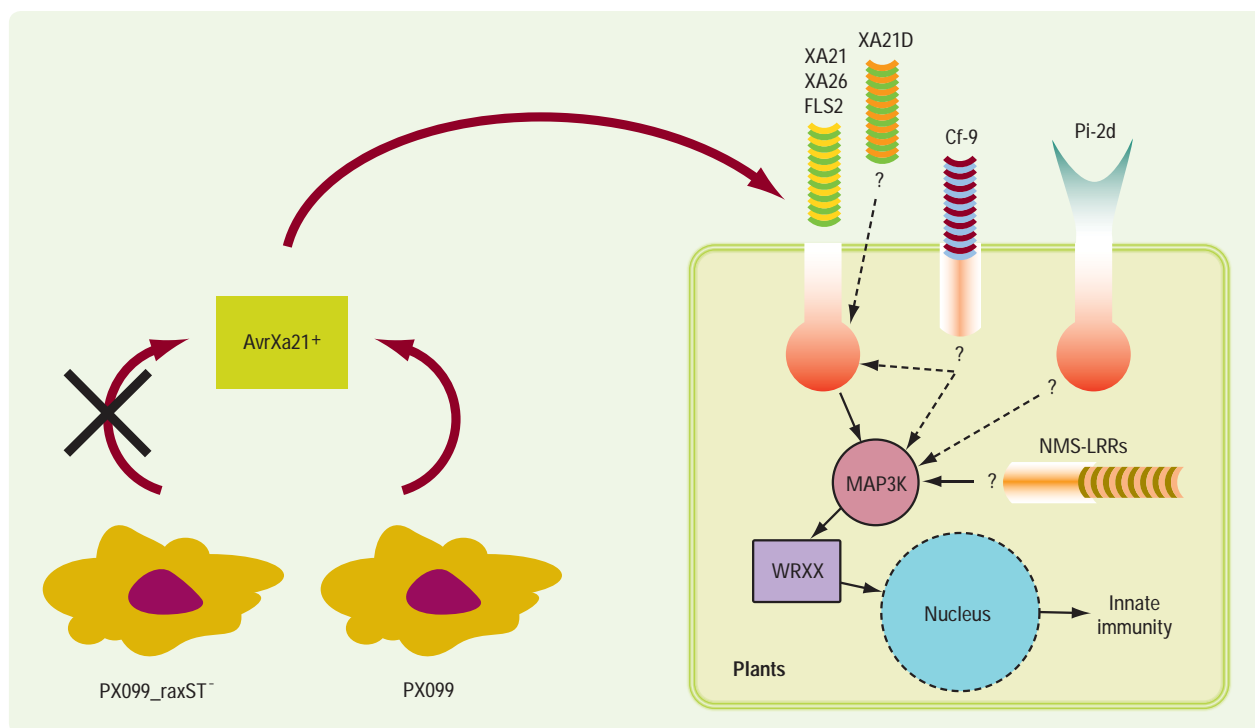


Figure 4. The schematic diagram shows the PX099 bacteria but not PX099_raxST⁻, secreting AvrXa21+ peptide. It binds Xa21 on transgenic rice (TP309-Xa21) that encodes a leucine rich repeat (LRR) domain in the receptor.

innate immunity mechanism that makes the transgenic rice resistant to the pathogenic bacteria. This mechanism is not activated in wild-type TP309 rice.

The purpose for including PX099_raxST⁻ bacteria in the study was to show that AvrXa21 peptide secretion is critical for imparting immunity to the transgenic rice. The rax gene family has an important role in AvrXa21 peptide secretion. By knocking out the raxST gene, a rax gene family member, we were able to study the metabolomics response of TP309_Xa21 transgenic rice when the peptide was absent. In that state, the transgenic rice becomes susceptible to bacterial infection because the peptide is not secreted and cannot bind to the Xa21 receptor.

Processing of rice samples

Figure 5 shows the sample-extraction workflow. Rice leaves were weighed, placed in tubes with a stainless steel ball bearing and loaded into liquid-nitrogen-cooled adapters before being homogenized for one minute in a Retsch Mill. The rice leaf extraction and processing method incorporates a -20° C, single-phase solvent mixture of acetonitrile/isopropanol/water at a ratio of 3:2:2, optimized for the extraction of polar, semipolar and nonpolar metabolites. It minimizes the extraction of waxes that are detrimental to the analytical instrumentation. The supernatant was transferred to sample vials for analysis after the tubes had been centrifuged to pellet RNA and protein. This procedure is an improvement over previous extraction protocols for plant materials

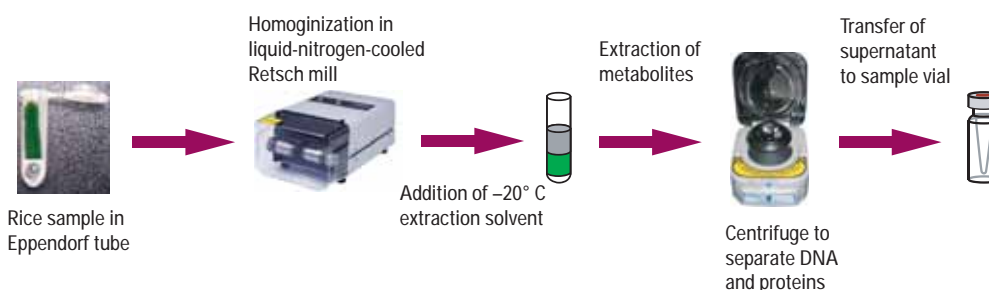


Figure 5. This was our workflow for the extraction of metabolites from rice leaves.

in that it is optimized for homogenizing as little as 20 mg of material in a single-phase solvent and enables analysis by both LC/MS and GC/MS instruments.

Analyzing extracted metabolites

Figure 6A summarizes the instrument conditions for LC/TOF MS on an Agilent 1200 LC equipped with a ZORBAX SB-Aq column (2.1 x 150 mm), which was used to separate the rice extracts. An Agilent 6210 TOF LC/MS equipped with an ESI source was used to acquire profiling data. Figure 6B shows the conditions for LC/Q-TOF MS, which was performed on an Agilent 6510 Q-TOF LC/MS equipped with an ESI source and was used to acquire accurate mass MS/MS data for metabolite identification.

Examining the data analysis workflow

Initial processing of the accurate-mass LC/TOF MS profiling data was done using MassHunter software (Figure 7). The feature

extraction and correlation algorithms located all the co-variant ions in a TIC. Background was subtracted and charge state was set to 1. The algorithm identified the monoisotopic mass and retention time and calculated an empirical formula for each feature. This information was imported into GeneSpring MS software for subsequent statistical analysis.

The workflow is summarized in Figure 8. Features were aligned and normalized and then checked for reproducibility of the sets of biological replicates in each class (condition) using hierarchical clustering analysis. To identify features with differential abundances across the different classes, we applied analysis of

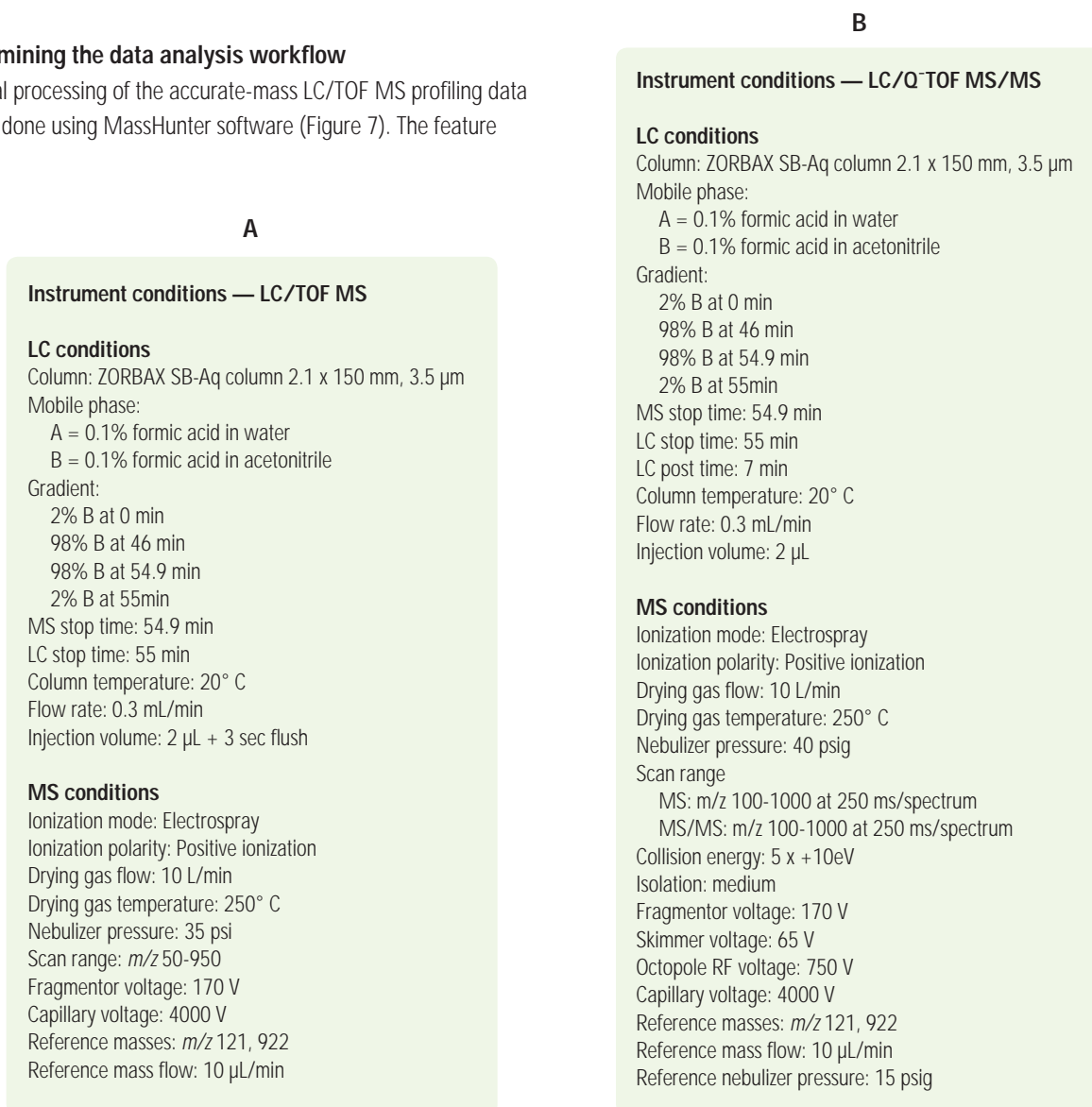


Figure 6. Summarizing the chromatographic and MS conditions used in the study, LC/TOF MS (A) was used for profiling and finding differential features and LC/Q-TOF MS (B) was used for identification of metabolites from a targeted inclusion list of ions that was generated by LC/TOF MS.

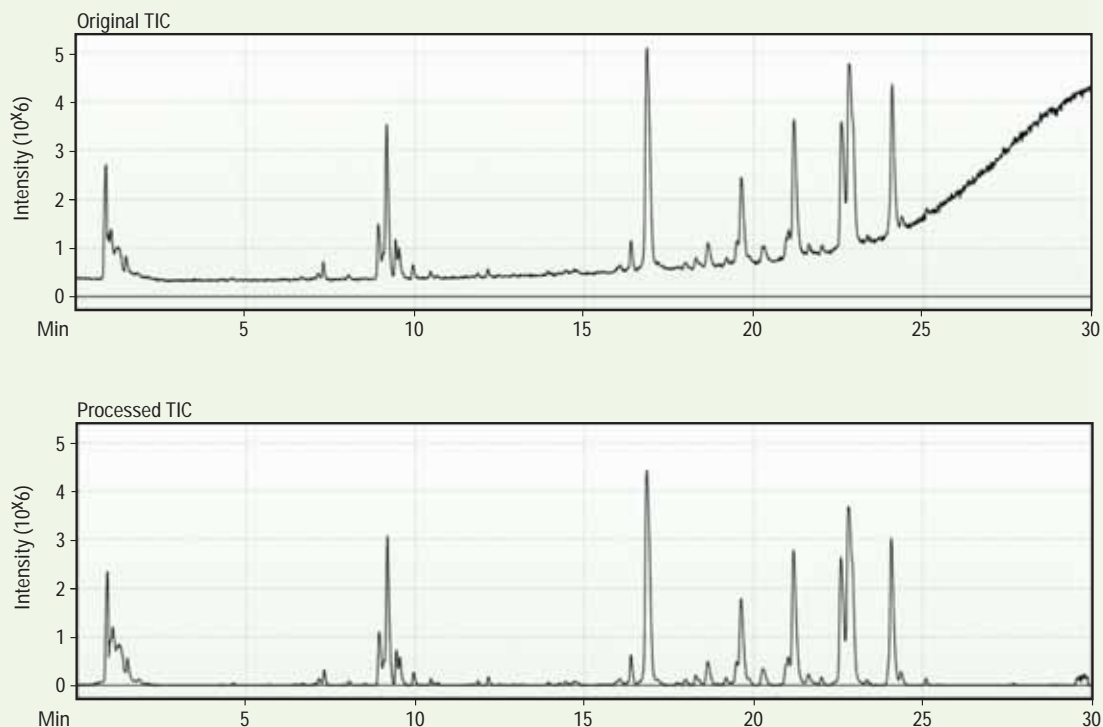


Figure 7. This shows rice LC/MS TICs before (original) and after (processed). Files were deconvoluted and background subtracted using Agilent MassHunter software.

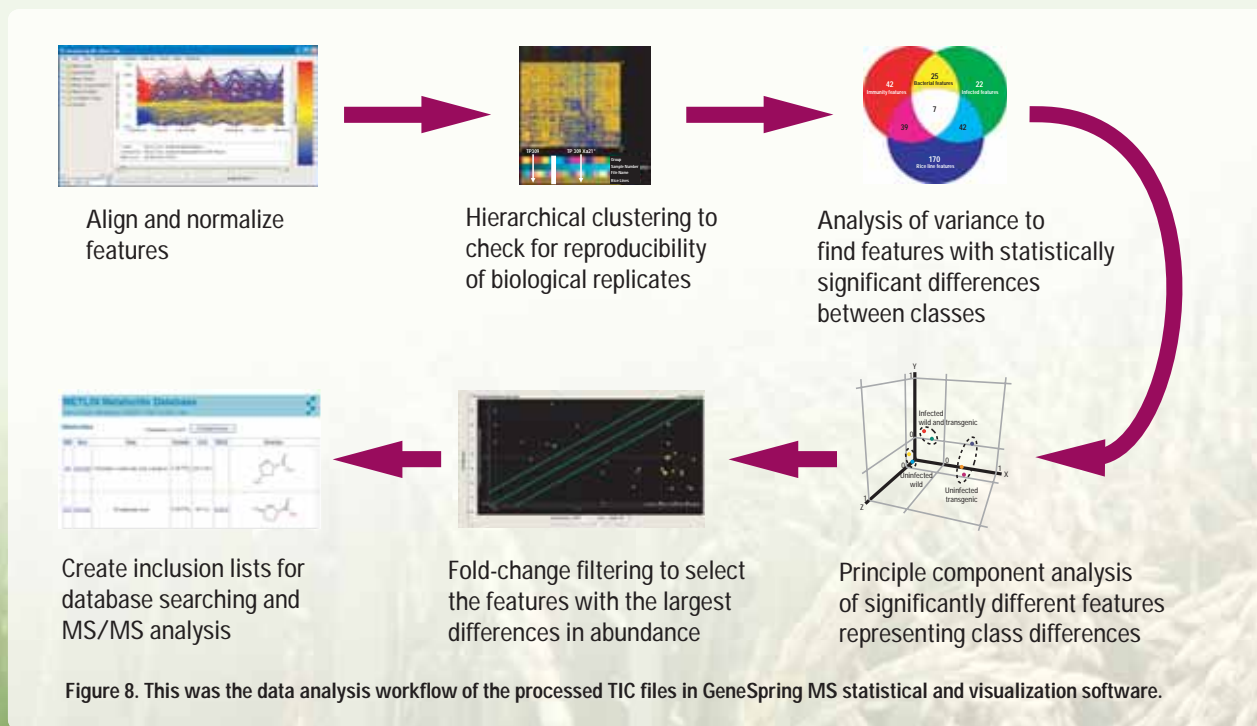


Figure 8. This was the data analysis workflow of the processed TIC files in GeneSpring MS statistical and visualization software.

variance (ANOVA) for multiple pair-wise comparisons. The results of the ANOVA were overlaid in a Venn diagram using three pairs of comparisons. For example, in one instance we compared only the significantly differential metabolites ($p < 0.05$) between TP309 (PXO99 vs. mock), TP309_Xa21 (PXO99 vs. mock) and TP309 mock vs. TP309_Xa21. From this we identified sets of feature ions that were specific to a particular class, specifically, TP309_Xa21/PXO99 features associated with resistance only and TP309/PXO99 features associated with susceptibility to infection. We then performed principle component analysis (PCA) of these feature sets to show how they visually discriminate the different treatment classes. We filtered the mass lists further to select features with the highest abundance and largest fold-change ratios. The mass lists were searched against the METLIN metabolite database. For example, Table 2 lists the METLIN search results for the neutral masses (not charged ions) that were induced in

the resistance-only (immunity) list. One of these masses, m/z 129.0414, with a single formula and six possible structures, was selected for further investigation by targeted MS/MS on the Q-TOF LC/MS system.

Examination of the MS/MS spectrum for its precursor ion, 130.0532, is shown in Figure 9. Only two of the six possible metabolites could logically have produced the spectrum. However, because the two compounds are enantiomers, they were indistinguishable by mass spectrometry. Their precise identity could be determined on a chiral LC column.

Clear differences between the two rice lines and infection states were detected. Identification of putative biomarkers of infection is ongoing and shows that metabolomic profiling can be a compelling research tool.

Table 2. This is a partial list of the induced (greater than two-fold change versus controls) feature ions from the TP309-Xa21/PXO99 condition, with their METLIN database search results. One of the highlighted neutral masses with six possible structures was subsequently analyzed by MS/MS.

Retention time (min)	Mass (U)	Fold Change	Empirical formula	Number of formulas	METLIN search (number of hits)
32.64	771.4705	2.4	C27H68N10013P	93	0
1.11	296.9389	2.8	C7HN08F2S	13	0
32.76	710.4604	4.2	C38H60N706	71	0
41.36	167.0575	6.1	C6H7N402	3	3
43.74	401.3279	9.7	C24H41N40	9	0
40.60	849.5386	10.7	C29H72N17010P	100	0
31.24	295.2517	11.5	C18H33N02	2	0
25.80	329.2925	11.9	C19H39N03	2	0
27.20	453.2855	12.4	C9H31N1903	20	0
32.66	739.4514	12.9	C32H65N7010S	85	0
47.38	934.5473	18.6	C53H79N2010P	100	0
46.41	660.5333	20.3	C25H62N1902	32	0
50.91	565.8811	20.7	C4HN6016F6PS	32	0
49.41	948.5989	23.2	C58H76N804	100	0
2.38	221.0538	24.8	C6H7N503	4	0
45.17	817.5082	25.0	C34H63N1903S	100	0
37.68	608.2646	27.8	C25H45N409PS	75	Harderoporphyrin
38.53	861.5044	28.0	C47H70N607P	100	erythromycin ethylsuccinate
2.07	129.0414	35.5	C5H7N03	1	6
2.10	122.0383	36.2	C7H6O2	2	benzoic acid

Developing new separation methods for metabolites

One outcome of the rice metabolomics study was to identify gaps in our analytical workflow. Our C18 ZORBAX SB-Aq LC column had limited capacity to bind and separate polar metabolites. We also encountered significant difficulties with GC separation and analysis of derivatized metabolites, resulting in MS source fouling and reduced column longevity. To address these issues, two new chromatographic separation methods are being developed. One uses a novel type-C silica material for separating metabolites by aqueous normal phase (ANP) LC that can be coupled to different sources for MS detection. The other builds a new metabolite derivatization module into the injection port of a GC oven, improving the analysis of labile metabolites by GC/MS.

Binding and resolving polar metabolites

At Agilent, we have recently been investigating new chromatographic materials for LC/MS analysis that can bind and resolve polar metabolites. Many endogenous metabolites are highly polar and unretained on standard reverse-phase high-pressure LC (HPLC) columns, even in a 100 percent aqueous mobile phase.

Chromatographers have tried many approaches to solving this problem but only hydrophilic interaction chromatography (HILIC) can possibly address the chemical diversity of hydrophilic metabolites. Unfortunately, the available HILIC materials have three important limitations: They are slow to re-equilibrate; the chromatography has poor reproducibility; and they require high levels of salts or buffers, which can cause problems in metabolomics analysis. Type-C silica (Figure 10) is an ANP stationary phase

with HILIC-like retention but without these disadvantages.

The principle of ANP is analogous to that found in normal-phase chromatography but the mobile phase has water as part of the binary solvent. "Normal phase" implies that retention is greatest for polar solutes such as acids and bases. We used amino acids to demonstrate the utility of ANP to separate polar metabolites. Figure 11 shows the extracted ion chromatograms (EICs) for a mixture of 19 amino acids that were separated on a silica-hydrate surface based on the polar properties of the individual amino acids. These would otherwise be unretained on a standard C18 column. All of the critical amino acid pairs — those that are isobaric or have masses within one mass unit — were separated under the gradient condition that was used (except for the leucine/isoleucine pair). Additional gradient formats and mobile phases are under investigation to address this issue.

Table 3 summarizes the reproducibility of retention times for nine amino acids separated approximately between eight and 12.2 minutes at two temperatures, 15° C and 30° C. Four replicates were performed at each temperature. The reproducibility was 0.28 percent or better for the amino acids, an excellent result representing a significant improvement over HILIC analyses.

Improving the analysis of labile metabolites

Many scientists who are proficient — but not expert — users of GC/MS desire a turnkey solution that includes *in situ* (rather than offline) derivatization of the sample in the instrument. For *in situ* derivatization to be successful, it must be performed in the heated GC injection port. However, the sample solvent, derivatization agents and samples can contain a number of unwanted components that reduce sample throughput by degrading column or

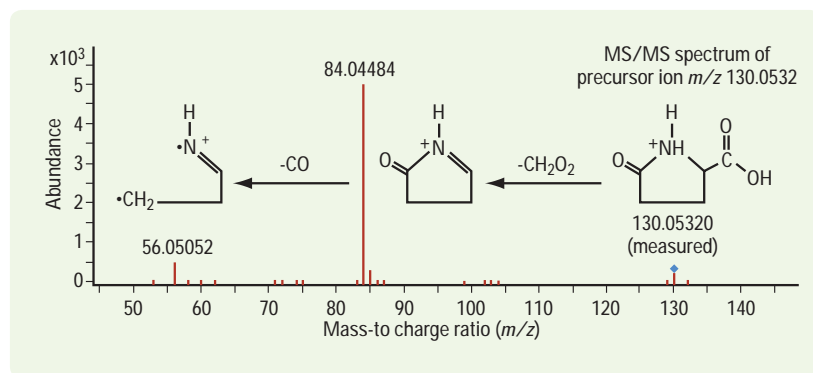


Figure 9. In this metabolite identification, the MS/MS spectrum of the precursor ion at m/z 130.0532 shows a base peak representing the loss of formic acid (CH_2O_2) and a peak representing a subsequent loss of CO. Evaluation of this information against the structures of the six possible identities generated by a search of the Metlin database reduced the list of possible identities to two.

detector performance. To address this issue we tested a “selective sample introduction” device that can be used to perform the *in situ* reaction. This device can be operated in such a manner as to reduce or remove the high boiling compounds and residual derivatizing agents. We believe such an approach can create new possibilities for reducing the amount of sample pretreatment necessary prior to GC/MS analysis, resulting in improved lab productivity, instrument reliability and analysis reproducibility. Figure 12 shows an Agilent 6890/5975C GC/MS system fitted with a ProSep precolumn separation device (Apex Technologies) that was developed to divert the low-boiling derivatizing agent and the bulk of the high-boiling compounds through the vent port. This also enabled the selection of components for introduction

onto the two GC columns joined by a purged tee. The purged tee permitted back-flushing of the first column to eliminate the very close eluting high boilers while the analysis continued on the second analytical column.

This was demonstrated in an experiment using C24-FAME (fatty acid methyl esters) standards and cholesterol esters. Fatty acids are an important class of lipid metabolites and can be identified by their retention on defined chromatographic systems and by mass spectrometry. We added fatty acid standards to cholesterol esters to provide a high-boiling cutoff marker. Other late-eluting components (such as triglycerides) would also be eliminated as they elute near or after the cholesterol.

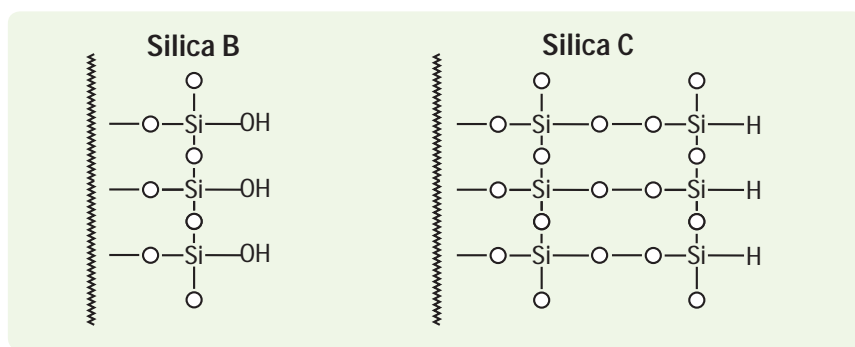


Figure 10. A new deactivated silica Type-C material with a high surface area and 4.0 μm particle size was developed for LC separation of polar metabolites. Type-B silica was converted to Type-C material having a silica hydride (Si-H) surface.

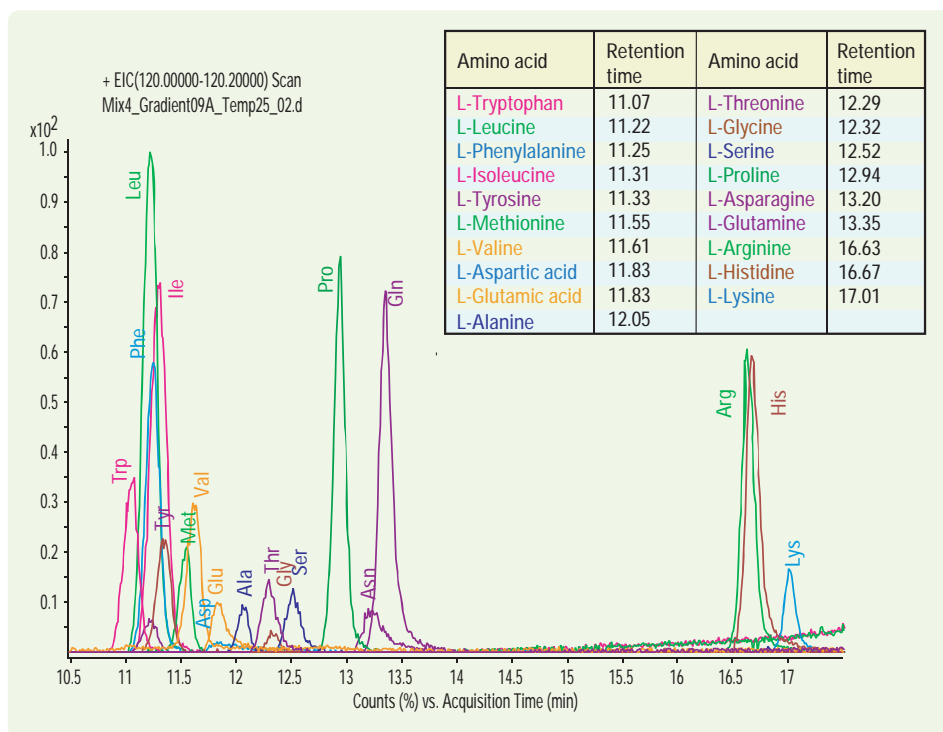


Figure 11. This EIC shows the separation of mixture containing 19 amino acids.

Table 3. Retention time reproducibility for nine amino acids at two temperatures: 15° C and 30° C. Four replicates were performed at each temperature and the percent relative standard deviation (% RSD) was calculated.

Amino Acid	G1B	G1B inj 2	Gr 1B inj 3	Gr 1B inj 4	% RSD	Gr 1B	Gr 1B inj 2	Gr 1B inj 3	Gr 1B inj 4	% RSD
Retention time	15° C	15° C	15° C	15° C		30° C	30° C	30° C	30° C	
L-Alanine	9.654	9.622	9.637	9.633	0.14	9.671	9.705	9.678	9.687	0.15
L-Glutamine	10.961	10.929	10.955	10.940	0.13	10.911	10.933	10.917	10.938	0.12
L-Histidine	12.178	12.180	12.183	12.180	0.02	12.162	12.173	12.168	12.178	0.06
L-Methionine	8.771	8.751	8.754	8.762	0.10	8.856	8.900	8.873	8.905	0.26
L-Phenylalanine	8.369	8.360	8.363	8.360	0.05	8.532	8.576	8.527	8.559	0.27
L-Proline	10.647	10.628	10.650	10.610	0.17	10.495	10.507	10.496	10.511	0.08
L-Serine	9.932	9.935	9.935	9.928	0.03	9.948	9.971	9.971	9.986	0.16
L-Threonine	9.731	9.745	9.746	9.738	0.07	9.725	9.770	9.736	9.774	0.25
L-Tyrosine	8.491	8.483	8.495	8.498	0.08	8.641	8.686	8.641	8.679	0.28

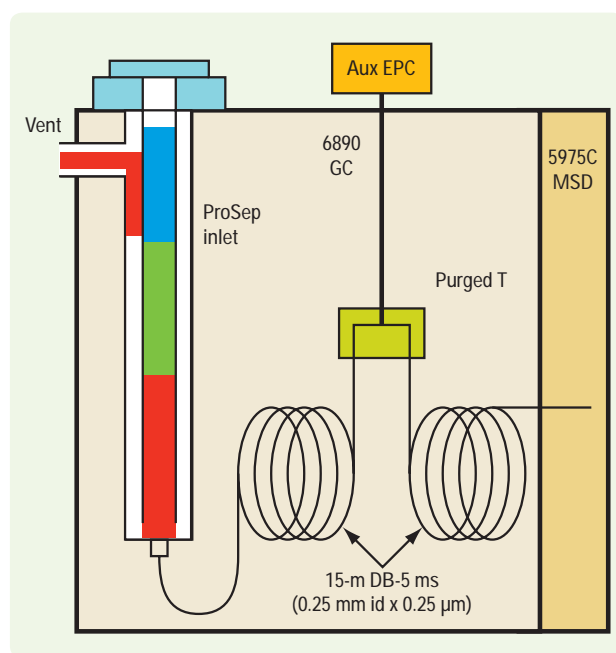


Figure 12. The GC/MS configuration used an Agilent 6890/5975C GC/MS system fitted with an APEX ProSep. Two 15-m DB-5ms (0.25 mm id x 0.25 µm) columns joined by a purged tee were used for the separation.

Figure 13 shows the result of two chromatographic runs, with and without derivatization in ProSep. The top chromatogram shows both the C24-FAME standards and cholesterol esters before removal with ProSep and column back-flushing. The bottom chromatogram shows the quantitative removal of all the cholesterol esters with essentially no reduction of the C24-FAME standard. This illustrates the high degree of selective elimination possible in this arrangement. The method was shown to be reproducible and was accomplished without loss of sensitivity.



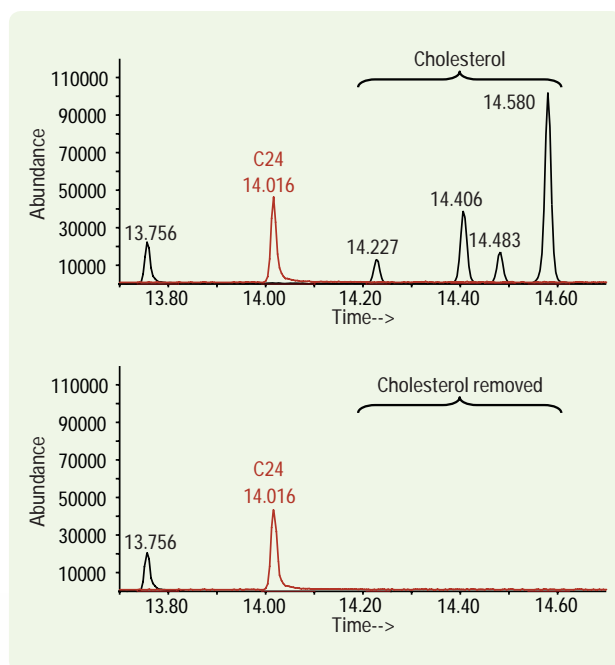


Figure 13. ProSep enabled selective removal of high-boiling components. The top chromatogram shows the C24-FAME and various cholesterol esters before removal using ProSep and column back-flushing. The bottom chromatogram shows the quantitative removal of all the cholesterol esters.


Conclusion

This collaborative study exemplifies the rapid progress that has been made in hardware, software and biological applications for metabolomics. We learned a significant amount about gaps in our analytical workflow and required improvements in both instrumentation and software, which are currently being addressed. Nevertheless, challenges remain for the unambiguous identification of metabolites, which will be greatly aided by the development of comprehensive, accurate mass libraries of metabolites.

References

1. Dr. Sana was the corresponding author for this article.
2. The METLIN database is available online at metlin.scripps.edu.
3. The Agilent metabolomics laboratory has a specific Web site to support researchers in the field: www.metabolomics-lab.com.





Measuring Stream Dynamics with Fiber Optics

Nick Tuffillaro

Member of Technical Staff, Agilent Technologies
nick_tuffillaro@agilent.com

John Dorigi

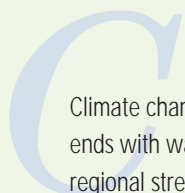
Application Engineer, Agilent Technologies
john_dorigi@agilent.com

Mike Collier

Graduate Student, Oregon State University
mike.collier@gmail.com

Dr. John Selker

Professor, Oregon State University
selkerj@enr.orst.edu



Climate change is a story that begins with temperature and often ends with water — melting glaciers, rising sea levels, storms and regional stresses on freshwater sources. Remote sensing from satellites provides the big picture, but a regional understanding of the impact of environmental change requires detailed measurements on the ground. One key measurement of a regional environment is “streamflow,” which hydrologists define as the movement of water in a natural channel.

Lakes and rainwater runoff are obvious places to start when looking for sources of streamflows. However, most of the available freshwater exists not on the surface but in the ground, and underwater springs, which are a significant contributor to streamflow, are currently not well measured or modeled. Locating and gauging these groundwater inputs requires measurements able to cover several kilometers with resolution as fine as one meter. Traditional “point measurement” instruments used in hydrology cannot handle this challenge; however, new distributed measurement technologies that use fiber optic temperature sensors can provide the required reach and resolution.

These sensors quickly measure temperature over a few kilometers with resolution down to a meter, and this temperature data can be used to uncover the groundwater interactions with stream water. However, instruments developed for *in situ* environmental measurements must also be field deployable, energy efficient (typically operating from batteries or solar cells) and pest-proof.

The Agilent N4386A distributed temperature system (DTS) uses fiber optics to meet these measurement challenges. The DTS is used in a wide range of applications: downhole oil and gas reservoir performance monitoring; power cable monitoring; pipeline and water dam leakage detection; and in security applications such as fire detection in tunnels, refineries or other special-hazard applications. Geophysical scientists are also using this instrument to address a variety of hydrological applications. This article highlights one such project, done in collaboration with Oregon State University, Corvallis, Oregon to measure the connection between surface streamflows and subsurface water sources.

Basics of DTS operation

The DTS uses light to measure temperature. It starts each measurement by launching a pulse of light from a semiconductor laser into a standard communications optical fiber and then measuring the backscattered light to first determine time-of-flight and then position.

Three important scattering mechanisms are present in an optical fiber: Rayleigh, Brillouin and Raman. The Agilent DTS uses the spontaneous Raman scattering signal and measures changes in the intensity at the Stokes line, which is temperature-dependent, and the Anti-Stokes line, which is mostly temperature independent. The temperature is then computed from the ratio of these two lines after performing a fiber-dependent calibration procedure. The basic relation is written as

$$\frac{I_{AS}}{I_S} \propto \exp\left(\frac{h\Delta\nu_R}{kT}\right)$$

where h is the Planck constant, k is the Boltzmann constant, T is the absolute temperature and $\Delta\nu_R$ is the separation between Raman Anti-Stokes/Stokes and probe-light frequencies.

In the DTS, temperature resolution varies with distance, spatial resolution and temporal averaging. A total of 8000 measurement points can be acquired during every averaging period. This allows spatial resolution down to 1.5 m for measurement spans of up to 12 km and down to 1 m for distances up to 8 km. For example, a temperature resolution of 0.11° C is possible at a distance of 2 km (1.5 m spatial resolution) with 10 minutes of temporal averaging. Reducing the temporal averaging to thirty seconds decreases the temperature precision to 0.35° C.

During set up and calibration in the field, temperature accuracy (along with precision) is typically checked with a few independent single-point temperature measurements. A two- or four-channel DTS offers additional capability for dual-ended or loop-back measurements. The ongoing auto-calibration present in a dual-ended measurement further simplifies the calibration and improves measurement accuracy.

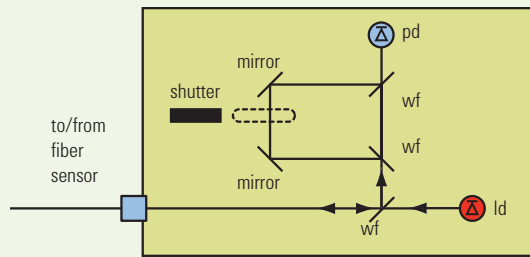


Figure 1. The integrated optical assembly in the Agilent DTS includes a low-power semiconductor laser (ld) and a single-receiver optical detector (pd). The concept uses a series of wavelength filters (wf) and mirrors direct the backscattered Stokes and Anti-Stokes lines from the fiber sensor to the photo diode. (Figure adapted from Reference 1.)

Looking inside the Agilent DTS

The core of the Agilent DTS is an integrated optical block that contains a laser source, filters and a single optical detector in a bulk optical assembly. The entire assembly is hermetically sealed and filled with an inert gas, isolating the components and preventing condensation from degrading instrument performance over its range of operating temperatures. A schematic of the optical assembly is shown in Figure 1. Two unique aspects of the design are its use of a low-power semiconductor laser and its single-receiver optical detector.

The DTS uses a low-power external-cavity diode laser operating at 1064 nm. A semiconductor laser ensures a long operating life, eliminating the need for field-replaceable parts. This is an important requirement for reliable, maintenance-free measurements in remote locations. Additionally, the average optical power from the source is ~17 mW, which classifies the laser as a Class 1M “eye safe” device — unlike other commercial instruments that use solid-state YAG lasers.

The optical path for the single-receiver design is also shown in Figure 1. Light from the source is coupled into the sensing fiber and backscattered light is directed toward the detector through a series of filters and reflectors. The Agilent DTS measures both the Anti-Stokes (1018 nm) and Stokes (1112 nm) lines using a single optical receiver. A single receiver improves the instrument’s measurement accuracy over a wide range of operating temperature by eliminating drift, which can occur in dual-receiver designs. The apparent change in temperature reported by the DTS is less than 1° C as the ambient operating temperature of the DTS changes over its entire 70° C range.

The choice of a power-efficient semiconductor laser carries a technical challenge: the resulting backscattered light has limited signal strength at the receiver, and this translates into a lower signal-to-noise ratio. Agilent engineers overcame this issue using a code-correlation technique to boost signal level and improve the signal-to-noise ratio, making it comparable to higher-power, single-pulse laser sources.² This approach was leveraged from Agilent’s 20 years of experience designing and manufacturing rugged, field-reliable optical time-domain reflectometers (OTDRs) and external-cavity diode lasers.

Making it field-ready

To address rugged, outdoor field applications, the Agilent DTS is designed around an integrated optical block. The instrument also includes an IP66 (NEMA 4) enclosure to prevent moisture from interfering with instrument operation (Figure 2). Additionally, the optical block is temperature stabilized, allowing operation from –10° C to +60° C. Operation at lower temperatures is made possible by adding insulation that traps heat generated by the instrument: With this extra warmth, the DTS will continue to function even if the external temperature drops below –10° C. In a trial, the DTS operated down to –40° C using only external insulation with no internal heating elements. The instrument can be operated with standard telecom fibers for normal temperature ranges or with special fibers that cover a temperature span of –273° C to +700° C, depending on sensor coating.



Figure 2. An IP66/NEMA4 enclosure prevents moisture from interfering with instrument operation.

In remote deployments, power consumption is a critical factor. The DTS offers a nominal power consumption of 15 W (< 40 W peak) and can use DC sources such as batteries and solar panels.

Measuring the water cycle

The water cycle begins with the sun heating the oceans and lifting moisture to the clouds. Precipitation falls to the Earth and starts its journey back toward the sea, driven by gravity. Water on the Earth's surface is easily seen in rainwater runoff to lakes, rivers and streams. Less visible is the water below the ground. Groundwater makes up 98 percent of available fresh water and its importance can not be underestimated: It supplies 40 percent of the fresh water in the United States and 70 percent in China.^{3,4} In addition to human uses, groundwater is essential as a freshwater source for springs, rivers, lakes and their surrounding habitats. Despite its critical role in the water cycle, the interaction of surface water and groundwater is difficult to measure and therefore difficult to understand, model and manage.

Getting a local look at the water cycle typically involves the use of hydrologic tracers. A variety of passive (O16/O18, tritium, CFCs) and active (dyes) tracers allow hydrologists to piece together a detailed picture of the path taken by water both above and below the ground. For instance, measurements of O16/O18 ratios allow the determination of "residence time," which is the average time the water spends in a given reservoir. These measurements often provide the key data needed to determine the origin and subsequent path water takes during its extended journey underground.⁵

Heat can also be used as a tracer. Because the temperatures of streams and subsurface springs differ, temperature measurements can provide a distributed, real-time look at the interaction of stream waters and their surrounding groundwater aquifers.

Examining stream dynamics with the DTS

New distributed temperature-sensing applications in hydrology are being developed at Oregon State University. Examples include measuring flow patterns in lakes via temperature, upwelling of water-borne pollutants in abandoned mine shafts, and the thermal interactions of air and snow.⁶

For temperature-based measurements of flow patterns, environmentally rugged — but otherwise standard — communications optical fibers are placed in streams as shown in Figure 3. The distributed temperature sensor locates groundwater sources by looking for steps in the temperature change indicative of groundwater influx. Several different methods, all based on conservation of energy and mass, enable not only the determination of the location of groundwater inputs but also quantitative estimates of the groundwater inputs to streamflow. One such method starts with measurements of temperatures upstream and downstream from the groundwater source. Coupling this information with knowledge of the groundwater temperature enables estimates of changes in the flow rate using the following relation:

$$Q_o = Q_i \left(\frac{T_g - T_i}{T_g - T_o} \right)$$

In this equation, Q_o is the streamflow after the groundwater source (usually reported in cubic feet per second), Q_i is the streamflow before the groundwater source, T_g is the groundwater temperature, T_i is the temperature before the groundwater source, and T_o is the temperature after the groundwater source.⁷

During the spring of 2007, an Agilent N4386A DTS was installed at watershed one of the H.J. Andrews Experimental Forest in the Cascade Mountain Range of western Oregon. The forest is one of the National Science Foundation's long-term ecological research (NSF-LTER) sites. One goal of the Andrews LTER studies is to understand how land use, natural disturbances and climate change affect key ecosystem properties such as carbon dynamics, biodiversity and hydrology.

The site is heavily instrumented and is used, for instance, to study effects of land use and climate change on essential environmental properties supporting ecosystems.⁸ The DTS installation includes one kilometer of rugged optical fiber with the last 600 meters installed in the stream. Metal ties secure the fiber along the stream bed. The instrumentation is powered using a bank of 12-V batteries.

Measurement results from the Andrews installation are shown in Figure 4, which reveals variations in the stream temperature and surrounding air over one week. This particular data set clearly illustrates how the local air temperature drives shallow-water stream temperatures.

In addition to its use for hydrological science, the installation is also used for training. During the fall of 2007, the Andrews installation will be the site of a workshop called "Fiber Optic Distributed Temperature Sensing for Ecological Characterization." Staff from Oregon State University and the U.S. Geological Survey (USGS) will lead the workshop.⁹



Figure 3. Installing fiber at the H. J. Andrews Experimental Forest in the western Cascade Range of Oregon.

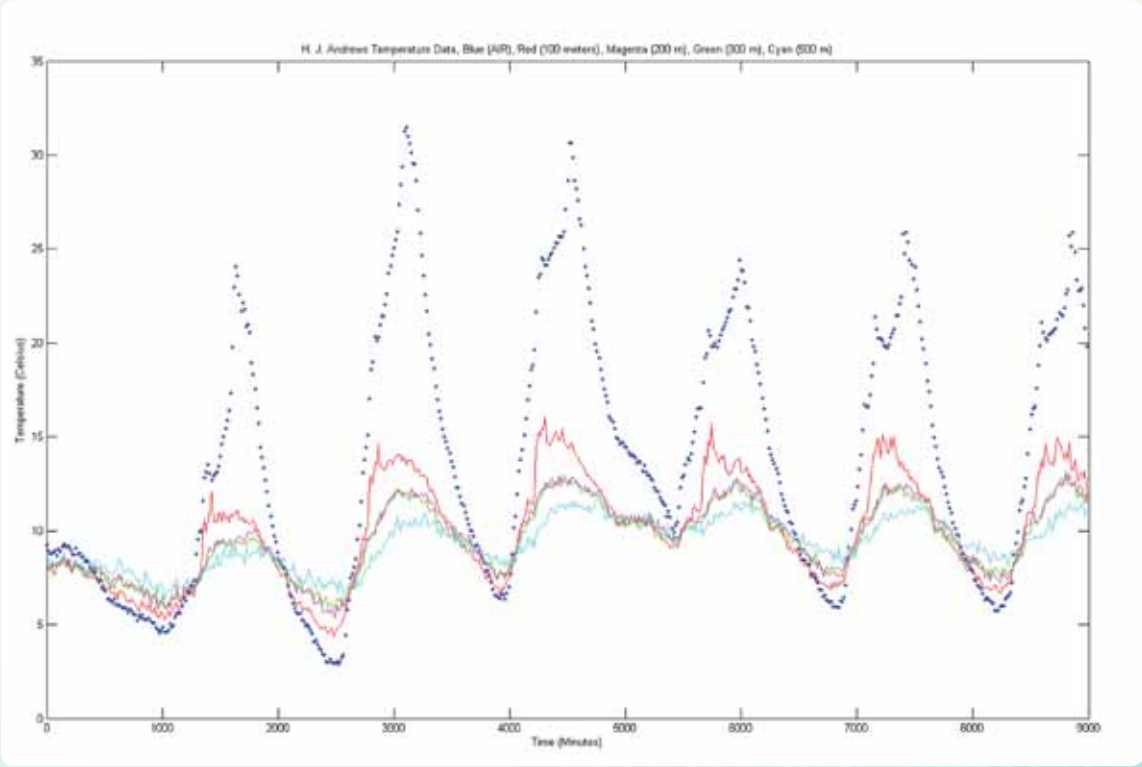
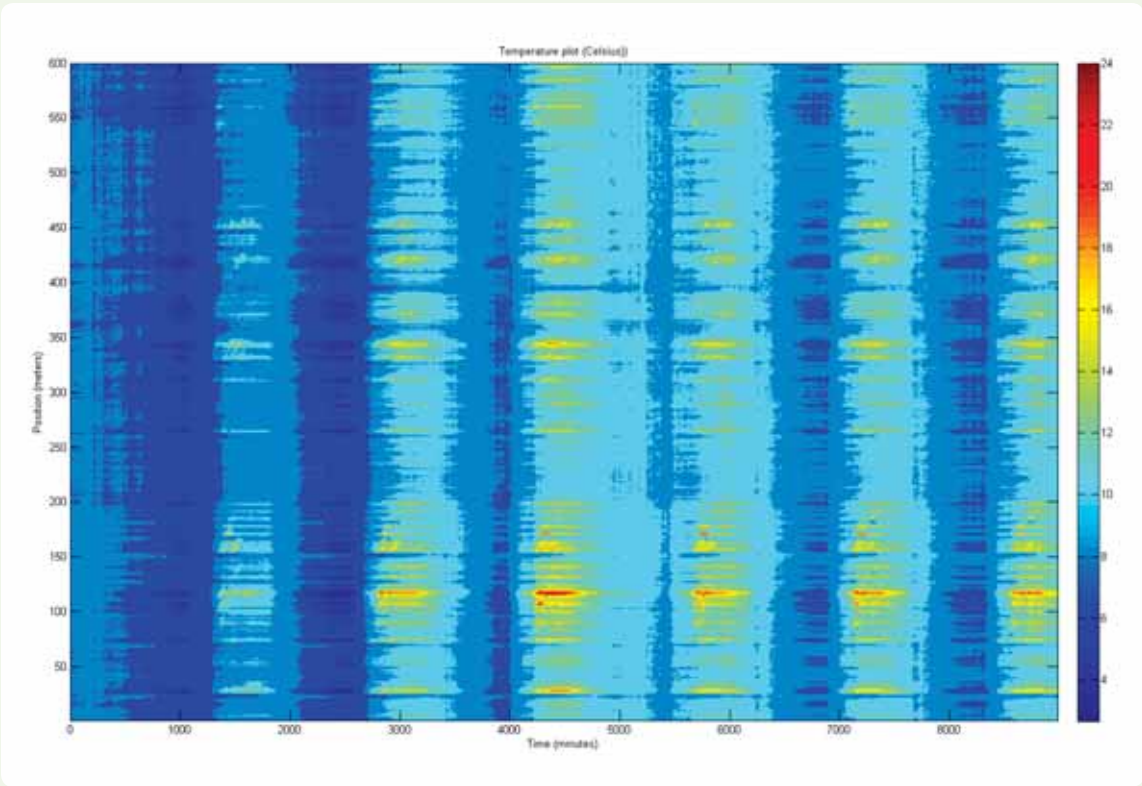


Figure 4. Temperature records from the Andrews installation at watershed one, May 12-19, 2007. Major oscillations are from diurnal cycle. The lower graph shows stream temperature at three positions; the dots show out-of-stream air temperatures also measured by the DTS system.

A second installation was deployed during the summer of 2007 in the Walla Walla region of southeastern Washington State. Walla Walla (literally “water, water” in the Native American Sahaptin language) is a rich agricultural area famous for sweet onions, winter wheat and, more recently, wine. The Walla Walla Basin Watershed Council is overseeing a number of hydrological monitoring projects, including a recharge project that takes a significant portion the Walla Walla River and directs it back into regional aquifers.¹⁰ Over the past 50 years, groundwater pump-down caused many streams to disappear, taking with them the fish and wildlife that depended on those streams. The Agilent DTS is aiding in both gauging the recharge of the aquifers and providing a first-hand look at the streams that are returning to the Walla Walla region after a 50-year absence.

Conclusion

Streamflow dynamics are the lifeblood of many ecological communities. Distributed temperature sensing is a unique new technology researchers can use to better measure and understand environments and ecologies. The technology opens new possibilities for assessing water quantity and quality in real-time with excellent resolution in both space and time. Today, the Agilent DTS is enabling a more thorough view of streamflow dynamics by providing a cost-effective way to make distributed measurements. Looking to the future, distributed sensor technologies will enable new *in situ* measurements that address concerns ranging from pollutant tracking for environmental protection to irrigation measurements for precision agriculture.

References

1. Soto, M.A., Sahu, P.K., Faralli, S., Sacchi, G., Bolognini, G., Di Pasquale, F., Nebendahl, B., and Rueck, C. 2007. High-performance and high-reliable Raman-based distributed temperature sensors based on correlation-coded OTDR and multimode-graded index fibers. *Proc. SPIE*, Vol. 6691, 66193B.
2. Sischka, F., Newton, S.A., and Nazarathy, M. 1988. Complementary Correlation Optical Time-Domain Reflectometry. *Hewlett-Packard Journal*, December 1988: 14-21.
3. Pielou, E.C. 2000. *Fresh Water*. University of Chicago Press.
4. Glennon, R.J. 2004. *Water Follies: Groundwater pumping and the fate of America's fresh waters*. Island Press.
5. Kendall, C., and McDonnell, J.J. (editors). 1998. *Isotope Tracers in Catchment Hydrology*. Elsevier Science.
6. Selker, J.S., Thévenaz, L., Huwald, H., Mallet, A., Luxemburg, W., van de Giesen, N., Stejskal, M., Zeman, J., Westhoff, M., and Parlange, M.B. 2006. Distributed Fiber Optic Temperature Sensing for Hydrologic Systems. *Water Resource Research* 42, W12202.
7. Selker, J.S., van de Giesen, N., Westhoff, M., Luxemburg, W, and Parlange, M. 2006. Fiber Optics Opens Window on Stream Dynamics. *Geophysical Research Letters*, DOI:10.1029/2006GLO27979.
8. An interactive map of the H. J. Andrews Experimental Forest is available at www.fsl.orst.edu/lter/
9. The workshop announcement is available online at oregonstate.edu/conferences/fiberoptic2007
10. For more information about hydrologic monitoring projects in the Walla Walla Basin see www.wwbwc.org/Projects/Monitoring_Research/Surface_Ground_Water_Hydrology.htm





Agilent Technologies